

UCLA

UCLA Electronic Theses and Dissertations

Title

Feedbacks and Interactions between Aeolian and Fluvial Processes and Vegetation Dynamics in Drylands

Permalink

<https://escholarship.org/uc/item/4qm130p2>

Author

Nadoum, Shereen

Publication Date

2019

Peer reviewed|Thesis/dissertation

UNIVERSITY OF CALIFORNIA

Los Angeles

Feedbacks and Interactions between Aeolian and Fluvial Processes
and Vegetation Dynamics in Drylands

A dissertation submitted in partial satisfaction of the
requirements for the degree of Doctor of Philosophy
in Geography

by

Shereen M GH M Nadoum

2019

© Copyright by
Shereen M GH M Nadoum
2019

ABSTRACT OF THE DISSERTATION

Feedbacks and Interactions between Aeolian and Fluvial Processes and Vegetation in Drylands

by

Shereen M GH M Nadoum

Doctor of Philosophy in Geography

University of California, Los Angeles, 2019

Professor Gregory Stewart Okin, Chair

Drylands cover more than 40% of the earth land surface and are home for more than 2 billion people. Despite the harsh environment and the extreme aridity conditions, drylands are among the most diverse ecosystems that contribute to more than 30 % of the global terrestrial net primary production. Assessing vegetation dynamics for dryland surfaces remain a challenge due to the appearance of soil and non-photosynthetic material that usually cause non-linear scattering of light. This aspect of remote sensing is investigated in this dissertation using mechanistic and unmixing remote sensing approaches to assess net primary productivity of the Chihuahuan Desert. The unmixing approach was demanded by the difficulties associated with assessing vegetation productivity with mechanistic remote sensing. We found that including soil and non-

photosynthetic surface covers contribute to the predictions of NPP with Multiple Endmember Spectral Mixture Analysis using Random Forest and stepwise regression.

Erosion is considered one of the main complex drivers that contribute to vegetation cover change. The feedbacks between wind erosion and other environmental, and biological driver have not been fully studied. Wind erosion remains one of the most understudied drivers of shrub encroachment despite the evidence of the association of aeolian transport with grass cover decline and shrub encroachment. In this research, we introduce wind erosion processes as major disturbances to vegetation cover in drylands affecting the health and mortality of vegetation species. We investigated the damaging effects of wind transport on major vegetation community types in the Chihuahuan Desert using a linear wind tunnel. We quantified the damaging effects of sandblasting using plant mapping methods to emphasize leaf loss, color change, stem loss and plant height change. Our sandblasting experiment shows some similarities between the grasses and the shrubs in the response to sandblasting. However, the grasses were more sensitive to sandblasting than the shrubs due to their growing point and growth form.

Aeolian and fluvial processes are fundamental drivers of arid land dynamics because of their effects on soil surfaces and microtopographies. In this research we investigate the coupling effects of wind and water transport in erosion and deposition in ephemeral streams in Moab, UT covering dry and wet periods. We used structure from motion and drone technologies to survey stream over 16 months period to investigate the soil surface elevation change due to wind and water activities. We performed differencing analysis and quantified soil erosion and deposition volume over 5 survey periods. The streams show a significant net soil erosion and deposition over the periods which indicate direct interaction between aeolian and fluvial processes in development and changes of channel morphologies.

The dissertation of Shereen M GH M Nadoum is approved.

Yongkang Xue

Thomas Welch Gillespie

Jasper F. Kok

Gregory Stewart Okin, Committee Chair

University of California, Los Angeles

2019

Table of contents

Dissertation Outline	1
Chapter 1: Introduction to drylands	3
1.1 Drylands characteristics	3
1.2 Socio-economic importance	5
1.4 Erosion interactions and implications	5
1.5 Erosion and vegetation	7
1.6 Above ground primary production	9
1.7 Vegetation and soil degradation	10
1.8 Bibliography	11
Chapter 2. The contribution of aeolian processes to vegetation state change: Damaging effects of sandblasting on native shrub and grass species in the Jornada Basin, NM.	21
2.1 Abstract	21
2.2 Introduction	22
2.3 Methods	25
2.3.1 Study area	25
2.3.2 Plant material	25
2.3.3 Wind tunnel treatments	26
2.3.4 In situ measurements	29
2.3.5 Quantification and mapping of above-ground biomass	30
2.4 Results	34
2.4.1 Total Abrader Mass (TAM)	34
2.4.2 Response of Plant Architecture to Aeolian Abrasion	34
2.4.3 In situ plants	47
2.5 Discussion	48
2.6 Conclusion	50
2.7 Future plans	51
2.7 Bibliography	52
Chapter 3. Remote sensing of net primary productivity of Chihuahuan Desert vegetation: Evaluation of data retrieval and statistical approaches.	58
3.1 Abstract	58
3.2 Introduction	59

3.3 Methods.....	62
3.3.1 Study site	62
3.3.2 Field data	65
3.3.3 MODIS Data products	65
3.3.4 Spectral unmixing of MODIS NBAR	66
3.3.5 Estimating NPP from MESMA fractions	67
3.3.5.1 Estimation of Error	69
3.4 Results	70
3.4.1 Standard MODIS GPP and NPP products	70
3.4.3 Multiple regression	73
3.4.5 Stepwise Regression	78
3.4.6 Random Forest.....	80
3.5 Discussion	80
3.5.1 Standard MODIS NPP and GPP products	81
3.5.4 The utility of MESMA-derived fractions	82
3.6 Conclusion.....	84
3.7 Acknowledgments.....	85
3.8 Bibliography.....	86
Chapter 4. Drone-based monitoring of hillslope-channel coupling by aeolian processes.....	91
4.1 Abstract	91
4.2 Introduction	91
4.2.1 Background.....	93
4.3 Methods.....	96
4.3.1 Study area	96
4.3.2. Ground control point (GCP)	98
4.3.2. Image acquisition.....	99
4.3.3. Image processing	100
4.3.4 Height accuracy/consistency assessment.....	101
4.3.5 Object classification and differencing analysis	102
4.4 Results	104
4.6 Conclusion.....	114
4.7 Acknowledgment	115

4.8 Bibliography.....	116
Chapter 5: Discussion and Conclusion	121
5.1 Bibliography	125

List of figures

Figure 1. Drylands distribution around the world (Millennium Ecosystem Assessment 2005).....	4
Figure 2. A 10-meter long wind tunnel was used treat 6 different treatment. (B) The hopper (green) was used to feed the wind tunnel with abrasders.	26
Figure 3. In situ samples of (A) <i>P. glandulosa</i> and (B) <i>A. canescens</i>	30
Figure 4. A diagram showing a plant map for <i>P. glandulosa</i> . B: A photo from field notes showing a plant map for <i>A. purpurea</i>	31
Figure 5. Leaf growth form for <i>S. Airoides</i> (A), <i>A. purpurea</i> (B), <i>B. eriopoda</i> (C).	32
Figure 6. (A) <i>B. eriopoda</i> LflHfr replicate showing stem loss. (B) <i>B. eriopoda</i> , (C) <i>S. airoides</i> , (D) <i>A. purpurea</i> treatments. Photos taken on October 1st, 2018.....	35
Figure 7. (A) <i>A. canescens</i> LflHfr replicate showing no indications of damage, (B) <i>A. canescens</i> , (C) <i>L. tridentata</i> , (D) <i>P. glandulosa</i> treatments. Photos were taken on October 1st, 2018.	36
Figure 8. Average leaflet loss % in response to sandblasting at sand flux treatments $g\ cm^{-1}$ and control for six species over six weeks.....	38
Figure 9. Average leaf loss % in response to sandblasting at sand flux treatments $g\ cm^{-1}$ and control for six species over six weeks.....	39
Figure 10. Leaf area loss (%) in response to sandblasting at sand flux treatments $g\ cm^{-1}$ and control for six species over six weeks.	42
Figure 11. Leaf color change (%) in response to sandblasting at sand flux treatments $g\ cm^{-1}$ and control for six species over six weeks.....	45
Figure 12. Plant height increase (%) in response to sandblasting at sand flux treatments $g\ cm^{-1}$ and control for six species over six weeks. Negative response indicate reduction in height.	46
Figure 13. Locations of the NPP sites in the Jornada Experimental Range (JER) and the Chihuahuan Desert Rangeland Research Center (CDRRC), both located in the Jornada Basin, NM (Havstad et al. 2006; Huenneke et al. 2002).	62

Figure 14. The overall correlation between in situ NPP and MODIS GPP at landscape scale (left), and the corrected NPP using MODIS GPP and in situ NPP (Right). The R² remained the same since only linear correction was applied. 72

Figure 15. (D) Community level stepwise regression analysis at seasonal (left) and annual scales (right). (E) Community level Random Forest analysis at seasonal (left) and annual scales (right). (F) Landscape level stepwise regression analysis (SW) and Random Forest analysis (RF) at seasonal (left) and annual scales (right). The annual scale display R² higher than the seasonal scale at most of the community types and at landscape (RF) levels..... 79

Figure 16. (A) A map of the Western United States showing the location of Moab, UT. (B) Satellite image (Google Earth assessed on 12/19/2018) showing the location of our study site. Bottom panel, orthomodels of the three streams. The NW stream image collection shown here was taken at sunrise 6:40 am (local time) which caused the appearance of deep shadow. 97

Figure 17. Masks were created for NW, SW, and NE streams indicating stream morphologies (bed, east wall, and west wall). 103

Figure 18. Soil surface elevation change (cm) over 16 months at (A) NW stream, (B) SW stream and (C) NE stream. 107

Figure 19. Soil surface elevation change (cm) over four different periods of time at (A-1-4) NW stream, (B-1-4) SW stream and (C-1-4) NE stream. 110

List of tables

Table 1. Aridity index of hyper-arid, arid and semi-arid lands. 3

Table 2. Native Chihuahuan desert shrub and grass species and their characteristics. The shrub species have high root mass compared to the grass species. 25

Table 3. TAM (mean ± standard deviation; g cm⁻¹) experienced by plants in four species over six weeks..... 34

Table 4. Leaf loss ANOVA analysis for each species and leaflet loss for *p. glandulosa*. 37

Table 5. Leaf area loss ANOVA test for each species..... 40

Table 6. Leaf color ANOVA test for each species. 43

Table 7. Plant height ANOVA test for each species..... 44

Table 8. Species, site, and average leaf loss (%) at sites of wind and abrasion effect (T) and control (C) standard deviation (STDEV) and coefficient of variance (CV) for plants in natural conditions. 48

Table 9. Site, dominant plants, soil type and year of fencing of our study sites. Each community includes three plots of most common plant communities. Fences were built to protect the plots from grazing and human interruption (Havstad et al. 2006; Huenneke et. 2002). Average NPP over 15 years for each plot ($\text{g m}^{-2} \text{y}^{-1}$).....	64
Table 10. Plot, community and landscape estimates of NPP, and “n” points of observation in each correlation in these scales. Coefficient of determination (R^2), y-intercept (b), slope of the regression between in situ NPP (Y) and MODIS NPP (X, left side of table) and MODIS uncorrected GPP (X, right side of table), RMSE ($\text{g m}^{-2} \text{y}^{-1}$), and ME ($\text{g m}^{-2} \text{y}^{-1}$) of the regressions between corrected MODIS GPP (GPP_C) and in situ NPP at plot, community and landscape scales. The regression between in situ NPP and corrected GPP is determined to be significant: p-value < 0.01 at all scales.	71
Table 11. Site, variable correlation coefficient (R^2), variable slope (c_{variable}), variable significance (p_{variable}), y-intercept (b), RMSE, R^2 and the significance of the 3-variable multiple regression models between in situ NPP and GV, NPV and soil (seasonal and annual) at plot community type and landscape scales.	74
Table 12. Site, variable correlation coefficient (R^2), slope (c_{variable}), variable significance (p_{variable}), y-intercept (b), RMSE, R^2 and the significance of the 2-variable multiple regression model between in situ NPP and GV and soil (seasonal and annual) at plot community type and landscape scales.	77
Table 13. Site, out-of-bag mean error, RMSE, normalized RMSE, relative error and RMS-relative error ($\text{g m}^{-2} \text{y}^{-1}$) at community and landscape scales using seasonal and annual derived-MESMA fractions.....	80
Table 14. Stream location reference direction, field transect measurements of length of survey (m) and mean width (m).	96
Table 15. Survey dates, max wind speed (m s^{-1}), 95th percentile wind speed (m s^{-1}), total rainfall (mm), number of days with maximum windspeed > 7 m/s ($\text{WS}>7$), and number of days with more than 10 mm rainfall ($\text{R}>10$) during the survey periods from Canyonland Weather Station near Moab, UT (ASOS Network 2017). Numbers in parentheses represent the percent of days during a time period with $\text{WS}>7$ and $\text{R}>10$	98
Table 16. Acquisition and processing parameters used for designing drone flights and generating 3D models.	99
Table 17. X, y and z errors (cm), overall error (cm), and reprojection pixel error of the estimated GCP marker positions.	104
Table 18. Comparison between heights (cm) measured with Trimble Total Station (TS) and heights retrieved from UAV (cm) for July 2017, and between heights of GCP retrieved from UAV (cm)	

for each survey date and overall for each site, mean difference (MD) cm, mean difference (MD) cm, mean absolute difference (MAD) cm..... 105

Table 19. Height uncertainty (MAD), pixel size, and volume uncertainty for each stream in the study..... 105

Table 20. Site, GCP order, GCP heights for each survey date (cm), and standard deviation cm (STDEV) for each GCP at all survey dates and average STDEV cm for each site..... 106

Table 21. Total erosion and deposition (cm³) at different portions of each stream..... 111

Acknowledgments

I would like to thank my advisor professor Gregory S. Okin for his continuous support and encouragement throughout my four years at UCLA. I have gained tremendous experience through his guidance, were it not for Greg's expertise in dryland ecosystems, this dissertation would not have been possible. I want to thank my committee members, professors Yongkang Xue, Thomas Gillespie, Jasper Kok for their input in my research. I would also like to especially thank Dr. Jayne Belnap for hosting my research in Moab Utah, working with you was a great pleasure. Dr. Steve Archer, no words can describe my admiration for your work, thank you for your guidance.

I am very thankful to Dr. Kebonye Dintwe, Dr. Junzhe Zhang, Dr. Abinash Battachan, Avishes Neupane and Austin Madson who made my time at UCLA beyond enjoyable. My gratitude goes to my colleagues Mike Fischella who help in field work and lab work and Dr. Furong Niu from the University of Arizona whom I learned a lot from. Thank you, guys.

I also want to thank the administrative staff Kasi McMurray, Nayla Huq, Jenee Misraje, Vanessa De La Rosa, and Brian Won at the department of geography UCLA.

I would also like to extend my gratitude to the Jornada Experimental Range staff David Thatcher, and Joe Martinez for providing us with comfortable accommodations throughout our field campaigns. John Anderson is very much appreciated for coordinating with LTER to accommodate our work sites.

Kuwait University and the High Ministry of Education of Kuwait, thank you for giving this opportunity and supporting me throughout the years of this scholarship, I look forward to starting a new chapter at Kuwait University. My Academic advisors at Kuwait Embassy Anna Tigen, and Mollie Yee, thank you for all the time and effort you put into working with me. Dr. Mansour Jaragh, Thank you for your support.

Above all, I thank my family for believing in me and giving me many opportunities to learn and be successful. I derive my strength from you.

VITA

EDUCATION

Ph.D. Candidate	Geography, University of California Los Angeles	(2017 - 2019)
Ph.D. Program	Earth Sciences, Colorado State University	(2014 - 2015)
Master of Arts	Geography, University of Arkansas	(2012 - 2014)
Bachelor of Arts	Geography, University of Kuwait	(2006 - 2010)

FELLOWSHIPS and AWARDS

Graduate Student Support – Kuwait University Scholarship Division	(2012 – 2019)
Teaching Assisting Scholarship – Kuwait University Scholarship Division	(2012 – 2019)

Dissertation Outline

Chapter 1: This chapter introduces the characteristics of dry regions including their location, climate, and aridity conditions. In addition, their biological and socio-economic importance are also discussed. The chapter introduces major discussion points of soil and vegetation dynamics and land cover alterations.

Chapter 2: Aeolian abrasion increases above-ground biomass stress and reduced productivity for some drylands vegetation which may contribute to shrub encroachment. In this study, we investigate the damaging effects of sandblasting on native grass (*Aristida purpurea*, *Bouteloua eriopoda*, and *Sporobolus airoides*) and shrub (*Artiplex canescens*, *Larrea tridentata* and *Prosopis glandulosa*) species in the Chihuahuan Desert. A ten-meter linear wind tunnel was used to simulate sandstorms and to expose the plants to different levels of sandflux and wind treatments. We quantified the damaging effects of sandblasting using “Plant mapping” techniques over the course of six weeks. We measured leaf loss (%), stem loss (%), leaf area loss (%), color change (%) and plant height change (%) using two sampling intervals. We found some similarities between *Bouteloua eriopoda* and *P. glandulosa* in the amount of leaf loss, however, we believe that grasses are usually more susceptible to sandblasting damages due to their growing point which doesn't exceed the saltation layer. The highest leaf loss (%), stem loss (%) and leaf color change (%) was found for *Bouteloua eriopoda*. Our results may explain the contribution of aeolian processes to shrub encroachment into grasslands.

Chapter 3: This chapter discusses remote sensing of net primary productivity using mechanistic and unmixing remote sensing approaches to estimate and predict NPP for the Chihuahuan Desert. Measurements of *In situ* NPP (2000-2015) from 12 NPP sites monitored by the Jornada Long Term Ecological Research Program were selected for this study. MODIS provided primary datasets for

our analysis, including GPP (MOD17A2H), NPP (MOD17A3H) and BRDF adjusted reflectance product (MCD43A4). We found that MODIS 17 products have no skill in predicting NPP at plot, community and landscape scales. Using BRDF, we estimated the fractional cover of seasonal and annual green vegetation (GV), non-photosynthetic vegetation (NPV) and soil using Multiple Endmember Spectral Mixture Analysis (MESMA), GV, NPV and soil were primary surface covers in the NPP predictions using multiple regression, stepwise regression and Random Forest. We found that random forest was best in explaining the variations in the annual *In situ* NPP (up to 93%) for all vegetation communities and landscape scale.

Chapter 4: Aeolian and fluvial activities are fundamental drivers of arid land dynamics because of their effects of sedimentation processes and erosion. In this chapter we investigate the coupling effects of wind and water transport in erosion and deposition in ephemeral streams in Moab, UT covering dry and wet periods. An unmanned-aerial vehicle (UAV) was used to survey three streams over the course of 16 months. We performed elevation differencing analysis (cm) to estimate the changes in soil surface elevation over four survey periods and used Trimble Total Station to assess the vertical accuracy of the models. We investigated the morphological traits of the streams and identified the spatial distribution of sediment erosion and deposition volume (cm³) onto the bed and the walls of the streams. We found that there's a direct linkage between aeolian and fluvial activities in channel development and sediment storage over time.

Chapter 5: This chapter highlights the long-term of environmental and ecological implications of the interactions between vegetation and soil dynamics.

Chapter 1: Introduction to drylands

1.1 Drylands characteristics

Drylands are found between latitudes 20 degrees north and 40 degrees south and cover about 40% of the earth's land surface (D'Odorico and Porporato 2006). Drylands ecosystems are characterized by lack of water, seasonal climatic extremes, and infrequent and unpredictable precipitation patterns (Knapp et al. 2008), frequently referred to as "water-limited ecosystems". These ecosystems include scrublands, shrublands, savannas, super deserts, and semi-deserts. Aridity is assessed based on climate variables: aridity index (AI) and/or the growing season in which water reaches a level that allows plant growth (FAO 2019). The AI is a measure of P/PET used to classify drylands into hyper-arid, arid, semi-arid and dry sub-humid, where water loss via potential evapotranspiration (PET) is higher than precipitation (P) almost all year long, registering P/PET of less than 0.65 (Middleton et al. 1997; World Atlas of Desertification 1997). This relationship between P and PET results in a short growing season, often less than 120 days in arid and semi-arid lands.

Table 1. Aridity index of hyper-arid, arid and semi-arid lands.

Climatic zones	Area coverage (%)	P/PET ratio	Annual precipitation (mm)
Hyper-arid	7.5	<0.05	60 -100
Arid	12.1	0.05-0.20	150- 250
Semi-arid	17.7	0.20-0.50	250 - 600

75% of the world's rangelands and roughly one third of the world's terrestrial biodiversity are found within these drylands; and 2 billion of the world's population depend on the resources

drylands provide (MEA 2005). Drylands also store one third of the world’s soil carbon. For these reasons, drylands are a crucial player in global climate patterns.

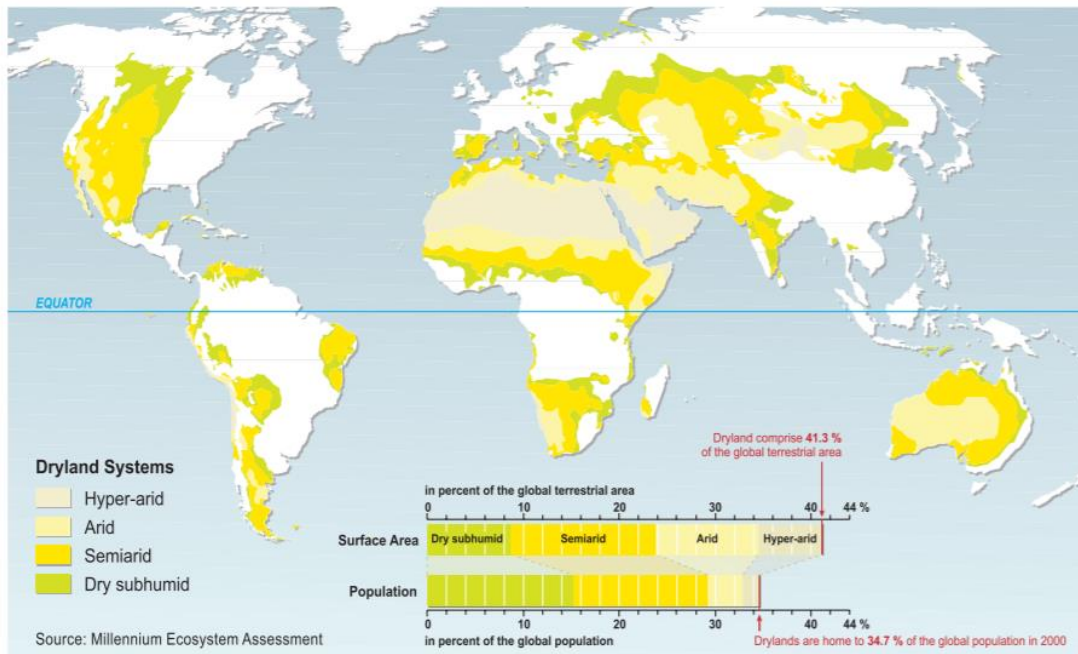


Figure 1. Drylands distribution around the world (Millennium Ecosystem Assessment 2005).

Despite the resource limitations and harsh environment, drylands support more than 38% of the human population. It was estimated that 10–20% of the drylands suffers from a severe ecosystem degradation (Alvaraz et al. 2011). These ecosystems are under increasing environmental stress caused by conditions of dryness and human activities. Drylands are vulnerable to climatic fluctuations such as droughts and increasing temperatures, while humans exacerbate these conditions with urbanization and suburbanization (Allred 1996; Buffington and Herbel 1965; Gibbens et al. 2005). This dual effect of disturbances from global climate change and anthropogenic factors lead to acceleration in soil erosion, decrease in soil stability, and decline in vegetation in arid and semi-arid lands (Schlesinger et al. 1990). Due to the fact that over 2 billion people inhabit drylands, these disturbances in turn lead to destabilizing habitats, the economy, and public health (Reynold and Stafford 2003). Understanding the dynamics of the controls and drivers

that affect these ecosystems will facilitate our understanding of the complex dynamic interactions between resources and the biotic and abiotic drivers in drylands.

1.2 Socio-economic importance

Dryland ecosystems hold great economic, social, and cultural value locally, regionally and globally. Locally, rural and local communities depend on natural resources and services that the ecosystem provides as they provide food, fuel, and water, in addition to spiritual and cultural values. Drylands support 35% of the world's population, of which 90% reside in developing countries (MEA 2005). In the developing countries, they contribute to the well-being of millions of people through sustaining the local livelihood and food production (Reed and Striger 2015). Globally, drylands provide not only sustenance to the world's populations, but also ingredients for food, medical, and cosmetic products to multinational businesses (FOA 2019).

1.3 Biological importance

Despite high levels of aridity and harsh environmental conditions, drylands include a wide range of biodiversity that is highly adapted to its ecology. The Sonora desert is considered the most biodiverse and productive dryland worldwide (Davies et al. 2012), including animals and plant species that are not found in any other ecosystem, in addition, the Kalahari Desert is also known for its biodiverse fauna and wildlife. All drylands combined include about 30% of sites that have important biodiversity and 28% of the total area of World Heritage Sites (WHS) (Reed and Striger 2015).

1.4 Erosion interactions and implications

The interactions among abiotic agents and their relative importance in drylands has been poorly studied. Abiotic disturbances in drylands are recognized in the high-frequency wind

dynamics and the episodic water movement, which are considered critical measures of erosion, since they serve as erosive agents (Okin et al. 2006).

The potential of erosion to cause environmental and climatic alterations has increased by 17% over the past century due to concentrated expansion of cropland, grazing, and anthropogenic activities that account for approximately 60% of all erosion drivers (Yang et al. 2003). Drylands in particular are most susceptible to aeolian and fluvial erosion due to the reduction in vegetation cover and soil moisture. Large bare soil surfaces provide aeolian and fluvial transport with supply, especially since the soil structure of drylands is weak due to low organic matter and weak physical and biological crusts (Belnap and Lange 2003; Sivakumar 2007). Today, drylands are known for their abundant soil supply of loose and dry soil particles, which are predicted to increase, as climate models suggest more intense and frequent wind and water storms in the future (Easterling et al. 1990; IPCC 2007).

Wind and water erosion have contributed to two billion tons of soil loss per year in the United States (NRCS 2000A; NRCS 2000B), eroding approximately 75 tons of soil annually (Pimentel et al. 2005). The case becomes especially problematic as current worldwide approximation of soil erosion ranges from 20 to 100 times greater than the average rate of soil renewal (Goudie and Middleton 2006). Changes in land cover, climate, and land use are likely to increase soil erosion and intensify the interaction between aeolian and fluvial erosion, leading to elevated rates of soil movement and degradation (D'Odorico et al. 2013). The effect of interactions in drylands is intensified due to reduction in plant cover, which increases the vulnerability of the soil surface, leading to acceleration of soil loss from wind- and water-borne materials (Easterling et al. 1990; IPCC 2007).

Erosion via water runoff and wind saltation can lead to disruption of micro-habitats, damaging soil microbial crusts and above-ground biomass (Schlesinger et al. 2000), causing loss of essential materials attached to the soil (Li et al. 2007b; Li et al. 2008; Okin, Gillette & Herrick 2006), and leading to reduced soil and water quality (Belnap et al. 2011). In addition, saltation of surface material on a small scale can initiate large-scale dust storms, which are predicted to increase in intensity and frequency by the end of the 21st century due to elevated drought conditions (Sheffield and Wood 2007). The expected increase in the rates of dust storms is also affected by alterations in vegetation cover, such as decreased vegetation cover and increased sediment uplift and transport (Jobbage and Jackson 2000; Li et al. 2007b; Li et al. 2008). A better understanding of small-scale mechanisms will allow us to better understand the large-scale events that cause climatic alterations.

Increasing evidence suggests that aeolian and fluvial interactions provide a major source of understanding of contemporary aspects of landscape formation such as channel formation and development of dunes. Sedimentological evidence shows that aeolian-fluvial interactions are important for reconstructing past climate, as their interactions exist in most climate zones, while contemporary feedbacks are most apparent in drylands (Belnap et al. 2011; IPCC 2013).

1.5 Erosion and vegetation

The frequency and intensity of abiotic factors are the main drivers of many ecological processes in dry regions, including activity of biomass, ANPP, nutrient cycling, and others such as soil texture and distribution. These abiotic and biotic feedbacks largely modulate the effects of climatic changes on drylands functionality and stability (Maestre et al. 2016). On various scales, soil erosive particles have been considered a primary driver of the decline in the production of vegetation, which has been understudied.

Despite difficulties associated with studying soil movement and its impact on soil and vegetated surfaces, soil movement has been very well addressed as a source of stress (Okin 2008). Shrub encroachment of honey mesquite and creosote bush into perennial grassland has been observed widely in Western United States (Van Auken 2000) and is a phenomenon that was the highlight of Long-Term Ecological Research (LTER) studies in the Jornada Basin in the early 1980s (Gibbens et al. 1983). In the Jornada Basin, southern New Mexico, Peters and Gibbons (2006) summarized the drivers that contribute to this shift in the ecosystem, which included droughts, fire suppression, overgrazing, and climate change, all factors that expand bare soil surfaces which in turn increase rates of aeolian transport in regions of low vegetation cover.

Wind erosion can be responsible for adding stress to perennial species in drylands, as wind can carry fine soil materials for long distances and deposit them when it encounters an obstacle or becomes weaker. It is observed that wind-carried materials are usually deposited under canopy creating a mound of loose materials (Gillette et al. 2006). We hypothesize that this encounter between vegetation canopy and soil carried by wind may have a damaging effect on the aboveground vegetation biomass; more investigation into this hypothesis would be well grounded. Sandblasting soil disturbs the health and mortality of vegetation cover. However, the potential contribution of soil erosion has been less frequently investigated in the context of biotic balance and stability. From an economic perspective, Baker (2007) and Baker et al. (2009) have concluded that sandblasting has damaging effects on cotton seedlings, where it has the potential to reduce cotton productions and increase labor cost in countries that depend on cotton production. The effects of soil erosion on vegetation productivity may lead to long-term ecological and environmental consequences. Biotic and abiotic drivers could strongly impact the net primary productivity of vegetation.

1.6 Above ground primary production

ANPP is a sensitive biotic stability measure of the ecosystem. It is affected by a number of complex feedbacks and interactions such as soil fertility, organic matter, microbial activities, and nutrient cycling (Peters et al. 2006; Yahdjian and Sala 2006).

Net primary production (NPP) represents the net carbon that is fixed (sequestered) by a plant community or ecosystem. Collectively, drylands contribute up to 30% of the global net primary production (Parton et al. 1995). NPP is the combined product of climatic, geochemical, ecological, and human effects. NPP makes up to 120 Pg C yr⁻¹ and GPP 58 Pg C yr⁻¹ globally (Hinsinger 2013; Schlesinger 1997). Drylands contribute significantly to global NPP: Savannas 17 Pg C yr⁻¹, grasslands 5.3, Mediterranean shrublands 1.3 Pg C yr⁻¹, and deserts 3.3 Pg C yr⁻¹ (Hinsinger 2013; Parton et al. 1995; Schlesinger 1997).

Despite scientific efforts at providing reliable methods, ANPP measurements and estimations in drylands are challenging due to the nature of dryland surface comprised of unvegetated surfaces and large soil background. Scientists continue to seek new methods for estimating ANPP. Experiments have been conducted on local (Flombaum and Sala 2008), regional (Gaitan et al. 2014a), and global (Maestre et al. 2012a) scales and their findings confirm positive relationships between species richness and key ecosystem measures such as ANPP (Havstad et al. 2006). Grazing, fire, climate, and biotic attributes along natural gradients have compounded effects, and it is often difficult to disentangle their independent effects and the interactions among them. There is a need to better understand how biological feedbacks operate in drylands and how abiotic agents can contribute to their alterations, as their interactions can affect the ecosystem fluctuations and determine the ecosystem's response to climate change in an untimely manner (D'Odorico et al. 2013; Schlesinger et al. 1990).

1.7 Vegetation and soil degradation

The consequences of dryland degradation include loss of vegetation cover, which in turn affects the carbon sequential and loss of soil resilience that affects more than one-fifth of drylands due to cultivation and grazing. Dryland degradation may have long-term consequences on the climate (Okin et al. 2001), i.e., soil degradation and drought together could cause soil movement that leads to soil suspension, thereby altering the radiation budget of the atmosphere. This atmospheric modification and temperature changes alter rates of evapotranspiration and patterns of rainfall frequency and distribution in the drylands. These changes will lead to elevated ecological stress (IPCC 1990).

Abiotic and biotic activities, including anthropogenics elevate the potential of environmental stress on drylands ecosystems. Vegetation and soil health are critical aspects of drylands functionality and stability, the disturbances on soil and vegetation cover could lead to ecosystem failure to sustain a healthy balance in the ecosystem.

1.8 Bibliography

Allred, K W. 1996. "Vegetation changes in New Mexico rangeland." *New Mexico Journal of Science* 36: 168-231.

Alvaraz, L J, H E Esteipan, and G S Okin. 2011. "Spatial patterns of grasses and shrubs in an arid grassland environments." *Ecosphere* 2 (9): 1-30.

Alvarez, Lorelei J, Howard E Epstein, Junran Li, and Gregory S Okin. 2012. "Aeolian process effects on vegetation communities in an arid grassland ecosystem." *Ecological and Evolution* 2 (4): 809-821.

Archer, S. 1989. "Have southern Texas savannas been converted to woodlands in recent history.134:545–61." *American Naturalist* 134 (4): 61.

Archer, S, D S Schimel, and E A Holland. 1995. "Mechanisms of shrubland expansion—land-use, climate or CO₂ ." *Climate Change* 29 (1): 91-99.

Baker, J. 2007. "Cotton seedling abrasion and recovery from wind blown sand." *Agronomy Journal* 99: 556-561.

Baker, J T, M Bobbie, J J Burke, D C Gitz, R J Lascano, and J E Ephrath. 2009. "and abrasion injury and biomass partitioning in cotton seedlings." *Agronomy Journal* 101 (6): 1297-1303.

Baker, Jeffrey T, Bobbie McMichael, John J Burke, Dennis C Gitz, Robert J Lascano, and Jhonathan E Ephrath. 2009. "Sand abrasion injury and biomass partitioning in cotton seedlings." *Agronomy Journal* 101 (6): 1297-1303.

Belnap, J, and O L Lange. 2003. *Biological soil crusts: Structure, function and management*. Verlag Berlin Heidelberg: Springer.

Belnap, J, S Munson, and J Field. 2011. "Aeolian and fluvial processes in dryland regions: the need for integrated studies." *Ecohydrology* 4: 615-622.

Belnap, Jayne. 1995. "Surface disturbances: Their Role in accelerating desertification." *Environmental Monitoring and Assessment* 37 (1-3): 39-57.

Belnap, Jayne, Seth M Munson, and Jason P Field. 2011. "Aeolian and fluvial processes in drylands regions: the need for integrated studies." *Ecohydrology* 4: 615-622.

Breshears, D D, J J Whicker, M P Johansen, and J E Pinder. 2003. "Wind and water erosion and transport in semi-arid shrubland, grassland and forest ecosystems: Quantifying dominance of horizontal wind-drive transport." *Earth Surface Processes and Landforms* 28: 1189-1209.

Breshears, David D, Jeffrey J Whicker, Mathew P Johansen, and John E Pinder. 2003. "Wind and water erosion and transport in semi-arid shrubland, grassland, and forest ecosystems: Quantifying dominance of horizontal wind-driven transport." *Earth Surface Processes and Landforms* 28: 1189-1209.

Bridges, E M, and L R Oldeman. 2010. "Global Assessment of Human-induced Soil Degradation (GLASOD)." *Arid Soil Research and Rehabilitation* 13 (4): 319-325.

Buffington, L C, and C H Herbel. 1965. "Vegetation changes on a semidesert grassland range from 1858 to 1963." *Ecological Monographs* 35: 140-164.

Buffington, Lee C, and Carlton H Herbel. 1965. "Vegetational Changes on a Semidesert Grassland Range from 1858 to 1963." *Ecological Monographs: Ecological Society of America* 35 (2): 139-164.

Bull, L J, and M J Kirkby. 2002. *Dryland rivers: Hydrology and geomorphology of semi-arid channels*. Chichester, England: John Wiley & Sons.

Bullard, Joanna E, and Grant H McTinish. 2003. "Aeolian-fluvial interactions in dryland environments: Example, concepts and Australia case Study." *Progress in Physical Geography* 27 (4): 471-501.

Capolupo, Alessandra, Stefania Pindozi, Collins Okello, Nunzio Fiorentino, and Lorenzo Boccia. 2015. "Photogrammetry for environmental monitoring: The use of drones and hydrological models for detection of soil contaminated by copper." *Science Of The Total Environment* 514: 298-306.

Castillo, C, R Perez, M R James, J N Quinton, E V Taguas, and J A Gomez. 2012. "Comparing the accuracy of several field methods for measuring Gully Erosion." *Science Society of America Journal* 76 (4): 1319-1332.

Chapin, F S, E S Zavaleta, V T Eviner, and R L Naylor. 2000. "Consequences of changing biodiversity." *Nature* 405 (6).

Cunliff, A M, R E Brazier, and K Anderson. 2016. "Ultra-fine grain landscape-scale quantification of dryland vegetation structure with drone-acquired structure-from-motion photogrammetry." *Remote Sensing of Environment* 183: 129-143.

Davies, J, L Poulsen, B Schulte-Herbruggen, K Mackinnon, N Crawhall, W D Henwood, N Dudley, J Smith, and M Gudka. 2012. *Conserving dryland biodiversity*. Nairobi : IUCN Drylands Initiative ; Cambridge, UK : UNEP-WCMC ; Bonn : UNCCD: IUCN.

D'Odorico, P, A Bhattachan, K F Davis, SD Ravi, and C W Runyan. 2013. "Global desertification: Drivers and feedbacks." *Advances in Water Resources* 51: 326-344.

D'Odorico, P, and A Porporato. 2006. "Ecohydrology of arid and semiarid ecosystems: An introduction." *Dryland Ecohydrology* 1-10.

D'Odorico, P, G Okin, and B Bestelmeyer. 2012. "synthetic review of feedbacks and drivers of shrub encroachment in arid grasslands." *Ecohydrology* 5 (5): 520-530.

D'Odorico, Paolo, Gregory S Okin, and Brandon T Besterlmeyer. 2012. "A synthetic review of feedbacks and drivers of shrub encroachment in arid grasslands." *Ecohydrology* 5 (5): 520-530.

Dodson, Carolyn. 2012. *A guide to plants of the northern Chihuahuan Desert*. Las Cruces: The University of New Mexico Press.

d'Oleire-Oltmanns, Sebastian, Irene Marzloff, Klaus Daniel Peter, and Johannes Ries. 2012. "Unmanned aerial vehicle (UAV) for monitoring soil erosion in Morocco." *Remote Sensing* 4 (11): 3390-3416.

Easterling, D, G Meehl, C Parmesan, and S Changnon. 1990. "Climate extremes: observations, modeling, and impacte." *Science* 289: 2068-2074.

Elnor, A, P Baumgart, H G Maas, and D Faust. 2014. "Multi-temporal UAV data for automatic measurments of rill and interill erosion on loess soil." *Earth Surface Processes and Landform* 40 (6): 741-755.

FAO. 2019. Food and Agriculture Organization of the United Nations. www.fao.org/.

Field, Christopher B, Michael J Behrenfeld, James T Randerson, and Paul Falkowski. 1998. "Primary production of the biosphere: Integrating terrestrial and cceanic components." *Science* 281 (5374). doi:DOI: 10.1126/science.281.5374.237.

Field, Jason P, David D Breshears, and Jeffrey J Whicker. 2009. "Toward a more holistic perspective of soil erosion: Why aeolian research needs to explicitly consider fluvial processes and interactions." *Aeolian Research* 1 (1-2): 9-17.

Flombaum, P, and O E Sala. 2008. "Higher effect of plant species diversity on productivity in natural than artificial ecosystems." *Proceeding the National Academy of Sciences of the United State of America* 105 (16): 6087-6090.

Fonstad, Mark A, James T Dietrich, Brittany C Courville, L Jennifer Jensen, and Patrice E Carbonneau. 2013. "Topographic structure from motion: A new development in photogrammetric measurement." *Earth Surface Processes and Landforms* 38 (4): 421-430.

Gaitan, J J, G E Oliva, D E Bran, F T Maestre, M R Aguiar, and et al. 2014a. "Vegetation structure is as important as climate to explain ecosystem functioning across Patagonian rangelands." *Journal of Ecology* 102: 1419-1428.

Gibbens, R P, and R F Beck. 1987. "Increase in Number of Dominant Plants and Dominance-Classes on a Grassland in the Northern Chihuahuan Desert." *Journal of Range Management* (40): 136-139.

Gibbens, R P, J Tromble, J T Hennessy, and M Gardenas. 1983. "Soil movement in mesquite dunelands and former grasslands of southern New Mexico from 1933 to 1980." *Journal of Range management* 36: 145-148.

Gibbens, R P, R P McNeely, K M Havstad, R F Beck, and B Nolen. 2005. "Vegetation changes in the Jornada Basin from 1858 to 1998." *Journal of Arid Environments* 61 (4): 651-668.

Gibbens, R P, R P McNeely, K M Havstad, R F Beck, and B Nolen. 2005. "Vegetation changes in the Jornada Basin from 1858-1998." *Journal of Arid Environments* 61: 651-668.

Gibbens, T J, J T Hennessy, and M Gardenas. 1983. "Soil movement in mesquite dunelands and former grasslands of southern New Mexico from 1933 to 1980." *Journal of Range Management* (36): 145-148.

Gillan, J K, J W Karl, A Elaksher, and M Duniway. 2017. "Fine-resolution repeat topographic surveying of dryland landscapes using UAS-based structure-from-motion photogrammetry: Assessing accuracy and precision against traditional ground-based erosion measurements." *Remote Sensing* 69: 95-107.

Gillan, J K, J W Karl, Nichole N Barger, Ahmed Elaksher, and Michael C Duniway. 2016. "Spatially explicit rangeland erosion monitoring using high-resolution digital aerial imagery." *Rangeland Ecology and Management* 69 (2): 95-107.

Gillette, D A, and A M Pitchford. 2004. "Sand flux in the northern Chihuahuan desert, New Mexico, USA, and the influence of mesquite-dominated landscapes." *Journal of Geophysical Research-Earth Surface* 109 (F4): F04003.

Gillette, D A, J E Herrick, and G A Herbert. 2006. "Wind characteristics of mesquite streets in the northern Chihuahuan Desert, New Mexico, USA." *Environment fluid Mechanisms* 6: 241-275.

Gillette, Dale A, and Ann M Pitchford. 2004. "Sand flux in the northern Chihuahuan desert, New Mexico, USA, and the influence of mesquite-dominated landscapes." *Journal od Geophysical Research* 109 (F04003).

- Glendell, M, G McShane, L Farrow, M R James, J Quinton, K Anderson, M Evans, et al. 2017. "Testing the utility of structure from motion photogrammetry reconstructions using small unmanned aerial vehicles and ground photography to estimate the extent of upland soil erosion." *Earth Surface Processes and Landforms* 42 (12): 1860-1871.
- Goncalves, J A, and R Henriques. 2015. "UAV photogrammetry for topographic monitoring of coastal areas." *ISPRS J. Photogrammetry and Remote Sensing* 104: 101-111.
- Goudie, A, and N Middleton. 2006. *Desert dust in the global system*. Vol. 2nd. Springer.
- Havstad, K M, L F Huenneke, and W H Schlesinger. 2006. *Structure and Function of a Chihuahuan Desert Ecosystem: The Jornada Basin Long-Term Ecological Research Site*. Oxford University Press.
- Hinsinger, P. 2013. *Plant-induced changes in soil processes and properties*. Blackwell Publishing Ltd.
- Huenneke, L F, J P Anderson, M Remmenga, and W H Schlesinger. 2002. "Desertification alters patterns of aboveground net primary production in Chihuahuan ecosystems." *Global Change Biology* 8 (3): 247–264.
- IPCC. 1996. *Climate Change 2013: The Physical Science Basis. Contribution of Working Group I to the Fifth Assessment Report of the Intergovernmental Panel on Climate Change*. . Cambridge and New York: Cambridge University Press.
- IPCC. 2013. *Climate Change. The physical science basis. Contribution of working group I to the fifth assessment report of the intergovernmental panel on climate change*. Cambridge, United Kingdom: Cambridge University Press.
- James, M R, and S Robson. 2012. "Straightforward reconstruction of 3D surfaces and topography with a camera: Accuracy and geoscience application." *Journal of Geophysical Research* 117 (F3).
- James, Mike R, and Stuart Robson. 2014. "Mitigating systematic error in topographic models derived from UAV and ground -based image network." *Earth Surface Processes and Landforms* 39 (10): 1413-1420.
- Jobbage, E G, and R B Jackson. 2000. "The vertical distribution of soil organic carbon and its relation to climate and vegetation." *ecological applications* 10: 423-436.
- Knapp, A K, C Beier, D D Briske, A T Classen, Y Luo, M Reichstein, M D Smith, et al. 2008. "Consequences of more extreme precipitation regimes for terrestrial ecosystems." *BioScience* 58: 811-821.

Knapp, Alan K, John M Briggs, Scott L Collins, Steven R Archer, M Syndonia Bret-Harte, Brent E Ewers, Debra P Peters, et al. 2008. "Shrub encroachment in North American grasslands: shifts in growth form dominance rapidly alters control of ecosystem carbon inputs." *Global Change Biology* 14 (3): 615-623.

Kok, J F, E J Parteli, T I Michaels, and D B Karam. 2012. "The physics of wind-blown sand and dust- Review." *Report on Progress in Physics* 10 (75). doi:doi: 10.1088/0034-4885/75/10/106901.

Lal, R. 2001. "Potential of desertification control to sequester carbon and mitigate the greenhouse effect." *Climate Change* 51: 35-72.

Lal, Rattan, Terry M Sobecki, John M Kimble, and Thomas Livari. 2003. *Soil degradation in the United States: Extent, Severity, and Trends*. Boca Raton: Lewis Publishers.

Le Houérou, H N. 1996. "Climate change, drought and desertification." *Journal of Arid Environments* 34 (2): 133-185.

Li, J, G S Okin, L Alvarez, and H Epstein. 2008. "Effects of wind erosion on the spatial heterogeneity of soil nutrient in two desert grassland communities." *Biogeochemistry* 73-88.

Li, J, G S Okin, L Alvarez, and H Esteipan. 2007. "Quantitative effects of vegetation cover on wind erosion and soil nutrient loss in a desert grassland of southern New Mexico, USA." *Biogeochemistry* 85: 317-332.

Li, J, G S Okin, L J Hartman, and H E Epstein. 2007b. "Quantitative assessment of wind erosion and soil nutrient loss in desert grasslands of southern New Mexico, USA." *Biogeochemistry* 85: 317-332.

Li, Junran, Gregory S Okin, and Howard E Esteipan. 2009. "Effects of enhanced wind erosion on surface soil texture and characteristics of windblown sediments." *JGR Biogeosciences* 114 (G2). <https://doi.org/10.1029/2008JG000903>.

Li, Junran, Gregory S Okin, Lorelei Alvarez, and Howard Esteipan. 2007. "Quantitative effects of vegetation cover on wind erosion and soil nutrient loss in a desert grassland of southern New Mexico, USA." *Biogeochemistry* 85 (3): 317-332.

Maestre, F T, D J Eldridge, S Soliveres, S Kefi, M Delgado-Baquerizo, M A Bowker, P Garcia-Palacios, et al. 2016. "Structure and functioning of drylands ecosystems in a changing world." *Annual Review of Ecological Evolution and Systematics* 47: 215-237.

Maestre, F T, J L Quero, N J Gotelli, A Escudero, V Ochoa, and et al. 2012a. "Plant species richness and ecosystem multifunctionality in global drylands." *Science* 335: 214-218.

MEA. 2005. Millennium Ecosystem Assessment: Desertification Synthesis. Washington DC: World Resource Institute.

MEA. 2005. Millennium ecosystem assessment: ecosystems and human well-being: desertification synthesis . Washington, DC: World Resources Institute.

Middleton, Nicholas J, Nick Middleton, United Nations Environment Programme, and David S Thomas. 1997. World Atlas of Desertification. Arnold.

2017. National Instruments. <http://www.ni.com/en-us.html>.

Nicholson, S E. 2001. "Climatic and environmental change in Africa during the last two centuries." *Climate Research* 17: 123-144.

Nicholson, S E, and J Kim. 1997. "The relationship of the El Nino-Southern Oscillation to African Rainfall." *International Journal of Climatology* 17: 123-135.

Nickling, W G, and C M Neuman. 1997. "Wind tunnel evaluation of a wedge-shaped aeolian sediment trap." *Geomorphology* 18 (3-4): 333-345.

Niethammer, U, M R James, S Rothmund, J Travelletti, and M Joswing. 2012. "UAV-based remote sensing of the Super-Sauze landslide: Evaluation and results." *Engineering Geology* 129: 2-11.

Okin, G S. 2008. "A new model of wind erosion in the presence of vegetation." *Journal of Geophysics Research* 113 (F2).

Okin, G S, A J Parsons, J Wainwright, J E Herrick, B T Bestelmeyer, D P.C Peters, and E L Fredrickson. 2009. "Do changes in connectivity explain desertification." *Biosciences* 59: 237-244.
Okin, G S, and D A Gillette. 2001. "Distribution of vegetation in wind-dominated landscapes: implications for wind erosion modeling and landscape processes." *Geophysics Research* 106: 9673-9683.

Okin, G S, B Murray, and W H Schlesinger. 2001. "Degradation of sandy arid shrubland environments: Observations, process modeling, and management implications." *Journal of Arid Environments* 47 (2): 123-144.

—. 2001a. "Desertification in an arid shrubland in the southwestern United States: process modeling and validation." *Land degradation: papers selected from contributions to the Sixth Meeting of the International Geographical Union's Commission on Land Degradation and Desertification*. Dordrecht, The Netherlands: Kluwer Academic Publisher. 53-70.

Okin, G S, D A Gillette, and J E Herrick. 2006. "Multi-scale controls on and consequences of aeolian processes in landscape change in arid and semi-arid environment." *Journal of Arid Environments* 65 (2): 253-275.

Okin, G S, D A Gillette, and J E Herrick. 2006. "Multi-scale controls on and consequences of aeolian processes in landscape changes in arid and semi-arid environments." *Journal of Arid environments* 65: 253-275.

Okin, G S, P D'Odorico, and S Archers. 2009. "Impact of feedbacks on Chihuahuan desert grasslands: transience and metastability." *Journal of Geographical Research-Biogeosciences* 114 (G1). doi:<https://doi.org/10.1029/2008JG000833>.

Okin, S G, D A Gillette, and J E Herrick. 2006. "Multi-scale controls on and consequences of aeolian processes in landscape change in arid and semi-arid environments." *Journal of Arid Environments* 65 (2): 253-275.

Osman, Khan Towhid. 2014. *Soil degradation, Conservation and Remediation*. Dordrecht, Netherlands: Springer.

Parton, W J, J M Scurlock, D S Ojima, D S Schimel, D O Hall, and M Scopegram Group. 1995. "Impact of climate change on grassland production and soil carbon worldwide." *Global Change Biology* 1: 13-22.

Peters, A J, and M D Eve. 1995. "Satellite monitoring of desert plant community response to moisture availability." *Environmental Monitoring and Assessment* 37 (1-3): 273-287.

Peters, D P, J E Bestelmeyer, E L Herrick, C M Fredrickson, and K M Havstad. 2006. "Disentangling complex landscapes: new insights into arid and semiarid system dynamics." *Bioscience* 56 (7): 491-501.

Peters, D PC, and R Gibbons. 2006. "Plant communities in the Jornada Basin: the dynamic landscape." In *Structure and function of a Chihuahuan Desert ecosystem: the Jornada Basin long-term ecological research site*, by W H Havstad, 211-231. Oxford, UK: Oxford University Press.

Peters, Debra P.C, Isabella Mariotto, Kris Havstad, and Leigh W Murray. 2006. "Spatial Variation in Remnant Grasses after a Grassland-to-Shrubland State Change: Implications for Restoration." *Rangeland Ecology and Management* 59 (4): 343-350.

Peters, DP C, B T Bestelmeyer, J E Herrick, E L Fredrickson, C Monger, and K M Havstad. 2006. "Disentangling complex landscapes: new insights into arid and semiarid system dynamics." *Bioscience* 56 (6): 491-501.

Pimentel, D, C Harvey, P Resosudarmo, K Sinclair, D Kurz, M McNair, S Crist, et al. 1995. "Environmental and Economic cost of soil erosion and conservation benefits." *Science* 267: 1117-1123.

Pimentel, D. 1993. *World Soil Erosion and conservation*. Cambridge, UK: Cambridge University Press.

Pimentel, David. 2006. "Soil erosion: A food and environmental threat." *Environment, Development and sustainability* 8 (1): 119-137.

Pimentel, David, C Harvery, P Resosudarmo, K Sinclair, D Kurz, M McNair, S Crist, et al. 1995. "Environmental and economic costs of soil Erosion and conservation benefits." *Science* 267 (5201): 1117-1123.

Racha, M D, G S Okin, C Alexander, J E Herrick, and D P Peters. 2015. "Modifying landscape connectivity by reducing wind driven sediment redistribution, Northern Chihuahuan Desert, USA." *Aeolian Research* 17: 129-137.

Ramawat, Gopal. 2010. *Desert Plants: Biology and Biotechnology*. Berlin Heidelberg: Springer.

Ravi, S, P D'Odorico, D Breshears, J Field, A Goudie, T Huxman, J Li, et al. 2011. "Aeolian Processes and the Biosphere." *Reviews of Geophysics* 49 (3). doi:<https://doi.org/10.1029/2010RG000328>.

Ravi, Sujith, David Breshears, Travis E Huxman, and D'Odorico Paolo. 2010. "Land Degradation in drylands: Interactions among hydrologic-aeolian erosion and vegetation dynamics." *Geomorphology* 116 (3-4): 236-245.

Reed, Mark S, and Lindsey C Striger. 2015. "Climate change and desertification: Anticipating, assessing & adapting to future change in drylands." 3rd UNCCD Scientific Conference, Cancun, Mexico.

Reynold, F James, D Mark Stafford Smith, Eric F Lambin, B L Turner II, Michael Mortimore, Simon P J Butterbury, Thomas E Dowing, et al. 2007. "Global desertification: Building a Science for Dryland Development." *Science* 316 (5826): 847-851.

Reynold, J F, and D M Stafford. 2003. "Global Desertification: Do humans cause deserts?" *Geographical Review* 93 (3): 413-415.

Reynold, James F, Mark Stafford Smith, Eric F Lambin, B L Turner II, Michael Mortimore, Simon P Butterbury, and Thomas E Dowing. 2007. "Global desertification: Building a Science for Dryland Development." *Science* 5826 (316): 847-851.

- Schlesinger, W H. 1997. *Biogeochemistry: An analysis of global change*. Academic Press.
- Schlesinger, W H, J F Reynold, G L Cunningham, LF Huenneke, W M Jarrell, R A Virginia, and W G Whitford. 1990. "Biological feedbacks in global desertification." *Science* 247: 1043-1048.
- Schlesinger, W H, T J Ward, and J Anderson. 2000. "Nutrient losses in runoff from grassland and shrubland habitat in southern New Mexico: II. Field plots." *Biogeochemistry* 49: 69-86.
- Sheffield, J, and E F Wood. 2007. "Projected changes in drought occurrence under future global warming from multi-model, multi-scenario, IPCC AR4 simulations." *Climate Dynamics* 31: 79-105.
- Sivakumar, M VK. 2007. "Interactions between climate and desertification." *Agricultural and Forest Meteorology* 142: 143-155.
- Stubbendick, James, Cheryl D Schmidt, Heidi L Hillhouse, and L M Landholt. 2010. "Influences of wind and sandblasting on the endangered blowout penstemon." *endangered Species Research* 9: 99-104. doi:doi: 10.3354/esr00246.
- Toy, T J, G R Foster, and K G Renard. 2002. *Soil Erosion: Processes, prediction, measurement and control*. New York: John Wiley & Sons.
- USDA. 2017. *Natural Resource Conservation Service: Plant Material Program*. <https://www.nrcs.usda.gov/wps/portal/nrcs/main/plantmaterials/pmc/>.
2013. *Valuing the Biodiversity of Dry and Sub-Humid Lands*. Secretariat of the, Montreal, Quebec, Canada H2Y 1N9: Secretariat of the Convention on Biological Diversity.
- Van Auken, O W. 2000. "Shrub invasion of North America semiarid grassland." *Annual Review of Ecology Evolution, and systematics* 31: 197-215.
- Visser, S M, G Sterk, and O Ribolzi. 2004. "Techniques for simultaneous quantification of wind and water erosion in semi-arid regions." *Journal of Arid Environment* 59: 699-717.
- Westoby, M J, J Brasington, N F Glasser, M J Hambrey, and J M Reynolds. 2012. "'Structure-from-motion' photogrammetry: A low-cost effective tool for geoscience application." *Geomorphology* 179: 300-314.
- Whicker, Ward, and Vincent Schutlz. 1982. *Radioecology: Nuclear energy an the environment*. Boca Ralton, Florida: CRC Press.
- Yahdjian, L, and O E Sala. 2006. "Vegetation structure constrains primary production response to water availability in the Patagonian steppe." *Ecology* 952-962.

Chapter 2. The contribution of aeolian processes to vegetation state change: Damaging effects of sandblasting on native shrub and grass species in the Jornada Basin, NM.

2.1 Abstract

The effects of windblown soil particles remain unquantified despite scientific efforts at addressing the role of aeolian processes in vegetation state change. The goal of our study was to examine and quantify the above-ground biomass damages caused by sandblasting in the absence of other disturbances. A total of 216 plants of native grass (*Aristida purpurea*, *Bouteloua eriopoda*, and *Sporobolus airoides*) and shrub (*Artiplex canescens*, *Larrea tridentata* and *Prosopis glandulosa*) species in the Jornada Basin NM, USA were used to examine the effects of sand blown by wind at six different treatments. We used a ten-meter-long wind tunnel to expose the plants to two wind frequency for the control treatments (low frequency: every other week, and high frequency: every week), with two sand flux (high flux: $120 \text{ g cm}^{-1} \text{ minute}^{-1}$, and low flux: $60 \text{ g cm}^{-1} \text{ minute}^{-1}$) for the sand flux treatments for six weeks. Morphological features of the plants were measured two days before the experiment to record the plants' morphological characteristics in their healthy state; then they were undestructively examined at the time of the sandblasting experiment during the 3rd and 7th weeks after exposure. For assessing the above-ground biomass damage we recorded the amount of leaf loss, leaflet loss, stem loss, leaf area reduction and observations of production using traditional sampling methods. The results displayed leaf loss up to 95% for *Bouteloua eriopoda*, 79% for *Sporobolus airoides*, and 81% for *Aristida purpurea*. *B. eriopoda* was the only grass species that experienced a considerable amount of stem loss. In the shrub category, *Prosopis glandulosa* recorded the largest amount of leaf loss (up to 94%) and leaflet loss (up to 95%); *Larrea tridentata* recorded up to 79% leaf loss; *Artiplex canescens* did not experience any major leaf loss (up to 10%). With increasing sand flux (high), the percentage

of leaf and leaflet loss increased. Leaflet loss for *Prosopis glandulosa* was also positively associated with sand flux and wind treatments, explaining about 81% of the relationship. The plants experienced reduction in leaf area (%) in response to increasing sand flux with the high frequency sand flux treatments. Our results support the hypothesis that aeolian processes are responsible to some degree for above-ground biomass damage, depending on the severity and the intensity of the aeolian events.

2.2 Introduction

Drylands cover more than 40% of the earth's land surface and are home to more than two billion people (MEA 2005; Reynold et al. 2007). Over the past 150 years, drylands in the United States and elsewhere have experienced drastic changes in vegetation cover observed in the form of shrub encroachment (Archer 1989; Bestelmeyer, et al. 2004; Bestelmeyer et al. 2015; Buffington & Herbel 1965; Gibbens et al. 2005; Okin et al. 2009; Peters & Herrick 2001; Peters et al. 2006; Turnbull, et al. 2002). This change in vegetation cover, from grasslands to shrublands, has been attributed to a number of environmental feedbacks including droughts, grazing, warming, and high levels of atmospheric CO₂ (Archer et al. 1995; D'Odorico et al. 2012; Gibbens et al. 1983; Gibbens & Beck 1987; Gibbens et al. 2005; Knapp et al. 2008; Okin et al. 2009; Peters et al. 2006). The shifts not only impact populations living in drylands and the possible land use therein, but might also have large-scale environmental and climatic implications. For instance, Knapp et al. (2008) found that the shift from grassland to shrubland alters the amounts and controls of carbon inputs into the ecosystem independent of those alterations in climatic drivers or resource levels. Grasslands account for 30 - 35% of global terrestrial net primary productivity (Field et al. 1998); thus, any changes in the patterns or controls of carbon inputs in grasslands will have global implications. Likewise, increases in shrub cover at the expense of grass cover has the potential to

increase atmospheric input of dust (e.g., Bergametti and Gillette 2010; Breshears et al. 2012; Gillette and Pitchford 2004) which could impact dust loading in the atmosphere with its attendant climatic and health consequences (Wiggs et al. 2003).

Despite the many proposed triggers for grass-to-shrub change, in most theoretical conceptualizations of the process, grazing and drought are implicated in processes that promote and enforce shrub encroachment (Van Auken 2000; Okin et al. 2009; Okin et al. 2015; Okin et al. 2018). The feedback between grazing and vegetation cover is very well-understood (e.g., D'Odorico et al. 2012). Grazing and drought tend to reduce fuel mass and thus reduce the ability of fires to limit shrub dominance (Peters et al. 2006). Droughts and extensive grazing cause reduction in vegetation cover and increase bare soil cover, thus increasing the rates of water erosion (Bullard and Livingstone 2002; Muhs and Holiday 1995) and aeolian transport (Okin et al. 2001; Gillette & Pitchford 2004; Li et al. 2007). Transport of soil resources by wind and water enforces islands of fertility (Schlesinger et al. 1990; Wainwright et al. 1999; Wainwright et al. 2002; Li et al. 2009).

The impact of plants on aeolian transport has been well-documented in literature, emphasizing the structural characteristics of plant communities such as their lateral cover and distribution, or the gap size between plants (Bhattachan et al. 2014; Gibbens et al. 2001; Li et al. 2007; Okin & Gillette 2001; Okin et al. 2006; Ravi et al. 2010; Ravi et al. 2011). Other things being equal, aeolian transport increases with increasing gap size (bare soil areas), meaning that, as vegetation is lost and the physical structure of the plant communities changes, aeolian transport increases (Gibbens et al. 2001; Li et al. 2007). However, beyond just movement of soil resources, aeolian processes have been implicated in direct impacts on vegetation that may promote shrub encroachment (e.g., Okin et al. 2006). In particular, it has been suggested that the low growing

points, relatively thin leaves, and shallow roots make grasses more susceptible to aeolian damage than shrubs.

In this study, we focus on above-ground biomass response to aeolian transport as a major ecosystem disturbance that could cause changes in the vegetation cover. Specifically, we investigate the impact of sandblasting on plant architecture. Sandblasting is a product of saltation which is the movement of aeolian material roughly in the range 70-200 μm (Kok et al. 2012). The effect of saltation on above-ground plant health and productivity has not been investigated in relation to shrub encroachment. In fact, there are few measurements of the effect of sandblasting on native vegetation, which is different from studies on agricultural plants (Baker et al. 2009).

Our overall goal is to test one component of the hypothesis that positive feedbacks associated with aeolian processes drive shrub encroachment in arid grasslands with wind-erodible soils. A positive feedback in this case requires aeolian processes to decrease vegetation cover, in a way that increases aeolian transport. We hypothesize that the different impacts of aeolian transport on grasses and shrubs, with grasses being more susceptible and shrubs being less susceptible, contributes to this feedback. Thus, we study the effect of sandblasting on plant architecture after periods of exposure to saltation in a linear wind tunnel. The elevated stress caused by aeolian processes may differ between shrub and grass communities, as some species may be more resilient than others and can adapt and reproduce despite high levels of imposed stress. We expect shrubs to be more tolerant to sandblasting than grasses; this finding will contribute to understanding feedbacks controlling shrub encroachment.

2.3 Methods

2.3.1 Study area

Our study took place in the Jornada Experimental Range (JER), outside of Las Cruces, New Mexico (32.6°N, -106.7°E), which has an elevation of around 1,300 meters. The JER is representative of hot desert ecosystems worldwide with a well-documented history of ecosystem disturbances and shrub encroachment. Three different shrub species – *Prosopis glandules* (PRGL), *Larrea tridentata* (LATR), *Atriplex canescens* (ATCA) – and grass species – *Bouteloua eriopoda* (BOER), *Sporobolus airoides* (SPAI), and *Aristida purpurea* (ARPU) – were selected for the aeolian sandblasting experiment (Table 1). These species are common in the JER and are representative of many other dryland vegetation types in the Western United States and around the world (Dodson 2012; Ramawat 2010). Each species was given a four-letter identifier consisting of the first two letters of the genus and species names.

Table 2. Native Chihuahuan desert shrub and grass species and their characteristics. The shrub species have high root mass compared to the grass species.

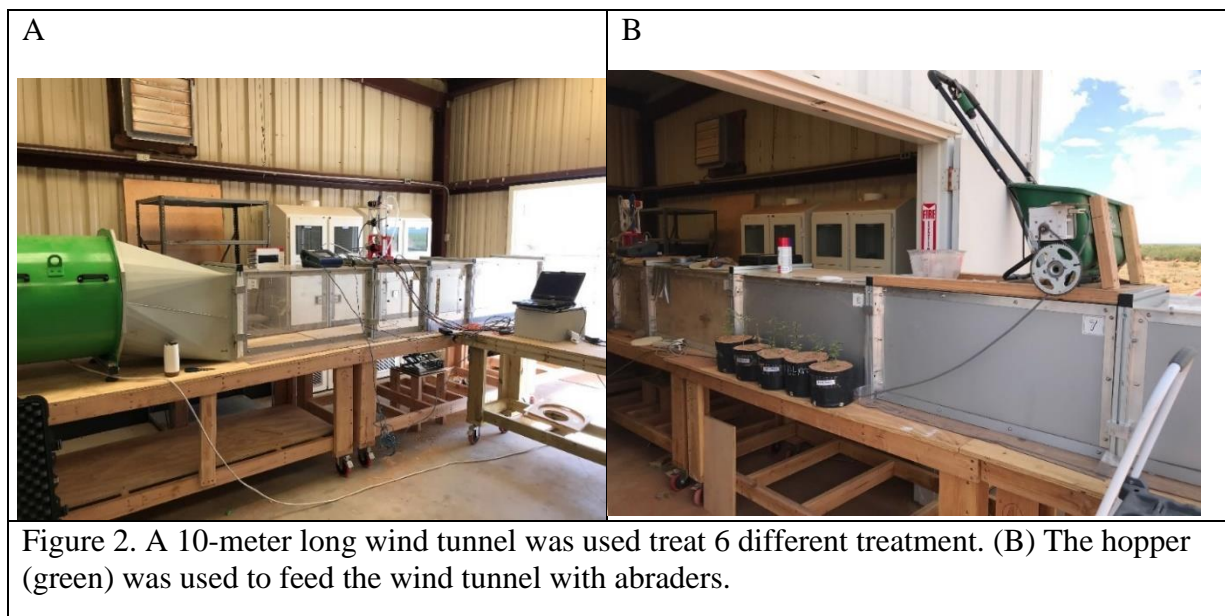
Type	Species					
	Shrub			Grass		
Sci-name	<i>Prosopis glandulosa</i>	<i>Larrea tridentata</i>	<i>Atriplex canescens</i>	<i>Aristida purpurea</i>	<i>Bouteloua eriopoda</i>	<i>Sporobolus airoides</i>
Common name	Honey mesquite	Creosote bush	Fourwing saltbush	Purple threeawn	Black grama	Alkali sacaton
Tag name	PRGL	LATR	ATCA	ARPU	BOER	SPAI

2.3.2 Plant material

Seeds for the selected shrub and grass species were obtained from local native plant nurseries (Plants of the Southwest 2017) and the NRCS Plant Material Center (USDA 2017). The seeds were planted in a greenhouse at The University of Arizona and maintained for three months until they reached a suitable height (average: shrub = 18 cm, grasses = 14 cm) for the sandblasting

experiment. The plants were then relocated to a common garden in the JER and were maintained for four weeks before they were sandblasted. The four-week transition between the greenhouse and the common garden allowed the plants to adapt to the new natural environment. A total of 216 plants were protected in a fenced area and were provided with a controlled amount of water for six weeks throughout the experiment period. The plants were given 0.5 liters (grasses, 3.9-liter pot), and 1 liter (shrubs, 7.6-liter pot) of water daily.

2.3.3 Wind tunnel treatments



We used a suction mode wind tunnel (10 m x 0.5 m x 0.5 m) to simulate sand storms and to expose the plants to different levels of sand flux and wind treatments over the course of six weeks. The wind tunnel design was modified from Aeolian Simulation Lab wind tunnel at the Ben Gurion University of the Negev (Katra et al. 2016). The tunnel was placed on a leveled table (11 m x 0.75 m x 0.75 m) allowing the pots to be below the table surface level and the plants at table surface level (Figure 2). The working section included an opening in the bottom to accommodate the plants.

Since the surface of the wooden table where the wind tunnel is placed was flat and smooth, the airflow was tripped by two arrays of wooden dowels at the entrance of the tunnel. The first array consisted of 3.5-cm diameter wooden dowels, cut to 10-cm height, and placed in an offset grid pattern with a density of 30 dowels occupy 1 cm² that spanned the width of the tunnel and was approximately 50-cm in length. The second array was placed just downwind of the first, and consisted of 3.5-cm diameter wooden dowels, cut to 7-cm height, and placed in an offset grid pattern with a density of 35 dowels occupy 1 cm² that spanned the width of the tunnel and was approximately 50-cm in length.

Abraders, consisting of sandy loam soils from the JER sieved using a 1 mm mesh, were added to the airflow across the full width of the tunnel to simulate sandblasting by aeolian sediment. Abraders were placed in a hopper located approximately 3 m upwind of the plants. The sediments were manually introduced into the wind tunnel for each run, the flow of sediments was monitored to ensure continuous dispersal of abraders.

Our experiment included six total treatments, including controls. The treatment combinations allowed separation of sandblasting from wind-only effects. All treatments and controls lasted 5 minutes, with a wind speed in the center of the tunnel, measured with a pitot tube, of ~11 m s⁻¹. With the tripping roughness, this translated to shear velocities of ~ 0.50 m s⁻¹ at the plants ($z_0 = 5.25 \times 10^{-6}$ m). Each treatment included 6 replicates. Control treatments did not include abraders and were conducted with two wind frequencies: 1) low frequency, every other week (LFC), 2) high frequency wind, every week (HFC). The treatments with sand included two levels of sand flux conducted at the same frequency: 1) low flux, low frequency (LflLfr); 2) low flux, high frequency (LflHfr); 3) high flux, low frequency (HflLfr); and 4) high flux, high frequency (HflHfr). The target horizontal flux for low flux treatments was 60 g cm⁻¹ min⁻¹ and the target

horizontal flux for the high flux treatments was $120 \text{ g cm}^{-1} \text{ min}^{-1}$. The low flux was chosen to imitate natural fluxes measured in mesquite dune areas the JER where approximately $10 \text{ g cm}^{-1} \text{ d}^{-1}$ has been measured on average over an entire year by Gillette and Pitchford (2004), assuming that that flux occurred during 10 stormy days and had transport for 10 minutes in each of those days:

$$\left(10 \frac{\text{g}}{\text{cm d}}\right) \frac{365 \text{ d}}{\text{yr}} \frac{1 \text{ yr}}{10 \text{ storm days}} \approx 30 \frac{\text{g}}{\text{cm min}} \text{ for 10 min} \quad (1)$$

High flux was set to twice the low flux. In practice, we found that it was more reliable to run our experiments for 5 minutes instead of 10 minutes, and therefore, to keep the total flux the same over the treatment, the low flux treatment was ultimately $60 \text{ g cm}^{-1} \text{ min}^{-1}$ for 5 min and the high flux treatment was $120 \text{ g cm}^{-1} \text{ min}^{-1}$ for 5 min. We assumed that doubling the flux while halving the time would, in addition to keeping the total flux per treatment the same as the above calculation, also keep the total damage to the plants the same. Bridges et al. (2005) found, for instance, that the total amount of aeolian abrasion to rocks scaled linearly with the total kinetic energy of the abrading particles. Because kinetic energy scales linearly with mass (as opposed to velocity, which we kept the same for all treatments and controls), we concluded that halving the time while doubling the mass flux would not change the total kinetic energy of the abraders.

To quantify the actual flux experienced by the plant, a 25-cm high wedge-shaped aeolian sediment trap based on the design of Nickling & Neuman (1997) was placed on the table behind the plants. The sediment samples were collected and weighed for each run, the total abrader mass (TAM; g cm^{-1}) was calculated using:

$$TAM = \frac{\text{total_Sediment}}{\text{width}} \quad (2)$$

where the *total_Sediment* is the total mass of the sediments (g) collected in the sediment trap during the run and *width* is the width of the trap opening (1 cm). The sediment samples were weighed for each replicate after every run.

Because we had six species, each day of the week was assigned to one species; treatments were repeated in the wind tunnel on a weekly basis, totaling six sandblasting events for each species over six weeks from July 1st, 2018 to October 1st, 2018.

2.3.4 In situ measurements

A total of 30 individuals for the same species chosen for wind tunnel treatments were selected for comparison from sites known for high erosion rates at the Jornada Basin: the Nutrient Effects of Aeolian Transport (NEAT: closest to the center of control (0 % grass cover removal) and upwind (50 % grass cover removal) and downwind perpendicular to the upwind location in block 3) experiment (Okin et al. 2001a), the “Scraped Site” (samples were selected closest to the center of downwind for treatment and upwind for control; Okin et al. 2001a; Alvarez et al. 2012), mesquite dune sites northwest of the JER headquarters, the controls located in this area were protected in a fenced site established in 2008 while the treatment samples were selected in the field of mesquite dunes. These sites were selected based on their history of aeolian transport, dominant species, and soil. The NEAT experiment and Scraped Site were established to study aeolian transport, with the NEAT experiment specifically designed to study the competition between grass and shrub species under conditions of increased aeolian transport. The mesquite dune sites were chosen because of the high rate of aeolian transport in these communities (Gillette and Pitchford 2004). The sites were flagged and individual plants were tagged indicating replicate order, location and orientation. We selected one branch (Figure 3) from each plant to where we counted leaves and leaflets to estimate leaf and leaflet loss over 6 weeks (Equation 3). The first measurements were made on June 28th, 2018 and then repeated on September 30th, 2018. Due to the difficulties in determining wind and sandblasting magnitude and frequency in each site, plants were not

assigned to treatments of different intensities and wind frequencies, but rather: 1) wind and no abrasion effect (control), and 2) plants under the effect of abrasion and wind.

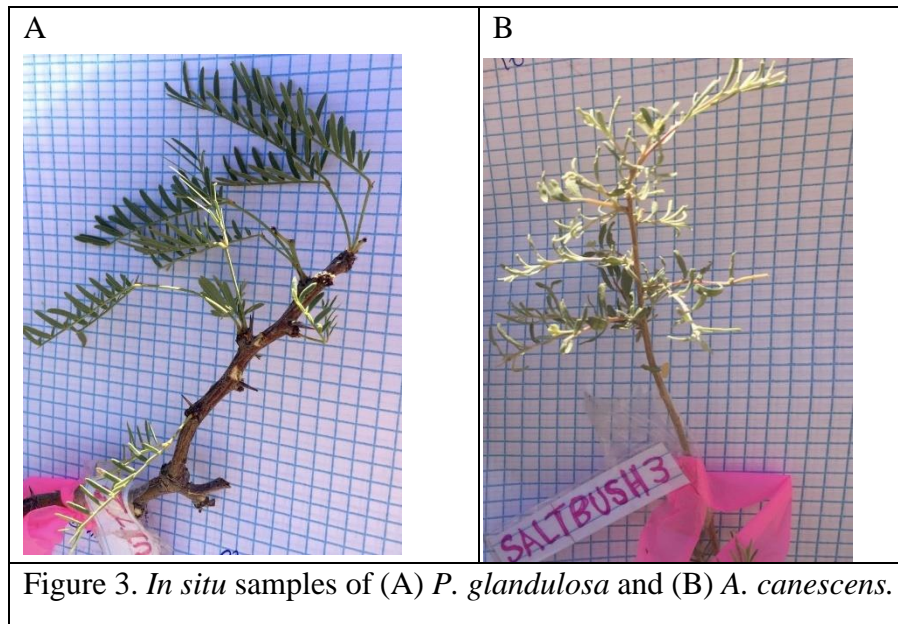
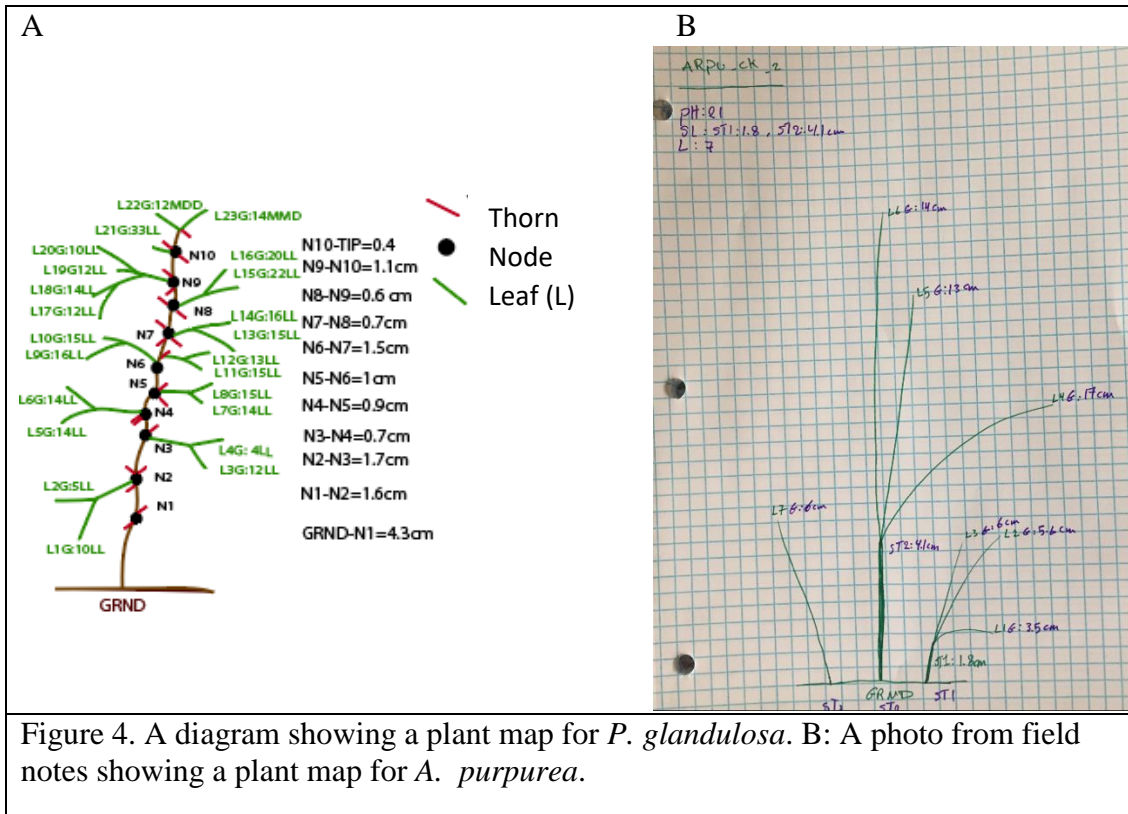


Figure 3. *In situ* samples of (A) *P. glandulosa* and (B) *A. canescens*.

2.3.5 Quantification and mapping of above-ground biomass

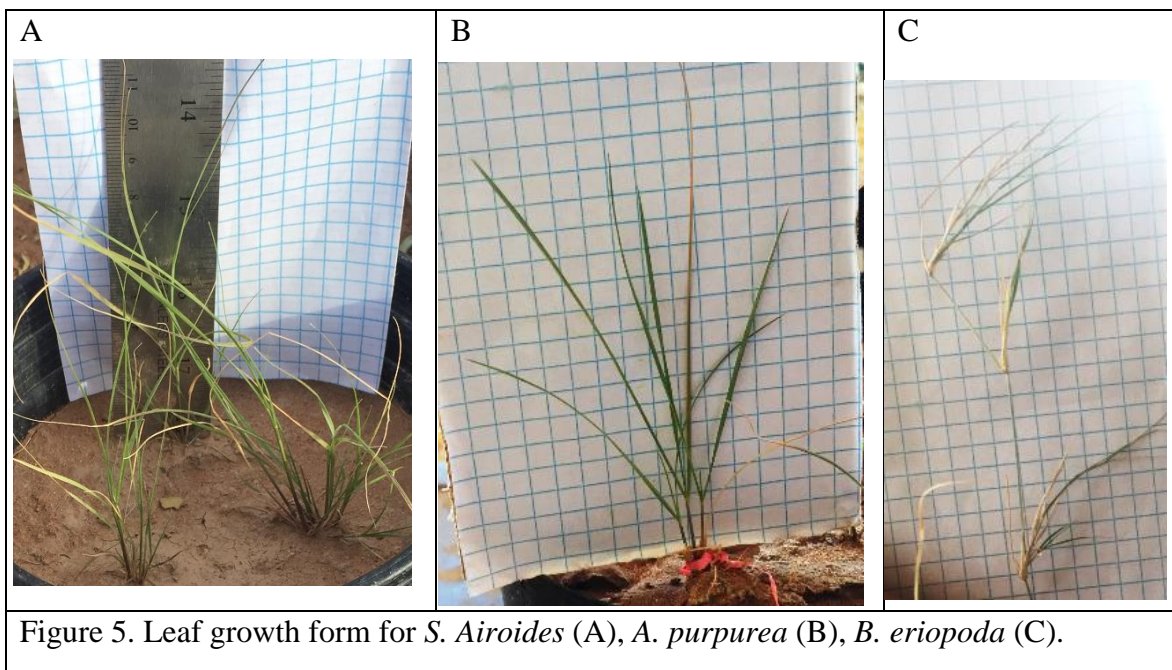
To assess the impacts of aeolian transport on plant architecture, physical characteristics were measured such as the number of leaves and leaflets, leaf area, leaf color, and seed production in a process we called “plant mapping”. The mapping was done twice, before the first sandblasting trial on July 1st, 2018 and after the last sandblasting trial on October 1st, 2018. The downwind (down-tunnel) direction of the plants was marked so that the plant mapping is always done from the same direction.



In our plant mapping, each leaf, node, thorn and minor stems was given a code (consisting of letters and numbers) as an identifier to follow the progress of the plants throughout the treatments (e.g., Figure 4). Different processes were used for grasses and shrubs. For shrubs, photos were taken of the plants with a grid of known line separation in the background, from which scale can be determined (Figure 3). The distance between the nodes was measured to keep track of the overall growth. Codes were created to track the changes throughout the treatments, i.e., for a *P. glandulosa*, the code 0701:N8:L15G,4CM,20LL:L16G,5CM,22LL:2T indicates that the date of the mapping is July 1st (0701), at the 8th node (N8) leaf number 15 (L15) was healthy green (G) and was 4 cm, this leaf had a count of 20 leaflets (20LL), node 8 also included leaf 16 which was also green and was 5 cm with 22 leaflets, node 8 had 2 thorns. *P. glandulosa* was the only bipennate plant, and therefore had leaflets. For the other shrub species, the ‘LL’ part of the code was omitted.

To differentiate between leaves that grow from the same node, we always used the same leaf order for mapping and used markers to reduce confusion when needed. Then, after the last sandblasting trail, a second code is created (e.g., 1001:N8:L16Y,3.9CM,12LL:L15B,5CM,19LL:1T) indicating morphological changes. To illustrate, the code created on October 1st indicate that leaf 15 turned yellow (L15Y) and lost 8 leaflets (12LL), while leaf 16 turned brown and lost 3 leaflets.

Leaf color was also quantified since each leaf was given a color code (G and B). leaf color is the total number of leaves that changed in color (%) by the end of the sandblasting experiments, lost leaves are included in the color quantification. Leaf area (cm²) was roughly estimated using traditional methods: length and width of the leaves using a millimetric ruler and gridded paper.



For grasses, photos with a grid were also taken (Figure 4). The grass mapping for *B. eriopoda* differed from the mapping for *S. airoides* and *A. purpurea*, *B. eriopoda* leaves grow at nodes above the ground level, while bunchgrass leaves grow mostly at ground level (Figure 4). Therefore, bunchgrass mapping, especially *S. Airoides* did not always include stem measurements.

The orientation of the mapping was indicated with labels and markings on the pots. The same coding technique used for the shrubs is followed for the grasses (Figure 4), (e.g., ARPU: 0701:GRND:L1G,14CM, 0.2CM then updated to 1001:GRND:L1B,13CM, 0.2CM). The code indicates that Leaf 1 (L1) was green and grows at ground level (GRND) and is 14 cm long and 0.2 cm wide, then turned brown (B) and decreased in length (13 cm) later in October. We selected one plant in each pot for mapping since more than one plant grew in the same pot (Figure 5A). The total height of the plants was also measured with a millimetric ruler to record the overall plant growth progress.

The first plant mapping was done two days before the first sandblasting trial, July 1st, 2018, and one week after the 6th (and last) sandblasting trial, October 1st, 2018. Percent change to measured plant characteristics was calculated as:

$$\text{Change (\%)} = \frac{\text{Measurement}_{\text{July}} - \text{Measurement}_{\text{October}}}{\text{Measurement}_{\text{July}}} \times 100 \quad (3)$$

where $\text{Measurement}_{\text{July}}$ is the measurement in July and $\text{Measurement}_{\text{October}}$ is the measurement in October. Leaf (leaflet) loss (%) was calculated using the measured total number of leaves (leaflets) for each plant. Leaf area change (%) was calculated using the measured total leaf area for the plants. Stem loss (%), using the measured number of stems, was calculated for *B. eriopoda* because there was a considerable amount of stem loss for some treatments for this plant. Leaf color change (%) is the total number of leaves that turned brown for each plant, and plant height increase (%) is the overall growth of each plant during the 6-week period of the experiment.

2.4 Results

2.4.1 Total Abrader Mass (TAM)

Table 3. TAM (mean \pm standard deviation; g cm⁻¹) experienced by plants in four species over six weeks.

Species	LflLfr	LflHfr	HflLfr	HflHfr
PRGL	806.4 \pm 134.1	884.0 \pm 36.5	2573.1 \pm 159.1	3320.3 \pm 195.5
ATCA	1474.7 \pm 168.1	929.9 \pm 129.4	2537.3 \pm 403.3	2633.5 \pm 345.0
LATR	782.5 \pm 78.3	900.9 \pm 274.5	2639.4 \pm 239.7	3274.7 \pm 337.7
BOER	941.3 \pm 37.4	1137.7 \pm 100.5	2937.2 \pm 147.0	3058.7 \pm 156.4
SPAI	948.3 \pm 119.6	919.3 \pm 77.7	2492.7 \pm 175.0	3201.5 \pm 225.3
ARPU	598.3 \pm 81.4	842.2 \pm 96.3	2993.2 \pm 281.1	3214.8 \pm 346.9

Given the final manner in which abrasers were introduced into the wind tunnel, the TAM for each species fall into two main groups (Table 3). Plants in the LflLfr and LflHfr treatments experienced 598-1475 g cm⁻¹ whereas plants in the HflLfr and HflHfr treatments experienced 2492-3320 g cm⁻¹ TAM. The considerable variability between individual plants, furthermore, meant that some individuals experienced considerably higher TAM than other individuals, even in the same treatment. Therefore, we pursued two approaches to statistical analysis of results. Two-factor ANOVA is consistent with the original layout of the experiment. Regression analysis using individual-plant information was used as an alternative to account for within-group abraded variability.

2.4.2 Response of Plant Architecture to Aeolian Abrasion

Physical damage caused by sandblasting was apparent at the end of the sandblasting experiment for some species, but not others (Figures 6 and 7).

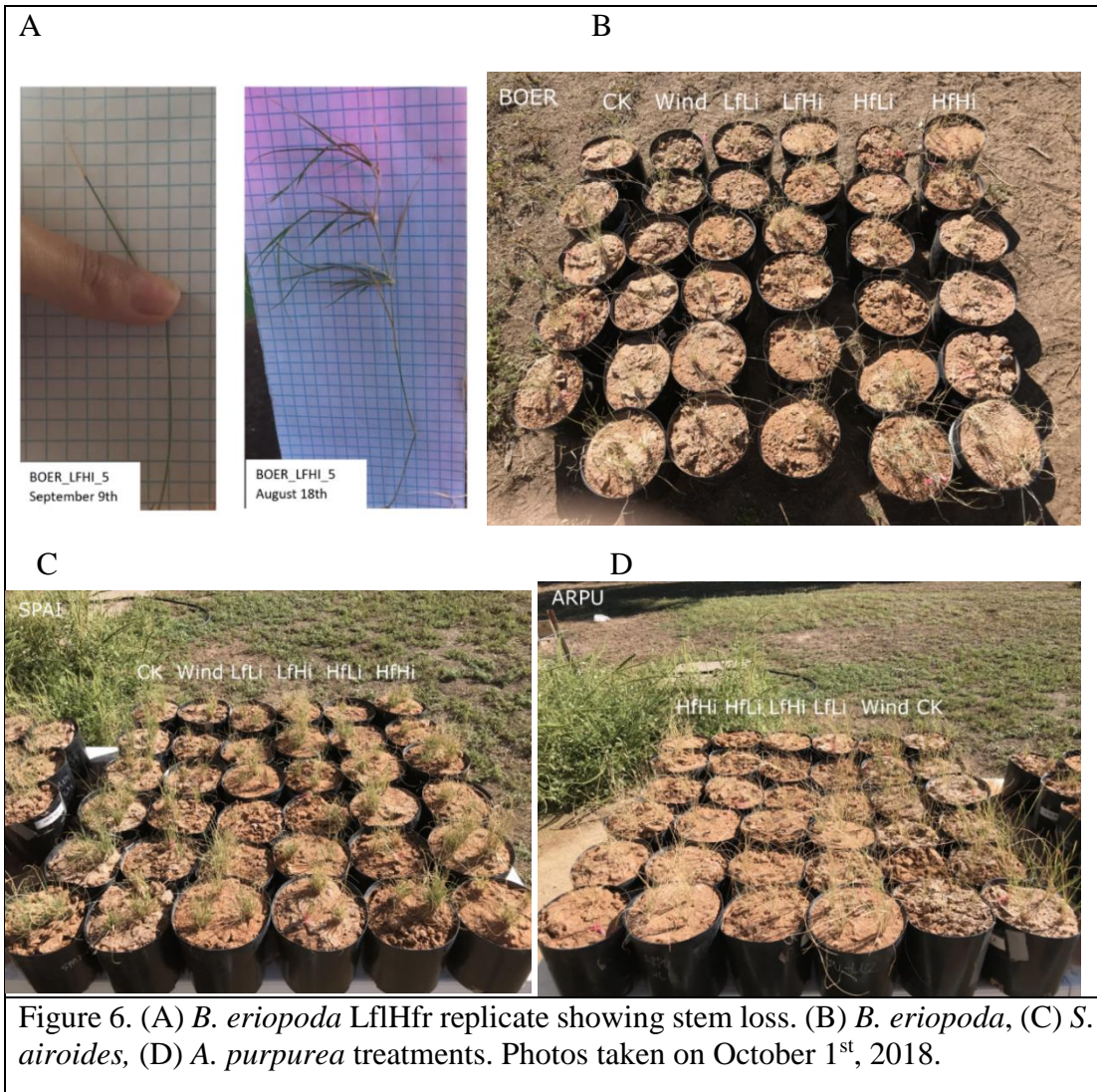


Figure 6. (A) *B. eriopoda* LfHfr replicate showing stem loss. (B) *B. eriopoda*, (C) *S. airoides*, (D) *A. purpurea* treatments. Photos taken on October 1st, 2018.

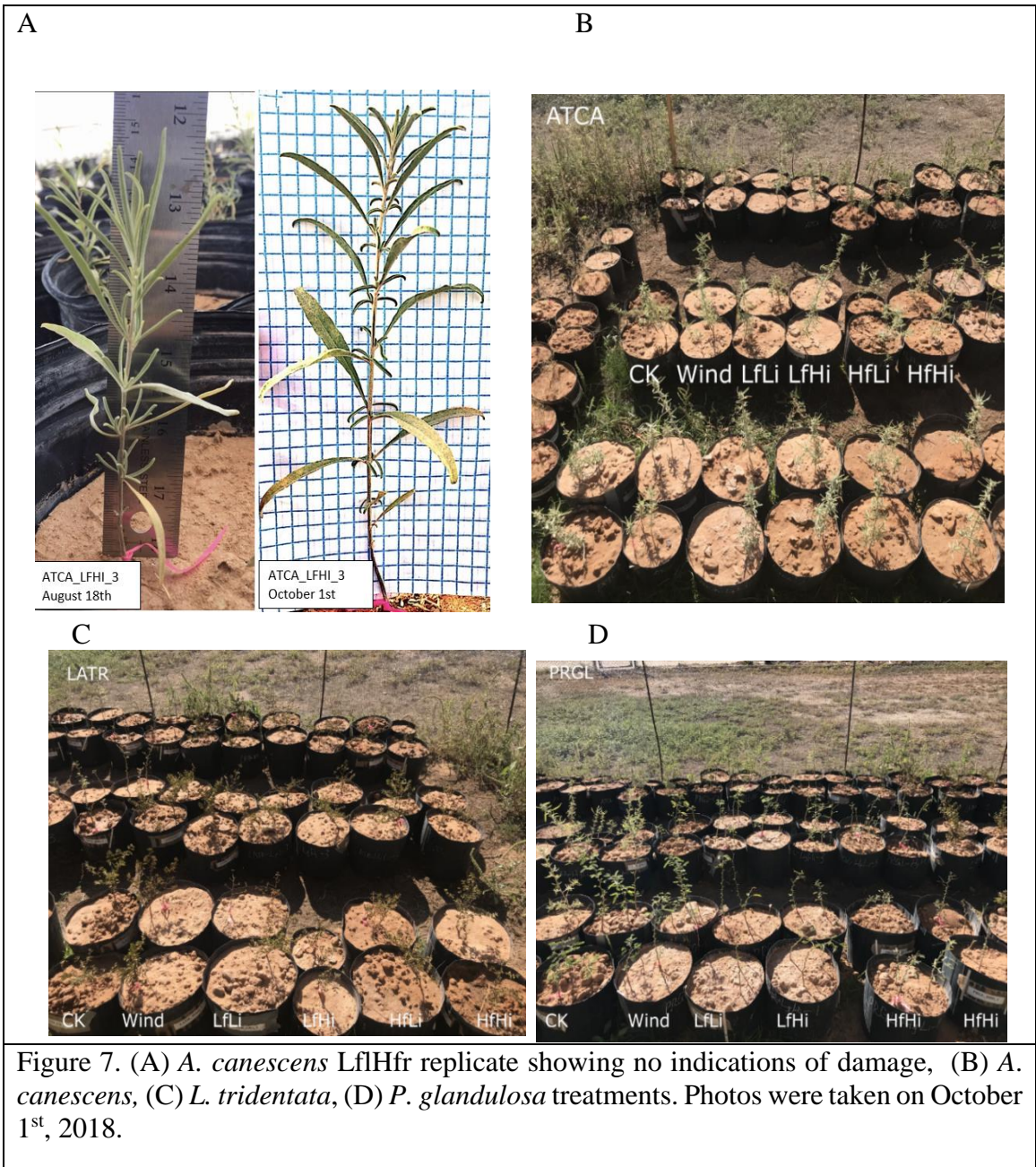


Figure 7. (A) *A. canescens* LfHfr replicate showing no indications of damage, (B) *A. canescens*, (C) *L. tridentata*, (D) *P. glandulosa* treatments. Photos were taken on October 1st, 2018.

2.4.2.1 Leaf and leaflet Loss

Table 4. Leaf loss ANOVA analysis for each species and leaflet loss for *p. glandulosa*.

Specie	Source of variation	Df	Sum of squares	Mean square	F	P > F
<i>P. glandulosa</i>	Flux	2	1.74	0.87	101.2	4.6E-14
	Frequency	1	0.76	0.76	88.1	2.0E-10
	Flux: Frequency	2	0.04	0.02	2.28	1.2E-01
	Residual	30	0.26	0.01		
p. glandulosa (Leaflet)	Flux	2	1.77	0.90	102.5	3.5E-12
	Frequency	1	0.72	0.72	83.6	1.8E-12
	Flux: Frequency	2	0.04	0.02	3.11	1.3E-02
	Residual	30	0.30	0.01		
<i>A. canescens</i>	Flux	2	0.0003	0.0001	0.30	7.4E-01
	Frequency	1	0.0005	0.0005	0.99	3.2E-01
	Flux: Frequency	2	0.0006	0.0003	0.65	5.3E-01
	Residual	30	0.0143	0.0005		
<i>L. Tridentata</i>	Flux	2	1.25	0.62	106.9	2.3E-14
	Frequency	1	0.14	0.14	24.7	2.5E-05
	Flux: Frequency	2	0.15	0.08	12.8	9.3E-05
	Residual	30	0.18	0.01		
<i>S. airoides</i>	Flux	2	1.74	0.87	211.2	2.0E-16
	Frequency	1	0.30	0.30	71.9	1.8E-09
	Flux: Frequency	2	0.03	0.02	4.10	2.8E-02
	Residual	30	0.12	0.004		
<i>A. purpurea</i>	Flux	2	1.22	0.61	82.5	6.4E-13
	Frequency	1	0.22	0.22	29.7	6.6E-06
	Flux: Frequency	2	0.04	0.02	3.01	6.5E-02
	Residual	30	0.22	0.01		
<i>B. eriopoda</i>	Flux	2	1.31	0.65	44.1	1.2E-09
	Frequency	1	0.22	0.22	14.5	1.0E-03
	Flux: Frequency	2	0.01	0.004	0.29	6.0E-03
	Residual	30	0.44	0.02		

ANOVA indicated significant effects of flux and frequency for the different groups for all species except *A. canescens*. All other plants exhibited significant interactive flux/frequency effects (at $\alpha = 0.05$) except *P. glandulosa* leaves (not leaflets) and *A. purpurea* though, for *A. purpurea*, the interactive effect was close to significant at $\alpha = 0.05$.

In the regression context, all species except *A. canescens* indicated a significant response to sand flux ($P > 0.01$), with $> 50\%$ leaf loss for all species (except *A. canescens*) at the higher sand flux treatments (Figure 7,8). For those species with significant responses, the intercepts of the regressions of leaf loss against TAM varied. For *P. glandulosa*, *L. tridentata*, and *S. airoides*,

the intercept was about 20 %, whereas for *A. purpurea*, it was slightly higher. *B. eriopoda* exhibits the highest intercept, as well as the highest leaf loss for the wind-only treatments. *B. eriopoda* also experienced the highest amount of leaf loss for all other treatments, compared to the other species.

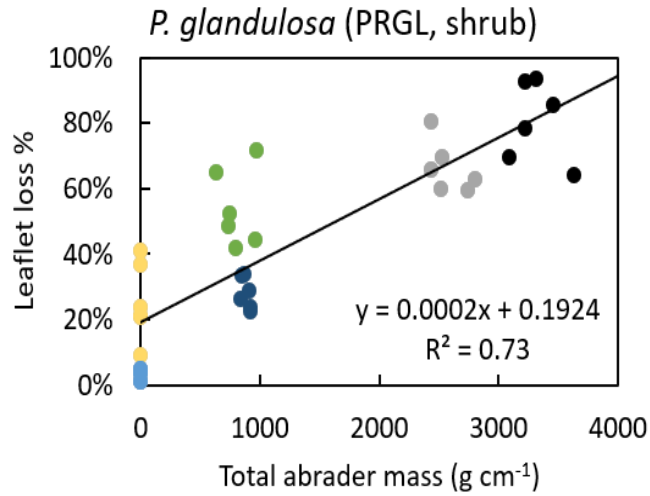


Figure 8. Average leaflet loss % in response to sandblasting at sand flux treatments g cm^{-1} and control for six species over six weeks.

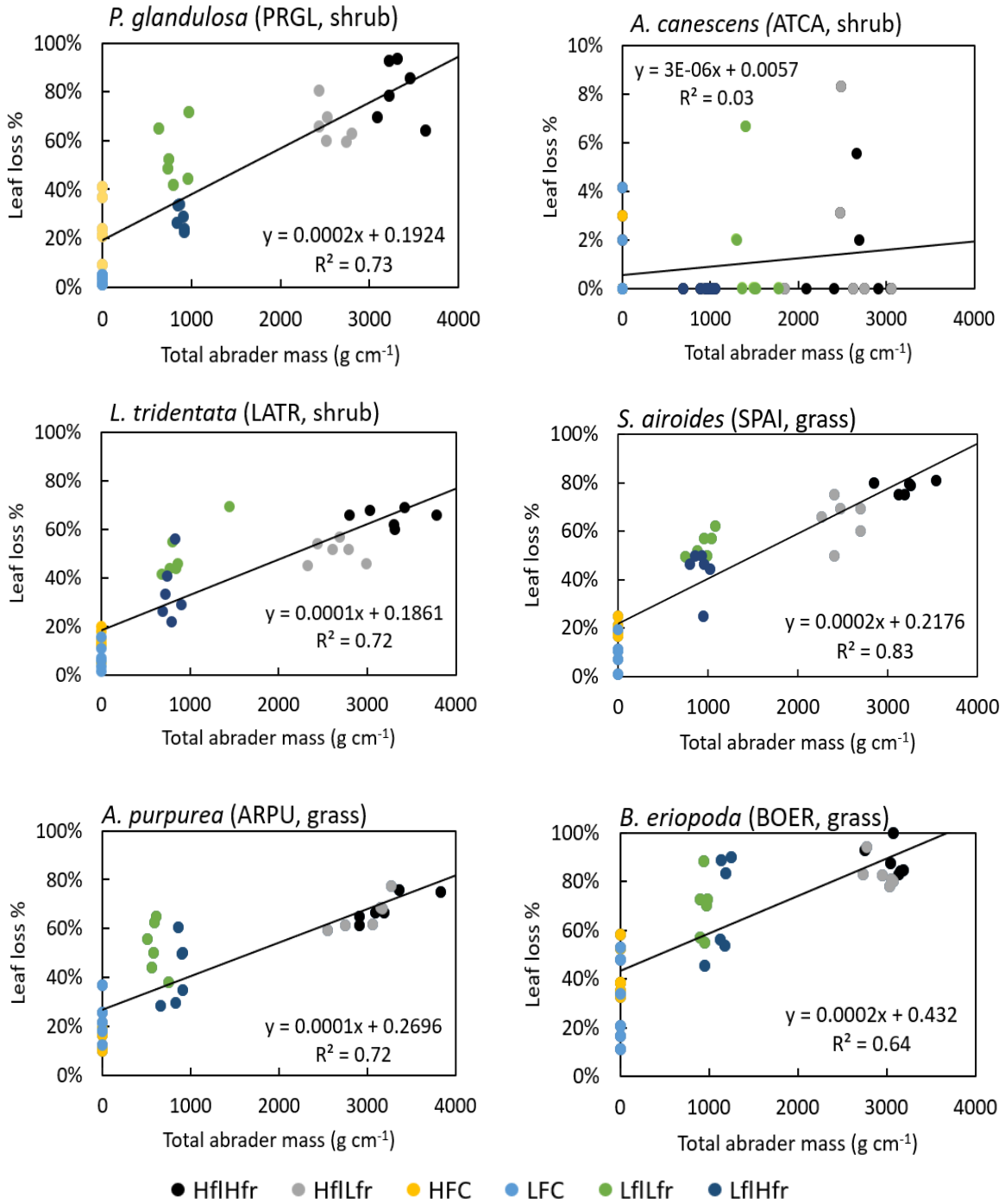


Figure 9. Average leaf loss % in response to sandblasting at sand flux treatments g cm^{-1} and control for six species over six weeks.

2.4.2.2 Total Leaf Area

Total leaf area characterizes the total amount of surface area is available for photosynthesis, and it is thus a good indicator of the impact that changes to plant architecture have on plant productivity. ANOVA analysis (Table 5) indicates significant effects associated with flux and frequency of treatments, as well as significant interactive effects ($P < 0.01$), for almost all species, except *A. canescens*. *A. canescens* did exhibit a significant response to flux ($\alpha = 0.05$), but not frequency.

Table 5. Leaf area loss ANOVA test for each species.

Specie	Source of variation	Df	Sum of squares	Mean square	F	P > F
<i>P. glandulosa</i>	Flux	2	0.31	0.16	3.55	4.0E-03
	Frequency	1	1.00	1.00	23.2	3.9E-05
	Flux: Frequency	2	1.01	0.51	11.7	1.7E-04
	Residual	30	1.30	0.04		
<i>A. canescens</i>	Flux	2	0.02	0.01	4.31	2.0E-02
	Frequency	1	0.01	0.01	3.22	9.0E-02
	Flux: Frequency	2	0.01	0.003	1.71	2.0E-01
	Residual	30	0.05	0.002		
<i>L. Tridentata</i>	Flux	2	0.96	0.48	54.8	9.7E-11
	Frequency	1	0.14	0.14	16.3	3.5E-04
	Flux: Frequency	2	0.06	0.03	3.60	4.0E-02
	Residual	30	0.26	0.01		
<i>S. airoides</i>	Flux	2	0.18	0.09	9.60	6.0E-04
	Frequency	1	1.04	1.04	112.5	1.1E-11
	Flux: Frequency	2	0.33	0.16	17.8	8.2E-06
	Residual	30	0.28	0.01		
<i>A. purpurea</i>	Flux	2	0.18	0.09	22.2	1.2E-06
	Frequency	1	0.73	0.73	180.2	3.2E-14
	Flux: Frequency	2	0.42	0.21	52.3	1.7E-10
	Residual	30	0.12	0.004		
<i>B. eriopoda</i>	Flux	2	0.06	0.03	3.95	3.0E-03
	Frequency	1	1.72	1.72	233.9	1.0E-15
	Flux: Frequency	2	0.66	0.33	45.0	9.3E-10
	Residual	30	0.22	0.01		

As with leaf loss, regression analysis indicates that all plants exhibited significant ($P < 0.05$) responses to the treatments except *A. canescens*. The intercepts for these relationships, however, were generally lower than their counterparts in leaf loss, except for *P. glandulosa*. For the grasses, an important component of leaf area loss was the loss of individual stems due to the

treatments. This is particularly clear in *B. eriopoda* which exhibits the highest degree of leaf area loss, with some plants in the strongest treatments exhibiting nearly 100% leaf area loss (Figure 10). However, some *P. glandulosa* individuals also exhibited nearly complete leaf area loss due to the denudation of leaflets from the leaves.

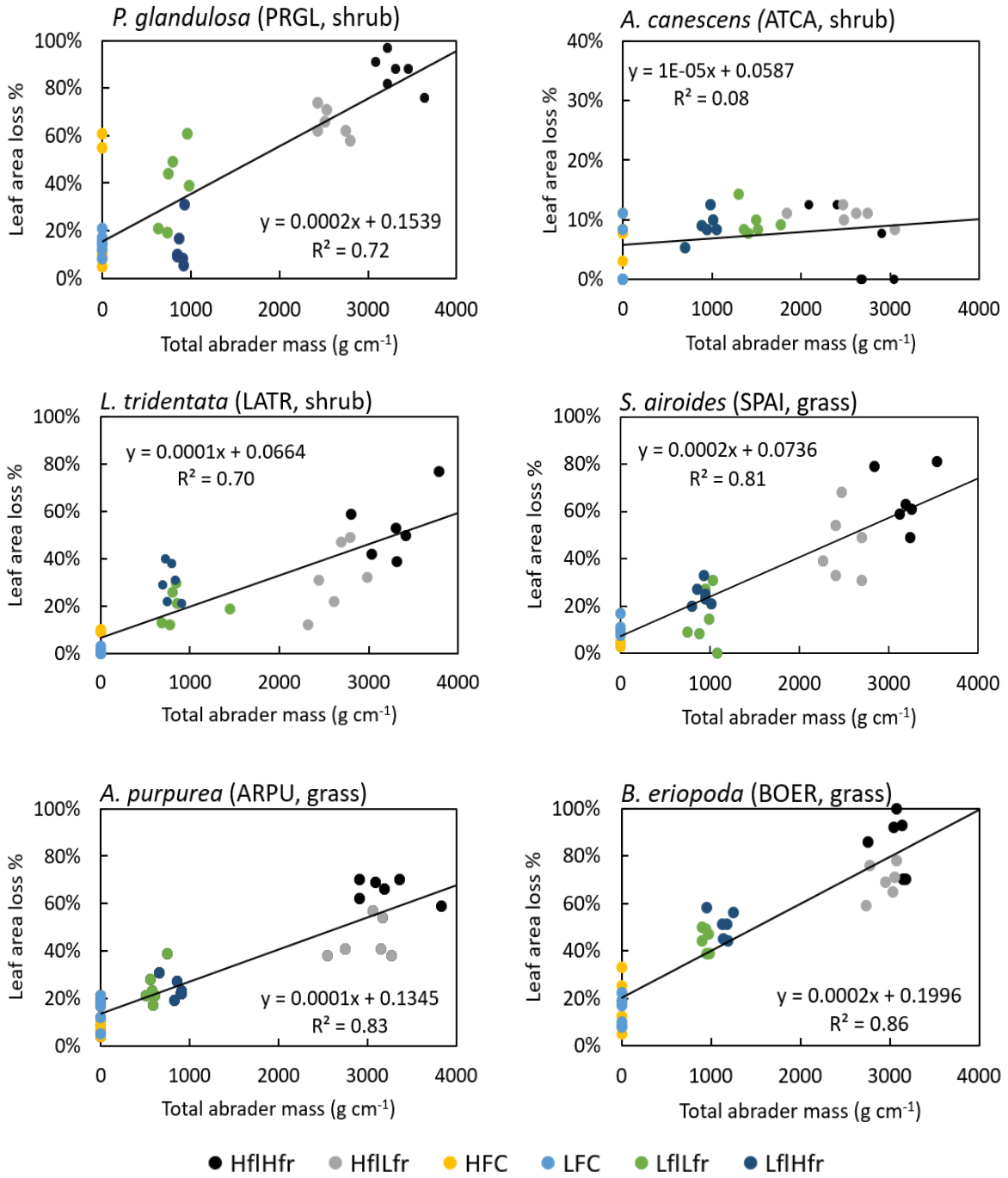


Figure 10. Leaf area loss (%) in response to sandblasting at sand flux treatments g cm^{-1} and control for six species over six weeks.

2.4.2.3 Other responses

Table 6. Leaf color ANOVA test for each species.

Specie	Source of variation	Df	Sum of squares	Mean square	F	P > F
<i>P. glandulosa</i>	Flux	2	1.66	0.83	291.9	5.2E-10
	Frequency	1	0.11	0.11	37.8	3.5E-07
	Flux: Frequency	2	0.00	0.002	0.62	5.4E-02
	Residual	30	0.09	0.003		
<i>A. canescens</i>	Flux	2	5.0E-05	2.5E-05	0.14	8.7E-01
	Frequency	1	0.0002	0.0001	1.50	2.3E-01
	Flux: Frequency	2	0.001	0.0003	1.36	2.7E-01
	Residual	30	0.006	0.0004		
<i>L. Tridentata</i>	Flux	2	0.42	0.21	135.9	1.6E-06
	Frequency	1	0.01	0.01	7.38	1.1E-02
	Flux: Frequency	2	0.01	0.01	3.95	3.0E-02
	Residual	30	0.05	0.002		
<i>S. airoides</i>	Flux	2	1.05	0.52	199.8	3.3E-08
	Frequency	1	0.03	0.03	10.4	3.0E-03
	Flux: Frequency	2	0.01	0.002	0.87	4.3E-01
	Residual	30	0.08	0.003		
<i>A. purpurea</i>	Flux	2	1.22	0.61	187.9	6.1E-07
	Frequency	1	0.004	0.004	1.38	2.5E-01
	Flux: Frequency	2	0.05	0.02	6.91	3.0E-03
	Residual	30	0.09	0.003		
<i>B. eriopoda</i>	Flux	2	1.91	0.94	154.2	7.2E-06
	Frequency	1	0.01	0.01	2.37	1.3E-01
	Flux: Frequency	2	0.02	0.01	1.27	3.0E-01
	Residual	30	0.20	0.01		

Table 7. Plant height ANOVA test for each species.

Specie	Source of variation	Df	Sum of squares	Mean square	F	P > F
<i>P. glandulosa</i>	Flux	2	0.04	0.02	1.99	0.15
	Frequency	1	0.05	0.05	4.15	0.05
	Flux: Frequency	2	0.11	0.06	5.19	0.01
	Residual	30	0.32	0.01		
<i>A. canescens</i>	Flux	2	0.01	0.01	0.39	0.68
	Frequency	1	0.0001	0.001	0.02	0.89
	Flux: Frequency	2	0.01	0.003	0.17	0.85
	Residual	30	0.53	0.018		
<i>L. Tridentata</i>	Flux	2	0.04	0.02	6.82	0.004
	Frequency	1	0.01	0.01	3.27	0.08
	Flux: Frequency	2	0.001	0.0001	0.13	0.88
	Residual	30	0.08	0.003		
<i>S. airoides</i>	Flux	2	0.004	0.002	3.64	0.04
	Frequency	1	0.0003	0.0001	0.23	0.64
	Flux: Frequency	2	7.2E-5	3.6E-5	0.06	0.94
	Residual	30	0.02	0.001		
<i>A. purpurea</i>	Flux	2	0.001	0.001	0.75	0.48
	Frequency	1	0.001	0.001	1.97	0.17
	Flux: Frequency	2	0.01	0.004	5.80	0.01
	Residual	30	0.02	0.001		
<i>B. eriopoda</i>	Flux	2	0.05	0.02	2.92	0.07
	Frequency	1	0.0003	0.0002	0.05	0.82
	Flux: Frequency	2	0.024	0.01	1.51	0.20
	Residual	30	0.24	0.01		

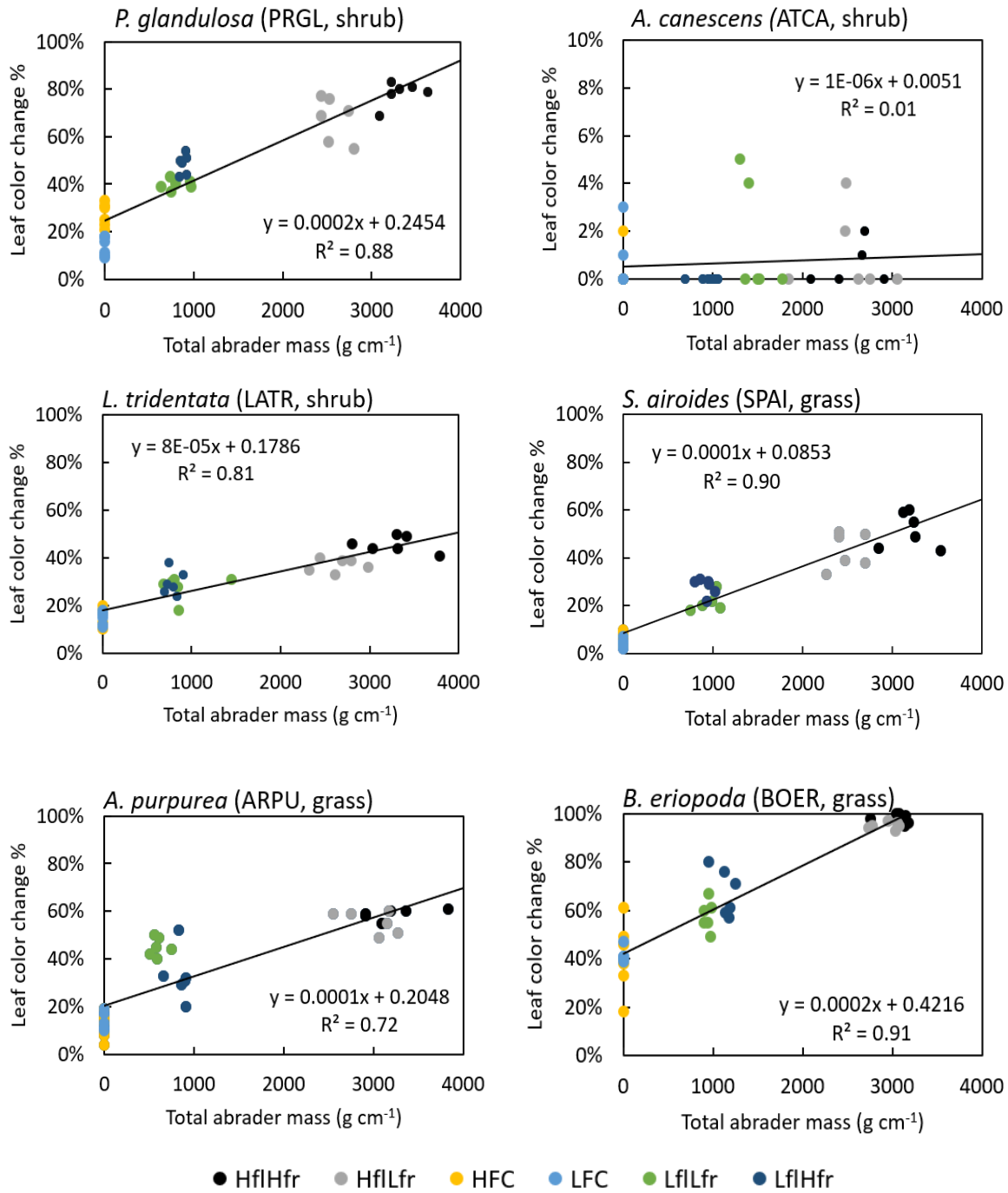


Figure 11. Leaf color change (%) in response to sandblasting at sand flux treatments g cm⁻¹ and control for six species over six weeks.

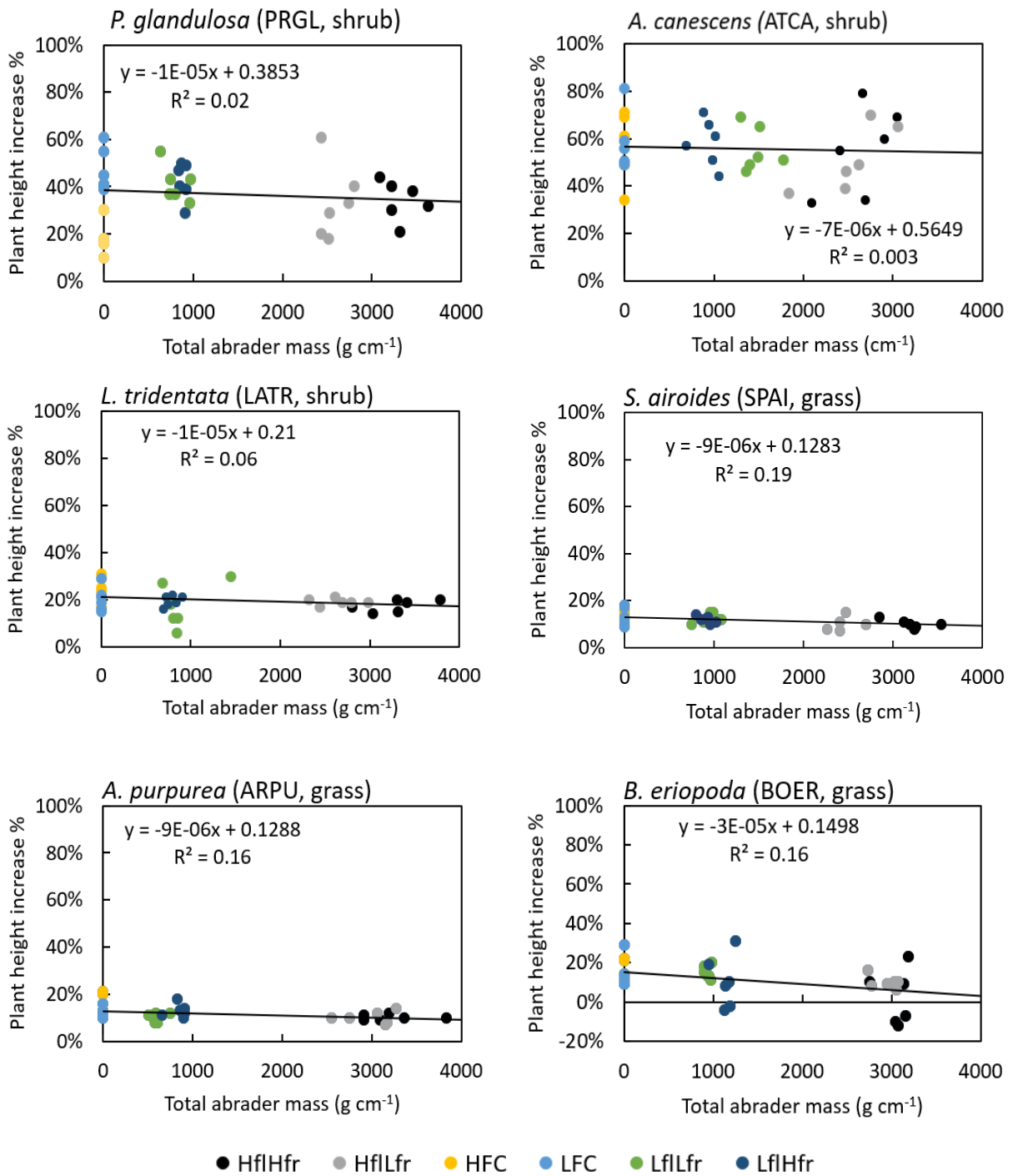


Figure 12. Plant height increase (%) in response to sandblasting at sand flux treatments $g\ cm^{-1}$ and control for six species over six weeks. Negative response indicate reduction in height.

ANOVA indicates significant effects of flux on the percent of leaves that changed color for all species except *A. canescens*, which exhibited no significant effects. *A. purpurea* and *B. eriopoda* were the only other plants that did not exhibit a significant frequency effect. Regression analysis indicates that the color change in response to flux was significant and positive for all species except *A. canescens*. As with leaf number and leaf area loss, *B. eriopoda* displayed the highest intercept for the regressions, indicating the strongest effect of wind-only treatments. The effect of treatments on plant height were less clear. Though ANOVA indicates some significant responses, the regression analysis indicates very low correlation with TAM. In most cases, the slope of these relationships is negative indicating that higher TAM led to reduced growth. Only *B. eriopoda* appeared to get shorter after the treatments.

No flower and seed production was observed for any of the plants except *L. tridentata* which most of its leaves remained green by the end of the experiment. In general, normal plant growth is observed in plant height increase (%) for all species except some replicates of *B. eriopoda* (Figure 12) which could be attributed to stem loss. Plant height response is insignificantly associated with treatments, regardless of the frequency and the flux treatments, the plants exhibit growth (Table 7).

2.4.3 *In situ* plants

Plants measured *in situ* showed some agreement in patterns of leaf loss with plants in the wind tunnel treatments (Table 8). In the grass category, the highest leaf loss was found for *B. eriopoda* (44 - 49%) for the wind and abrasion effect sites (T), while control (C) was 31 - 34% and no stem loss was observed. *A. purpurea* (T = 12 - 20% and C = 4 - 9%) and *S. airoides* (T = 19 - 21% and C = 9 - 13%) displayed lower leaf loss, but the treatment plants did exhibit more loss than the control plants. In the shrub category, *P. glandulosa* recorded the highest leaf loss (T = 63

- 78% and C = 22 - 34%) among all shrub species at all sites, *A. canescens* had leaf loss between 17 and 22% at C and 21-62% at T sites.

Table 8. Species, site, and average leaf loss (%) at sites of wind and abrasion effect (T) and control (C) standard deviation (STDEV) and coefficient of variance (CV) for plants in natural conditions.

species	Location		Leaf Loss %	STDEV	CV	Leaflet Loss %	STDEV	CV
<i>P. glandulosa</i>	NEAT	C	34	10.8	0.3	31	13.0	0.2
		T	63	12.1	0.2	56	15.3	0.3
	Scraped	C	22	13.5	0.6	44	13.4	0.3
		T	69	10.3	0.3	48	15.1	0.3
	Shrub dune	C	31	9.0	0.3	67	16.1	0.1
		T	78	11.0	0.1	66	15.3	0.2
<i>A. canescens</i>	NEAT	C	22	10.4	0.2			
		T	42	12.6	0.3			
	Scraped	C	17	5.5	0.3			
		T	21	10.5	0.5			
	Shrub dune	C	21	11.7	0.5			
		T	62	35.5	0.6			
T		36	7.6	0.2				
<i>A. purpurea</i>	NEAT	C	9	1.1	0.1			
		T	20	13.5	0.6			
	Scraped	C	4	1.7	0.4			
		T	12	1.5	0.1			
<i>S. airoides</i>	NEAT	C	13	8.1	0.6			
		T	19	8.5	0.5			
	Scraped	C	6	4.0	0.7			
		T	21	13.1	0.5			
<i>B. eriopoda</i>	NEAT	C	31	11.2	0.2			
		T	49	15.5	0.3			
	Scraped	C	34	24.2	0.7			
		T	44	12.5	0.3			

2.5 Discussion

Our results demonstrate unequivocally the damaging effects of sandblasting and wind on above-ground biomass. At plant level, the growth form determines the vulnerability to sandblasting, especially as saltation flux decreases with height. In general, our plants' heights were below 25 cm and fell within the saltation boundary in the wind tunnel. Among the grasses *B. eriopoda* appeared to be the most sensitive in all measures, to wind and abrasion. Among the shrubs, it was clear that the treatments had almost no impact on *A. canescens* by any measure. In

all measures except plant height change, *A. purpurea* appeared to be more sensitive to both wind and abrasion than *L. tridentata*. Overall, this variability makes it impossible to say whether, given the measures made here, grasses or shrubs were more susceptible to wind and abrasion effects.

Due to the limitations of the experiment, namely the need to place plants inside a 50 cm x 50 cm wind tunnel, individuals used in this study were necessarily smaller than mature adults found *in situ*. Despite the fact that our experiments did not exhibit any obvious differences between the response of grasses and shrubs to wind and abrasion (with the exception of *A. canescens*), we do not take them as a refutation of the idea that aeolian processes impact grasses and shrubs differently at the level and lifetime of a whole plant. In particular, grasses rarely grow higher than 30 - 40 cm, with the exception, perhaps of elevated flower/seed stalks. The shrubs that we have studied here, on the other hand, can exceed 1 m height as mature adults. The perennial grasses we worked with start regrowing leaves at the beginning of the season close to the base of the plant, whereas the leaves on shrubs are typically toward the end of woody branches that can be elevated above the ground. *P. glandulosa* is, furthermore, deciduous meaning that leaf and leaflet loss that occurs during the growing season will be replaced in the following year.

With the exception of *B. eriopoda*, all of the plants increased in height during the 6 weeks of the experiment. For the grasses on an interannual timeframe, this does not matter. However, for the shrubs, their ability to grow (even if reduced) means that they will, eventually, grow out of the saltation zone. Thus, even though *A. purpurea* and *L. tridentata* plants appeared to be impacted considerably by wind, our results do not provide any reason to believe that, with time, these plants would not be able to grow to heights where the photosynthetic material is out of the saltation zone. For grasses, this will never be the case.

Among grasses *B. eriopoda* appeared to be most sensitive to wind and abrasion. This helps explain, perhaps, why the loss of this grass has been so extensive across the Chihuahuan Desert, whereas other grasses, including *Aristida* spp. and *Sporobolus* spp. have managed to maintain higher cover even in the face of the opening of bare gaps and increases in aeolian transport. *B. eriopoda* has an additional disadvantage in that it is a stoloniferous grass meaning that it spreads through vegetative reproduction using stolons that grow close to the ground, where they would be most susceptible to damage from aeolian transport. Thus, aeolian transport has the potential to not only damage existing biomass, but to damage the plant's means of reproduction as well, limiting future expansion.

2.6 Conclusion

Our experiments clearly indicated that many species of grass and shrub were susceptible to damage due to both wind-only effects and sandblasting. These results support the hypothesis of Okin et al. (2006) that aeolian transport directly effects biomass and may close a positive feedback loop whereby increased aeolian transport damages plants, which reduces vegetation cover and therefore increases aeolian transport. Although we originally hypothesized that grasses would be more susceptible than shrubs to the damage due to aeolian transport, this was only clearly true for *B. eriopoda* helping explain, perhaps, why loss of this grass (and grasses of this genus) has been so extensive in the perennial grasslands of the southwestern US. Nonetheless, the ability of shrubs to continue growing (and therefore increasing the height of their leaves and growing point) despite considerable damage argues that their functional type gives them an intrinsic advantage over grasses even if small shrubs are as susceptible to damage as grasses.

2.7 Future plans

This work is part of a 3-year project that focuses on aeolian processes as major disturbances to the ecosystem encouraging state change from grassland to shrubland in collaboration with the University of Arizona, Dr. Steve Archer. The plants were transported back to the greenhouse in Tuscan, AZ in October 2018 and have been monitored since. Many of the plants have survived the dormant winter season and have started to grow again. In Summer, 2019 new treatments using the same plants, as well as new ones, will be continued, and the suite of measurements described here will be repeated.

Two important changes will be made to the experiments done in Summer, 2019. First, a shortage of plants in Summer, 2018 precluded the ability to do two wind-only treatments while also having a no-wind control. At the time, we were interested in investigating whether there was a significant wind effect. Our results indicate that there is, and yet, cannot clarify fully whether some of the damage observed in the wind-only treatments was due only to transportation of plants to/from the wind tunnel and manipulation required to do the measurements. In Summer, 2019, a set of control plants that will provide the opportunity to observe this potential effect will be included. In addition, although the TAM used in these experiments were consistent with measurements by Gillette and Pitchford (2004), the experimental impact on the plants was surprisingly high. Therefore, in Summer, 2019 lower flux treatments will be used. This will require some changes to the experimental set up including replacement of the hopper system to allow for lower and more carefully controlled flux rates.

Acknowledgment

This research was supported by the NSF-funded Jornada Basin LTER program.

I would like to express my gratitude to those who participated in this work. The PIs, Dr. Gregory Okin and Dr. Steve Archer, are very much appreciated for their continuous support and guidance. Dr. Furong Niu, Mike Fischella, and the Jornada HQ team, thank you for all your help and support. Special thanks to Kuwait University and Kuwait Embassy for their continuing support of my research.

2.7 Bibliography

Alvaraz, L J, H E Esteipan, and G S Okin. 2011. "Spatial patterns of grasses and shrubs in an arid grassland environments." *Ecosphere* 2 (9): 1-30.

Alvarez, Lorelei J, Howard E Epstein, Junran Li, and Gregory S Okin. 2012. "Aeolian process effects on vegetation communities in an arid grassland ecosystem." *Ecological and Evolution* 2 (4): 809-821.

Archer, S. 1989. "Have southern Texas savannas been converted to woodlands in recent history.134:545–61." *American Naturalist* 134 (4): 61.

Archer, S, D S Schimel, and E A Holland. 1995. "Mechanisms of shrubland expansion—land-use, climate or CO₂ ." *Climate Change* 29 (1): 91-99.

Baker, Jeffrey T, Bobbie McMichael, John J Burke, Dennis C Gitz, Robert J Lascano, and Jhonathan E Ephrath. 2009. "Sand abrasion injury and biomass partitioning in cotton seedlings." *Agronomy Journal* 101 (6): 1297-1303.

Bergametti, G, and D A Gillette. 2010. "Aeolian sediment fluxes measured over various plant/soil complexes in the Chihuahuan desert." *Journal of Geophysics Research* 115, F03044.

Bestelmeyer, Brandon T, Gregory S Okin, Michael C Duniway, Steven R Archer, Nathan F Sayre, Jebediah C Williamson, and Jeffrey E Herrick. 2015. "Desertification, land use, and the transformation of global drylands." *Frontiers in Ecology and the Environment* 13 (1): 28-36.

Bestelmeyer, Brandon T, Jeffrey E Herrick, Joel R Brown, David A Trujillo, and Kris M Havstad. 2004. "Land Management in the American Southwest: A State-and-Transition Approach to Ecosystem Complexity." *Environmenta; Managment* 34 (1): 38-51.

Bhattachan, A, P D'Odorico, K Dintwe, G S Okin, and S L Collins. 2014. "Resilience and recovery potential of duneland vegetation." *Ecosphere* 5 (1). <http://dx.doi.org/10.1890/ES13-00268>.

- Breshears, David D, Thomas B Kirchner, Jeffrey J Whicker, Jason P Field, and Craig D Allen. 2012. "Modeling aeolian transport in response to succession, disturbance and future climate: Dynamic long-term risk assessment for contaminant redistribution." *Aeolian Research* 3 (4): 445-457.
- Buffington, Lee C, and Carlton H Herbel. 1965. "Vegetational Changes on a Semidesert Grassland Range from 1858 to 1963." *Ecological Monographs: Ecological Society of America* 35 (2): 139-164.
- Bullard, Joanna E, and Ian Livingstone. 2002. "Interactions between aeolian and fluvial systems in dylands." *Research in Geography* 34 (1): 8-16.
- Chapin, F S, E S Zavaleta, V T Eviner, and R L Naylor. 2000. "Consequences of changing biodiversity." *Nature* 405 (6).
- D'Odorico, P, G Okin, and B Bestelmeyer. 2012. "synthetic review of feedbacks and drivers of shrub encroachment in arid grasslands." *Ecohydrology* 5 (5): 520-530.
- D'Odorico, Paolo, Gregory S Okin, and Brandon T Besterlmeyer. 2012. "A synthetic review of feedbacks and drivers of shrub encroachment in arid grasslands." *Ecohydrology* 5 (5): 520-530.
- Dodson, Carolyn. 2012. *A guide to plants of the northern Chihuahuan Desert*. Las Cruces: The University of New Mexico Press.
- Field, Christopher B, Michael J Behrenfeld, James T Randerson, and Paul Falkowski. 1998. "Primary production of the biosphere: Integrating terrestrial and oceanic components." *Science* 281 (5374). doi:DOI: 10.1126/science.281.5374.237.
- Gibbens, R P, and R F Beck. 1987. "Increase in Number of Dominant Plants and Dominance-Classes on a Grassland in the Northern Chihuahuan Desert." *Journal of Range Management* (40): 136-139.
- Gibbens, R P, J M Tromble, J T Hennessy, and M Gardenas. 2001. "Soil movement in mesquite dunelands and former grasslands of Southern New Mexico from 1933 to 1980." *Journal of Range Management* 36 (2): 145-148.
- Gibbens, R P, R P McNeely, K M Havstad, R F Beck, and B Nolen. 2005. "Vegetation changes in the Jornada Basin from 1858 to 1998." *Journal of Arid Environments* 61 (4): 651-668.
- Gibbens, T J, J T Hennessy, and M Gardenas. 1983. "Soil movement in mesquite dunelands and former grasslands of southern New Mexico from 1933 to 1980." *Journal of Range Management* (36): 145-148.

Gillette, D A, and A M Pitchford. 2004. "Sand flux in the northern Chihuahuan desert, New Mexico, USA, and the influence of mesquite-dominated landscapes." *Journal of Geophysical Research-Earth Surface* 109 (F4): F04003.

Gillette, Dale A, and Ann M Pitchford. 2004. "Sand flux in the northern Chihuahuan desert, New Mexico, USA, and the influence of mesquite-dominated landscapes." *Journal of Geophysical Research* 109 (F04003).

Huenneke, L F, J P Anderson, M Remmenga, and W H Schlesinger. 2002. "Desertification alters patterns of aboveground net primary production in Chihuahuan ecosystems." *Global Change Biology* 8 (3): 247–264.

Knapp, Alan K, John M Briggs, Scott L Collins, Steven R Archer, M Sydonia Bret-Harte, Brent E Ewers, Debra P Peters, et al. 2008. "Shrub encroachment in North American grasslands: shifts in growth form dominance rapidly alters control of ecosystem carbon inputs." *Global Change Biology* 14 (3): 615-623.

Kok, J F, E J Parteli, T I Michaels, and D B Karam. 2012. "The physics of wind-blown sand and dust- Review." *Report on Progress in Physics* 10 (75). doi:doi: 10.1088/0034-4885/75/10/106901.

Li, J, G S Okin, L Alvarez, and H Esteipan. 2007. "Quantitative effects of vegetation cover on wind erosion and soil nutrient loss in a desert grassland of southern New Mexico, USA." *Biogeochemistry* 85: 317-332.

Li, Junran, Gregory S Okin, and Howard E Esteipan. 2009. "Effects of enhanced wind erosion on surface soil texture and characteristics of windblown sediments." *JGR Biogeosciences* 114 (G2). <https://doi.org/10.1029/2008JG000903> .

Li, Junran, Gregory S Okin, Lorelei Alvarez, and Howard Esteipan. 2007. "Quantitative effects of vegetation cover on wind erosion and soil nutrient loss in a desert grassland of southern New Mexico, USA." *Biogeochemistry* 85 (3): 317-332.

MEA. 2005. *Millennium ecosystem assessment: ecosystems and human well-being: desertification synthesis* . Washington, DC: World Resources Institute.

Muhs, Daniel R, and Vance T Holiday. 1995. "Evidence of Active Dune Sand on the Great Plains in the 19th Century from Accounts of Early Explorers." *Quaternary Research* 43 (2): 198-208.

2017. National Instruments. <http://www.ni.com/en-us.html>.

Nickling, W G, and C M Neuman. 1997. "Wind tunnel evaluation of a wedge-shaped aeolian sediment trap." *Geomorphology* 18 (3-4): 333-345.

Okin, G S, A j Parson, J Wainwright, J E Herrick, B T Bestelmeyer, D PC Peters, and E L Fredrickson. 2009. "Do Changes in Connectivity Explain Desertification?" *BioScience* 59 (3): 237-244.

Okin, G S, and D A Gillette. 2001. "Distribution of vegetation in wind-dominated landscapes: implications for wind erosion modeling and landscape processes." *Geophysics Research* 106: 9673-9683.

Okin, G S, B Murray, and W H Schlesinger. 2001a. "Desertification in an arid shrubland in the southwestern United States: process modeling and validation." *Land degradation: papers selected from contributions to the Sixth Meeting of the International Geographical Union's Commission on Land Degradation and Desertification*. Dordrecht, The Netherlands: Kluwer Academic Publisher. 53-70.

Okin, G S, D A Gillette, and J E Herrick. 2006. "Multi-scale controls on and consequences of aeolian processes in landscape change in arid and semi-arid environments." *Journal of Arid Environments* 65 (2): 253-275.

Okin, G S, Mariano Moreno de las Heras, P M Saco, H L Throop, E R Vivoni, A J Parsons, J Wainwright, and D PC Peters. 2015. "Connectivity in dryland landscapes: Shifting concept of spatial interactions." *Ecological Environment* 13 (1): 20-27.

Okin, G S, O E Sala, E R Vivoni, J Zhang, and A Bhattachan. 2018. "The Interactive Role of Wind and Water in Functioning of Drylands: What Does the Future Hold?" *BioScience* 68 (9): 670-677.
Okin, G S, P D'Odorico, and S Archers. 2009. "Impact of feedbacks on Chihuahuan desert grasslands: transience and metastability." *Journal of Geographical Research-Biogeosciences* 114 (G1). doi:<https://doi.org/10.1029/2008JG000833>.

Okin, Gregory S, and Dale A Gillette. 2001. "Distribution of vegetation in wind-dominated landscapes: Implications for wind erosion modeling and landscape processes." *Journal of Physical Research* 106 (D9): 9673-9683.

Okin, S G, D A Gillette, and J E Herrick. 2006. "Multi-scale controls on and consequences of aeolian processes in landscape change in arid and semi-arid environments." *Journal of Arid Environments* 65 (2): 253-275.

Peters, A J, and M D Eve. 1995. "Satellite monitoring of desert plant community response to moisture availability." *Environmental Monitoring and Assessment* 37 (1-3): 273-287.

Peters, Debra P.C, Isabella Mariotto, Kris Havstad, and Leigh W Murray. 2006. "Spatial Variation in Remnant Grasses after a Grassland-to-Shrubland State Change: Implications for Restoration." *Rangeland Ecology and Management* 59 (4): 343-350.

- Peters, Debra, and Jeffrey Herrick. 2001. "Modelling vegetation change and land degradation in semiarid and arid ecosystems: An integrated hierarchical approach." *Monitoring and Modeling* 1 (2): 1-29.
- Peters, Debra, Isabella Mariotto, Kris Havstad, and Leigh Murray. 2006. "Spatial variation in remnant grasses after a grassland-to-shrubland state change: Implications for restoration." *Rangeland Ecology and Management* 59 (4): 343-350.
- Peters, DP C, B T Bestelmeyer, J E Herrick, E L Fredrickson, C Monger, and K M Havstad. 2006. "Disentangling complex landscapes: new insights into arid and semiarid system dynamics." *Bioscience* 56 (6): 491-501.
- Pimentel, David. 2006. "Soil erosion: A food and environmental threat." *Environment, Development and Sustainability* 8 (1): 119-137.
- Pimentel, David, C Harvery, P Resosudarmo, K Sinclair, D Kurz, M McNair, S Crist, et al. 1995. "Environmental and economic costs of soil Erosion and conservation benefits." *Science* 267 (5201): 1117-1123.
- Racha, M D, G S Okin, C Alexander, J E Herrick, and D P Peters. 2015. "Modifying landscape connectivity by reducing wind driven sediment redistribution, Northern Chihuahuan Desert, USA." *Aeolian Research* 17: 129-137.
- Ramawat, Gopal. 2010. *Desert Plants: Biology and Biotechnology*. Berlin Heidelberg: Springer.
- Ravi, S, D D Breshears, T E Huxman, and P D'Odorico. 2010. "Land degradation in drylands: Interactions among hydrologic–aeolian erosion and vegetation dynamics." *Geomorphology* 116 (3-4): 236-245.
- Ravi, S, P D'Odorico, D Breshears, J Field, A Goudie, T Huxman, J Li, et al. 2011. "Aeolian Processes and the Biosphere." *Reviews of Geophysics* 49 (3). doi:<https://doi.org/10.1029/2010RG000328> .
- Ravi, S, P D'Odorico, D D Breshears, J Field, A Gousie, T E Huxman, J Li, et al. 2011. "Aeolian Processes and the Biosphere." *Reviews in Geophysics* 49: 1-45.
- Reynold, James F, Mark Stafford Smith, Eric F Lambin, B L Turner II, Michael Mortimore, Simon P Butterbury, and Thomas E Dowing. 2007. "Global desertification: Building a Science for Dryland Development." *Science* 5826 (316): 847-851.
- Schlesinger, W H, J F Reynolds, G L Cunningham, L F Huenneke, W M Jarrell, R A Virginia, and W G Whitford. 1990. "Biological feedbacks in global desertification." *Science* 247: 1043-1048.

Stubbendick, James, Cheryl D Schmidt, Heidi L Hillhouse, and L M Landholt. 2010. "Influences of wind and sandblasting on the endangered blowout penstemon." *endangered Species Research* 9: 99-104. doi:doi: 10.3354/esr00246.

Turnbull, L, B P Wilcox, S Ravi, P D D'Odorico, D Childers, W Gwenzi, G Okin, J Wainwright, K K Caylor, and T Sankey. 2002. "Understanding the role of ecohydrological feedbacks in ecosystem state change in drylands." *Ecohydrology* 174-183.

USDA. 2017. Natural Resource Conservation Service: Plant Material Program. <https://www.nrcs.usda.gov/wps/portal/nrcs/main/plantmaterials/pmc/>.

Van Auken, OW. 2000. "Shrub invasions of North American semiarid grasslands." *Annual Review of Ecology and Systematics* 31: 197–215.

Wainwright, J, A J Parsons, and A D Abrahams. 1999. "Rainfall energy under creosotebush." *Journal of Arid Environments* 43 (2): 111-120.

Wainwright, J, A J Parsons, W H Schlesinger, and A D Abrahams. 2002. "Hydrology–vegetation interactions in areas of discontinuous flow on a semi-arid bajada, Southern New Mexico." *Journal of Arid Environments* 51 (3): 319-338.

Wiggs, Giles F, Sara L O'hara, Johannah Wegerdt, Joost Van Der Meer, Ian Small, and Richard Hubbard. 2003. "The dynamics and characteristics of aeolian dust in dryland Central Asia: possible impacts on human exposure and respiratory health in the Aral Sea basin." *The Geographical Journal* 169 (2): 142-157.

Chapter 3. Remote sensing of net primary productivity of Chihuahuan Desert vegetation: Evaluation of data retrieval and statistical approaches.

3.1 Abstract

An accurate assessment of net primary productivity (NPP) would be of great utility for regional and global studies of vegetation dynamics in drylands. We used two different remote sensing retrieval approaches and several statistical approaches to determine the ability of remote sensing to predict *in situ* estimates of NPP in the Chihuahuan Desert. We use Moderate Resolution Imaging Spectrometer (MODIS) estimates of vegetation productivity from the GPP (MOD17H3) and NPP (MOD17H2) products. In addition, we used a linear unmixing approach with MODIS nadir BRDF-adjusted reflectance (NBAR; MCD43A4) to retrieve cumulative estimates of green vegetation (GV), non-photosynthetic vegetation (NPV) and soil cover at seasonal and annual scales using multiple-endmember spectral mixture analysis (MESMA). Several statistical approaches were utilized to make predictions of *in situ* NPP, with this given set of remote sensing inputs, including simple regression, multiple regression, stepwise regression, and machine learning (Random Forest; RF). Our results indicate a very poor relationship between *in situ* NPP and standard NPP estimates from MODIS, though MODIS GPP was strongly correlated with *in situ* NPP with an overall coefficient of determination (R^2) of 0.52. When *in situ* NPP was regressed against MODIS GPP to allow a correction of MODIS-derived GPP, the overall root mean squared error (RMSE) was $64 \text{ g m}^{-2} \text{ y}^{-1}$. The correlations, corrections and associated errors varied were, nonetheless, different for each community type. MESMA-retrieved fractions were used to predict *in situ* NPP with multiple regression (with and without NPV) with the best R^2 (0.76) using annual average covers. Using stepwise regression, correlations between *in situ* NPP and predicted values improved significantly, the best correlation was found using annual estimates of tarbush cover ($R^2=0.91$,

RMSE = 5.5 g m⁻² y⁻¹). Random Forest using annual estimates of GV, NPV, and soil produced the best estimates of cover at community scale ($R^2 = 0.75 - 0.93$), at seasonal landscape ($R^2 = 0.86$, RMSE = 19.6 g m⁻² y⁻¹) and annual landscape ($R^2 = 0.92$, RMSE = g m⁻² y⁻¹) scales. RF was capable of capturing patterns of diversity and examining the complex relationship between *in situ* NPP and MESMA-derived fractions.

3.2 Introduction

As the main energy input to terrestrial ecosystems, net primary productivity (NPP) reflects the capacity of ecosystems to sustain life (Jobbagy et al. 2002; Sala et al. 1988; Yahdjian and Sala 2006). NPP is a primary factor in determining the amount of carbon sequestered in an ecosystem, and therefore it also controls an ecosystem's interplay with the global carbon cycle. As in other biomes, the response of NPP to climate is a key determinant of the functioning of the world's drylands (Baudena et al. 2007; Peters et al. 2006; Yahdjian and Sala 2006). In many regions of the world, including drylands, which cover ~ 40% of the Earth's terrestrial surface (Millenium Ecosystem Assessment 2005), environmental and climatic changes influence changes in vegetation productivity (Chapin et al. 2000; Havstad et al. 2006; Peters et al. 1995; Peters et al. 2006).

As a result, scientists and natural resource managers have called for new and more powerful approaches to identify and forecast trends in the dynamics of vegetation (Helman et al. 2014; Sims et al. 2007; Turner et al. 2006). Remote sensing is widely used to study vegetation structure and dynamics by monitoring the Earth surface. In the world's drylands, assessing vegetation structure and dynamics through remote sensing is a particular challenge because of specially-adapted leaf properties (leaf hairs, thick cuticles, heliotropism) that impact the spectral signature, low leaf area overall, and high soil cover that leads to multiple scattering (Huete 1988; Okin et al. 2001; Roberts

et al. 1997). In addition, heterogeneity of the soil spectral signature, which can be considerably greater than that of the green vegetation (GV) and nonphotosynthetic vegetation (NPV) components, can contribute to variability in drylands where the soil component tends to dominate spectral reflectance (Escafa del and Huete 1991; Okin 2010; Okin et al. 2012; Smith et al. 1990). The difference in spectral signature between soil and vegetation has made the estimation of productivity from the world's drylands using remote sensing especially difficult. Reeves et al. (2006), for example, found the presence of significant NPV material as a source of error and suggested that NPP in grasslands is best estimated during years of high productivity. Turner et al. (2006) found that estimation of gross primary productivity (GPP), a fundamental input for estimating NPP, in dryland sites was often affected by poor estimation of the fraction of photosynthetically active radiation that is absorbed (FPAR), possibly due to contamination by the soil signature. Sims et al. (2007) have also reported that FPAR is underestimated in regions where the surface is heterogeneous. The MODIS NPP algorithm is primarily dependent on live woody and biomass respiration at 20°C and leaf annual growth respiration (Running and Zhao 2015). MODIS NPP has been reported to unreliably estimate biomass productivity at regions of high temperature and low vegetation cover, which is to say, hot deserts (Sims et al. 2007).

In this paper, we revisit the ability to adequately estimate NPP in drylands using optical remote sensing using a unique, relatively long time series of *in situ* aboveground NPP measurements that coincide with the MODIS era. We utilize aboveground NPP data from Chihuahuan Desert shrub and grass communities in the Jornada Basin in south-central New Mexico, USA, where, as part of the NSF Long Term Ecological Research (LTER) program, where NPP has been measured for nearly three decades (Huenneke et al. 2002; Huenneke et al. 2003; Peters et al. 2006).

To emphasize the need for new approaches, we first examine standard MODIS GPP and NPP products (MOD17A2H and MOD17A3H, respectively). The MODIS NPP product includes both above and belowground components of annual productivity, whereas our *in situ* data only estimate aboveground annual productivity. Despite this, we anticipate that, if the MODIS NPP product is making useful estimates, linear relationships with aboveground *in situ* NPP will appear.

Because spectral contamination by NPV and the soil has been implicated in degrading the ability of optical remote sensing to estimate NPP in drylands (Reeves et al. 2006), we hypothesize that approaches that include these components may be able to improve dryland NPP estimates. Linear spectral unmixing (Shimabukuro and Smith 1991) is a common approach for separating the spectral contributions of GV, NPV, and soil (Asner and Heidebrecht 2002; Guerschmann et al. 2009; Okin et al. 2001; Roberts et al. 1998). Considerable variability in spectral reflectance, particularly of NPV and soil, is a challenge to simple spectral unmixing in drylands (Okin et al. 2001). Therefore, in this study, we use multiple endmember spectral mixture analysis (MESMA), which was developed to deal with spectral variability of endmember classes (Dennison and Roberts 2003; Roberts et al. 1998).

Because the fractional covers of GV, NPV, and soil have not been put into a mechanistic framework for estimating NPP, we rely on empirical approaches here, including simple regression, multiple regression, stepwise regression, and machine learning. Machine learning comprises a relatively new set of tools for finding relationships in data. Here, we use Random Forest (RF; Breiman 1996) which, because of its bagging (i.e., bootstrap aggregating) approach, allows even small dataset to be sampled multiple times, making RF models resilient to sample insufficiency (Breiman 2001).

3.3 Methods

3.3.1 Study site

The Jornada Basin LTER site is in the northern Chihuahuan Desert, approximately 25 km northeast of Las Cruces, NM around 32.6°N, -106.7°E at an elevation of 1315 meters. The Jornada is one of the premier sites globally to study changes in dryland ecosystems especially the conversion of grasslands to shrublands, often considered a form of land degradation (Fredrickson et al. 2005; Havstad et al. 2006). At the Jornada, over the past 150 years, grassland communities have become increasingly dominated by shrubs, with honey mesquite (*Prosopis glandulosa*) and creosote (*Larrea tridentata*) being the most widespread grass-replacing species (Gibbens et al. 2005; Peters et al. 2006).

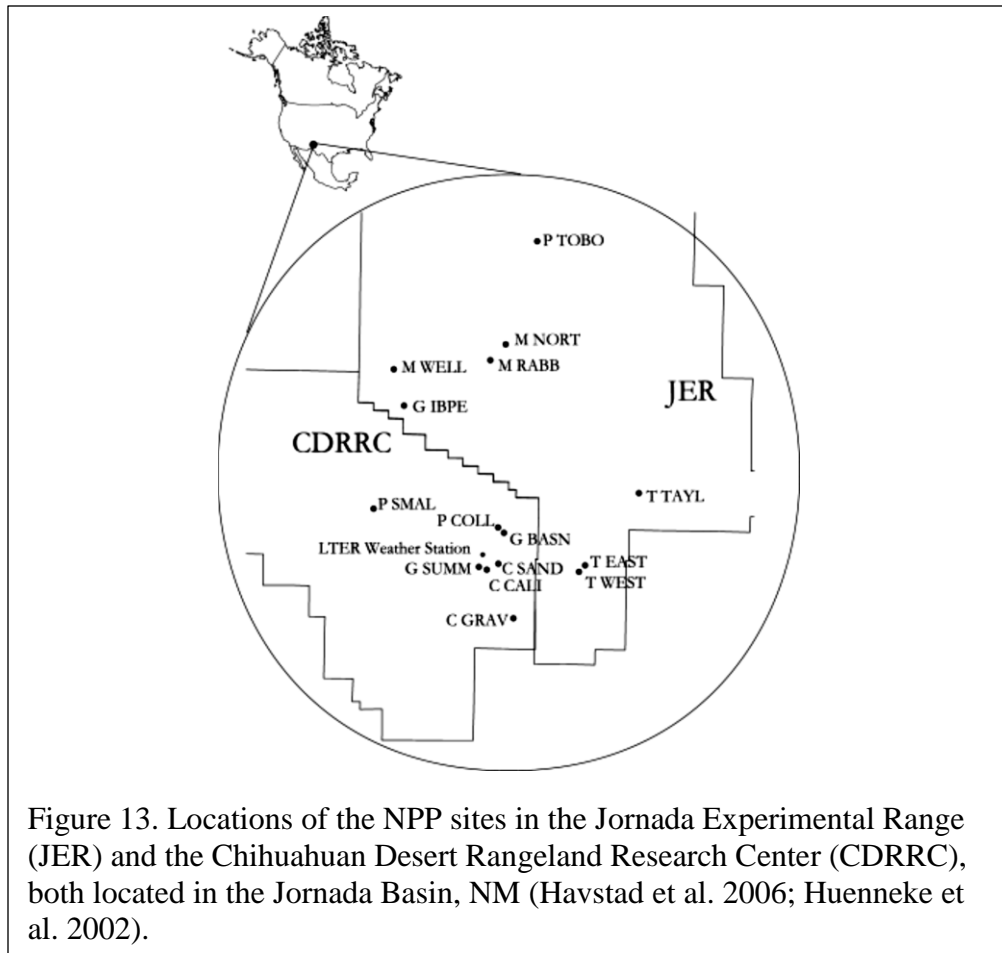


Figure 13. Locations of the NPP sites in the Jornada Experimental Range (JER) and the Chihuahuan Desert Rangeland Research Center (CDRRC), both located in the Jornada Basin, NM (Havstad et al. 2006; Huenneke et al. 2002).

Most of the annual precipitation (80%) at Jornada occurs during the summer monsoon season, with little spring rainfall (Oliver 2008; Wainwright et al. 1995). The basin has a mean annual precipitation of ~240 mm, and average temperatures that range between 13°C (winter) and 36°C (summer) (Alvarez et al. 2011; Dodson 2012; Gibbens et al. 2005; Peters et al. 2006). Our study includes seven plots located in the 78,266-acre Jornada Experimental Range (JER) operated by USDA Agricultural Research Service, and five plots at the Chihuahuan Desert Rangeland Research Center (CDRRC) (Figure 13; Havstad et al. 2006; Huenneke et al. 2002). At these 12 long-term NPP sites, NPP of the entire community has been measured since 1989 (Peters et al. 2006). There are three plots in each of five vegetation communities dominated by either grass, mesquite, creosote, tarbush, or playa vegetation. Individual sites are labeled with a first letter indicating the vegetation community (e.g., M for mesquite) and an additional four-letter identifier. Some plots indicate soil type such as C-GRAV, which refers to gravel soil. We did not include the playa sites in this study because the playas are smaller compared to the size of a 500-m MODIS pixel. When these sites were installed, they were not chosen as replicates, but rather to represent the diversity of sites with different communities across the basin (Table 9). In this sense, they are ideal for the present study because of this variability.

Table 9. Site, dominant plants, soil type and year of fencing of our study sites. Each community includes three plots of most common plant communities. Fences were built to protect the plots from grazing and human interruption (Havstad et al. 2006; Huenneke et al. 2002). Average NPP over 15 years for each plot ($\text{g m}^{-2} \text{y}^{-1}$).

Site	Dominant Plants	Soil Type	Year Fenced	Average NPP
<i>Creosote Bush</i>				
Caliche (CALI)	<i>Larrea tridentata</i> <i>Xaathocephalum microplalum</i> <i>Aristida wrightii</i>	Algerita	1970s	41.1
Gravel (GRAV)	<i>L. Tridentata</i> <i>Prosopis glandulosa</i> <i>Muhlenbergia partieri</i>	Casito-Terino	1970s	95.2
Sand (SAND)	<i>L. tridentate</i> <i>Muhlenbergina porter</i> <i>Opuntia imbricata</i>	Onite-Pajarito loamy soil	1982	129.5
<i>Grasslands</i>				
Basin (BASN)	<i>Bouteloua eriopoda</i> <i>Sporobolus cryptandurus</i> <i>Ephedra trifurca</i>	Berino-Dona Ana sandy loam	1982	151.2
IBP (IBPE)	<i>Yucca elata</i> <i>B. eriopoda</i> <i>S. flexuosus</i>	Onite-Pajarito loamy sand	1962	140.9
Summerford (SUMM)	<i>Y. elata</i> <i>B. eriopoda</i> <i>E. trifurca</i>	Alladin gravel-sandy loam	1970s	184.2
<i>Mesquite</i>				
North (NORT)	<i>P. glandulosa</i> <i>X. saranthrae</i> <i>M. porteri</i>	Onite-Pintura loamy sand	1931	130.4
Rabbit (RABB)	<i>P. glandulosa</i> <i>Portulaca retusa</i> <i>Salsala kali</i>	Onite-Pintura loamy sand	1931	151.4
West Well (WELL)	<i>P. glandulosa</i> <i>X. saranthae</i> <i>M. porteri</i>	Wink-Harrisburg sandy loam	1989	136.2
<i>Tarbush</i>				
East (EAST)	<i>Flourensia cernuo</i> <i>M. porter</i> <i>Lycium berlandieri</i>	Stellar clay loam	1989	88.9
Taylor Well (TAYL)	<i>F. cernuo</i> <i>Scleropagan brevifolius</i> <i>M. porteri</i>	Dona Ana-Reagan sandy loam	1989	71.0
West (WEST)	<i>F. cernuo</i> <i>Scleropagan brevifolius</i> <i>Pleuraphis mutica</i>	Stellar clay loam	1989	69.0

3.3.2 Field data

Our analysis includes 15 years of NPP data from 2000 to 2015 for 12 NPP measurement sites that overlap the MODIS era, which began in 2000. Each NPP site is a 70 m x 70 m grid of 49 permanent 1-m² quadrats separated by 10-m in each cardinal compass direction. Sampling occurs three times per calendar year and is done on a per-species basis. Additional information on the sampling methods can be found in Huenneke et al. (2002). In this study, NPP summed over all species in the plots was used and thus represents community-wide productivity. The mean annual *in situ* NPP over all communities of the 15-year record (2000-2015) was 120 g m⁻² y⁻¹.

3.3.3 MODIS Data products

The MODIS 500-m resolution annual NPP product (MOD17A2H) as well as the 16-day 500-m GPP product (MOD17A3H) were downloaded from NASA's EarthData tool (<https://search.earthdata.nasa.gov>) and were used as the benchmark for our accuracy assessment. The MODIS17 products are based on the radiation use efficiency and assumes the productivity of vegetation under stable moisture and fertilization conditions is related to the amount of absorbed solar radiation (Turner et al. 2006; Zhao et al. 2004). Daily GPP estimates are based on the conversion of the fraction of photosynthetically active radiation to gross carbon uptake via a biome-specific efficiency parameter (light use efficiency), minimum temperature, vapor pressure deficit, and incoming shortwave radiation (Zhao et al. 2004). Annual NPP is the sum of daily rates over the growing season, once estimated biome-specific respiration costs have been deducted.

Pixels containing each NPP site at Jornada were extracted from images (i.e., nearest neighbor) for the appropriate time periods. NPP data are available as annual estimates. Annual GPP values were calculated as the sum of 16-day GPP composite estimates over each year.

A linear correction was applied in which *in situ* NPP was regressed against the uncorrected estimates of GPP (GPP_U) using linear least squares to obtain a gain and offset term so that corrected NPP (NPP_C) could be calculated:

$$NPP_C = offset + gain * GPP_U. \quad (3)$$

3.3.4 Spectral unmixing of MODIS NBAR

MESMA is a variant of spectral mixture analysis that unmixes each pixel with many models (i.e., sets of spectral endmembers) and chooses the best model based on some criterion (here, the spectral root mean squared error). The basic unmixing equations is:

$$\rho' = \sum_{i=1}^m f_i * \rho_i + \varepsilon, \quad (4)$$

where ρ' is the pixel spectrum, ρ_i is the reflectance spectrum of endmember i , f_i is the fraction of each endmember, and m is the number of endmembers. The residual is expressed as ε which represents the unmodeled spectral error, from which a spectral root mean squared error (RMSEs) can be calculated.

Here, we used three sets of endmembers representing GV, NPV and soil. In our analysis, we normalized the estimated GV, NPV and soil by dividing each endmember fraction by the sum of all three endmember fractions to force the endmember fractions to sum to one after linear least squares unmixing. Details on the unmixing approach used in this study can be found in Okin and Gu (2015).

To generate models for MESMA, an extensive library of endmember spectra of GV, NPV, and soil is needed (Adams et al. 1993; Bell et al. 2002; Dennison and Roberts 2003; Okin et al. 2001; Okin et al. 2012). Our library consisted of 326 spectra of GV, 330 spectra of NPV, and 160 spectra of soil. Spectra were derived from a combination of our own field measurements (Meyer and Okin 2015) and field and laboratory spectra available in several datasets, including the USGS

Spectral Library (Kokaly et al. 2017), the ASTER spectral library (Baldrige et al. 2009) and the ISRIC soil spectral library (ISRIC 2010). A total of 1000 three endmember models, randomly selected from all possible combinations among the GV, NPV, and soil endmember spectra were used in these computations.

For spectral unmixing, we used 16-day 500 m MODIS nadir BRDF-adjusted reflectance (NBAR) data (MCD43A4) available on EarthData. Pixels containing each NPP site at the Jornada Basin were extracted from images (i.e., nearest neighbor). All dates (i.e., 46 images per year) from 2000 to the end of 2015 were unmixed using MESMA for NBAR pixels corresponding to each of the 12 NPP sites. Two approaches were used to obtain yearly GV, NPV, and soil values that could be compared with the annual *in situ* NPP estimates. In the first approach (called hereafter ‘seasonal’), total growing season fractional cover was estimated by summing MESMA endmember fractions derived by unmixing 16-day composite NBAR data for which the first day of the 16-day composite falls between April 1st to October 31st (28 values per year). In the second approach (called hereafter, ‘annual’), MESMA endmember fractions were summed over the entire year (46 values per year).

3.3.5 Estimating NPP from MESMA fractions

Three approaches were used to estimate NPP from MESMA-derived GV, NPV, and soil fractions: multiple regression, stepwise regression, and random forest (RF). Seasonal and annual estimates of total fractional cover were utilized separately so that we could assess the best provided estimates. Regression models treated *in situ* NPP as the dependent variable and either seasonal or annual estimates of total fractional cover of GV, NPV and soil as the independent variables.

Analysis were done at plot, community, landscape scales. In the plot-level analyses, separate models were made for each NPP plot utilizing the 15 years of data for each plot (n =15).

In the community-level analyses, plots representing the same communities (i.e., creosote, mesquite, grass, tarbush) were pooled using all years of data ($n = 3 \times 15 = 45$). In the landscape level analyses, all plots were pooled, regardless of community and year ($n = 12 \times 15 = 180$).

Multiple regression was performed in two ways. In the first, we used the fractional cover of GV, NPV, and soil as predictors:

$$NPP_{Estimated} = c_0 + c_{GV} f_{GV} + c_{NPV} f_{NPV} + c_{soil} f_{soil}, \quad (5)$$

where c_0 is a constant, c are coefficients and f refer to the fractional cover (annual or seasonal totals) estimates for GV, NPV, and soil. Exploratory analysis indicated that NPV contributed least to the multiple regression predictions of NPP and had the lowest R^2 when correlated with *in situ* NPP. Since the fractions must sum to one, and therefore removal of one endmember does not necessarily result in a loss of information, a second set of multiple regression estimates were made using only GV and soil fractions.

Stepwise Regression utilizing the forward selection process was used (Efroymson 1960). Stepwise regression is designed to find the most useful variables to include in the regression model by exhausting all possible combinations of predictor variables without losing a significant portion of the explanatory power of the dataset. Here we use all three variables (fractional cover of GV, NPV, and soil) as inputs to the stepwise regression model. At each step, an independent variable is added based on its ability to improve root mean squared error (RMSE) of the estimates:

$$RMSE = \left(\sum_{j=1}^n (NPP_{Estimated}^j - NPP_{in\ situ}^j)^2 \right)^{1/2} \quad (6)$$

where NPP^j represents the NPP estimate for the j^{th} pixel or plot from either the regression ('Estimated') or field estimate ('*in situ*'), respectively, and n is the total number of plot-years under consideration. The value of n varied depending on whether analyses were being done at the plot, community, or landscape levels.

Random forest (RF; Breiman 2001), a machine learning algorithm, is an ensemble method often used for non-linear regression analysis in various disciplines (Pal 2007). RF has three qualities that make it useful in this study. Specifically, it is resilient to sample insufficiency, relatively insensitive to outliers, and robust against overfitting (Breiman et al. 2006).

RF is characterized by a bagging approach which depends on creating a set of bootstrapped samples as training data. RF builds multiple trees independently by using different bootstrapped sample subsets of the training data. Each tree in the forest consists of nodes, where each node in a tree splits by using a randomly chosen independent variable among the entire set of the independent variables in the dataset. After one tree is built, the model chooses the best split at each node which is determined based on the homogeneity measures (here, mean squared error; Auret and Aldrich 2012; Breiman 2001). After all trees are built, the average values of the prediction of each tree are recorded and outputted as the final result.

In this study, we treated GV, NPV, and soil cover (either seasonal or annual) as independent variables while *in situ* NPP was treated as the dependent variable. Analyses were done at community and landscape levels. Each forest contained 50 trees. We used a 70%/30% split between training and out-of-bag (OOB) data for cross validation.

3.3.5.1 Estimation of Error

For all predictions, RMSE (Eq. 7) and coefficient of determination (R²) were calculated. In addition, we calculated mean error (ME), which is an indicator of bias:

$$ME = \sum_{j=1}^m (NPP_{Estimated}^j - NPP_{in\ situ}^j). \quad (7)$$

For all correlations between *in situ* and predicted values we estimated the significance (i.e., p-value) of the relationship using an F-test for the significance of the slope.

3.4 Results

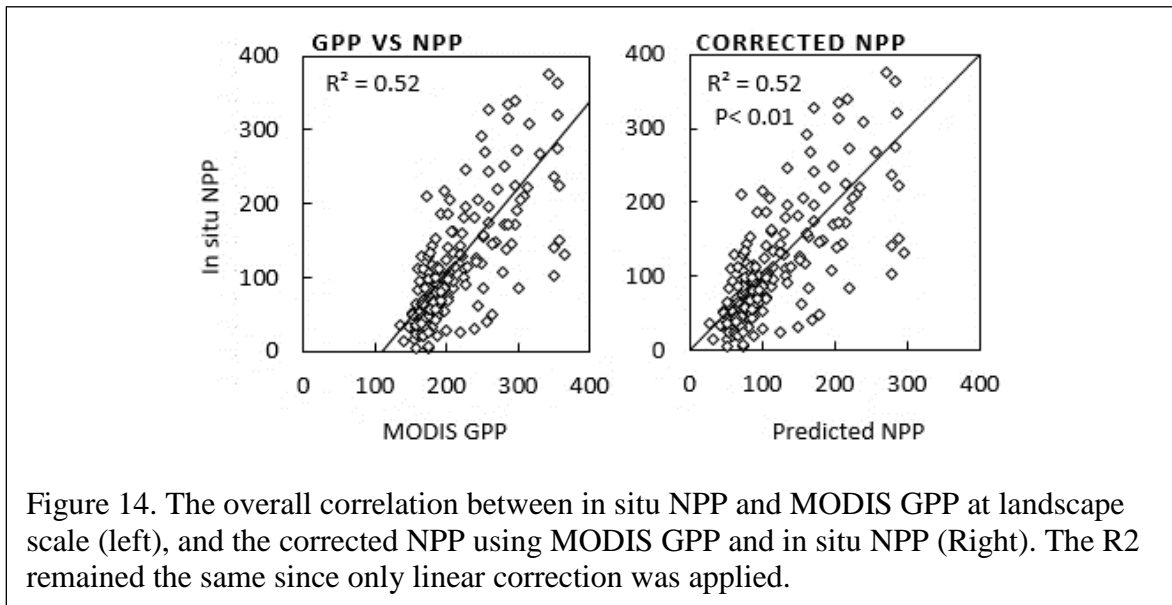
3.4.1 Standard MODIS GPP and NPP products

We found no correlation between *in situ* NPP estimates and MODIS-derived NPP (MOD17A3H) at the plot, community or landscape scales, with R^2 not exceeding 0.08 in any case (Table 10).

Table 10. Plot, community and landscape estimates of NPP, and “n” points of observation in each correlation in these scales. Coefficient of determination (R^2), y-intercept (b), slope of the regression between in situ NPP (Y) and MODIS NPP (X , left side of table) and MODIS uncorrected GPP (X , right side of table), RMSE ($\text{g m}^{-2} \text{y}^{-1}$), and ME ($\text{g m}^{-2} \text{y}^{-1}$) of the regressions between corrected MODIS GPP (GPP_C) and in situ NPP at plot, community and landscape scales. The regression between in situ NPP and corrected GPP is determined to be significant: p -value < 0.01 at all scales.

Site	n	NPP			GPP			RMSE	ME
		R^2	b	Slope	R^2	b	Slope		
<i>TWEST</i>	15	0.04	114	<0.1	0.65	99	0.97	112	0.5
<i>TEAST</i>	15	0.01	117	<0.1	0.69	100	0.92	90	0.4
<i>TTAYL</i>	15	0.02	110	0.1	0.46	98	0.57	61	0.5
<i>Tarbush</i>	45	0.01	112	<0.1	0.53	89	0.87	26	0.5
<i>MRABB</i>	15	0.01	180	<0.1	0.46	86	0.53	83	16
<i>MWELL</i>	15	0.02	126	<0.1	0.62	91	0.54	110	7.3
<i>MNORT</i>	15	0.06	146	<0.1	0.69	99	0.64	119	-16
<i>Mesquite</i>	45	0.04	130	<0.1	0.61	96	0.57	51	1.2
<i>GIBPE</i>	15	0.01	143	<0.1	0.25	74	0.31	57	0.1
<i>GSUMM</i>	15	0.07	130	0.1	0.42	79	0.33	48	14
<i>GBASN</i>	15	0.07	104	0.1	0.86	76	0.82	110	2.0
<i>Grass</i>	45	0.03	140	0.1	0.43	88	0.42	53	5.0
<i>CCALI</i>	15	0.03	145	<0.1	0.36	84	0.35	84	10
<i>CSAND</i>	15	0.08	164	<0.1	0.34	80	0.78	60	-5.0
<i>CGRAV</i>	15	0.03	132	<0.1	0.73	119	0.72	72	7.0
<i>Creosote</i>	45	0.02	137	<0.1	0.34	77	0.36	44	1.0
<i>Landscape</i>	180	0.05	98	0.2	0.52	85	0.94	64	0.2

In contrast, coefficients of determination between *in situ* NPP estimates and MODIS-derived GPP (MOD17A2H) were considerably higher, ranging from $R^2 = 0.25 - 0.86$ at the plot scale, and $R^2 = 0.34 - 0.61$ at the community scale (Table 10). High variability in the correlation between *in situ* NPP and MODIS-derived GPP was observed among plots within communities, ranging, in the extreme case (grass), from $R^2 = 0.25$ (GIBPE), the lowest correlation seen among all plots, to $R^2 = 0.86$ (GBASN), the highest correlation seen among all plots. Using all plots, at the landscape scale, MODIS GPP explained about half of the variance in the *in situ* data ($R^2 = 0.52$). The coefficients of determination of the regression of *in situ* NPP against MODIS-derived GPP varied from 0.34 – 0.61 at the community level. The landscape level, $R^2 = 0.52$. In all cases, the intercepts of these regressions were positive with some slopes close to 1 (Table 10).



Since only linear correction was applied on MODIS-derived GPP, R^2 of the corrected MODIS GPP regressed against *in situ* NPP were identical to those found in the correlation between *in situ* NPP and uncorrected MODIS GPP at plot, community and landscape scale (Table 10).

RMSE at the plot scale ranged between 48 – 112 g m⁻² y⁻¹ and 26 – 53 g m⁻² y⁻¹ at community level. At landscape level, RMSE was 64 g m⁻² y⁻¹ with very low ME (0.2 g m⁻² y⁻¹).

3.4.3 Multiple regression

Generally, GV and NPV fractions showed positive correlations with *in situ* NPP, whereas soil showed negative correlations with NPP (Table 11). The individual correlations between *in situ* NPP values and MESMA-derived GV and soil fractions were more frequently significant than those of NPV fractions, regardless of whether annual or seasonal MESMA results were used. This is true at the plot, community, and landscape scales.

Table 11. Site, variable correlation coefficient (R2), variable slope (c_{variable}), variable significance (p_{variable}), y-intercept (b), RMSE, R2 and the significance of the 3-variable multiple regression models between in situ NPP and GV, NPV and soil (seasonal and annual) at plot community type and landscape scales.

Site	GV	c _{GV}	p _{GV}	NPV	c _{NPV}	p _{NPV}	Soil	c _{soil}	p _{soil}	b	RMSE	R ²
TWEST _{seasonal}	0.45	937	<0.01	0.19	519	0.09	0.30	146	<0.01	-214	27.5	0.55
TEAST _{seasonal}	0.51	1331	<0.01	0.19	614	0.09	0.28	350	<0.01	-371	25	0.65
TTAYL _{seasonal}	0.03	140	0.12	0.05	-318	0.20	0.04	721	0.80	19.5	38.8	0.41
<i>Tarbush</i> _{seasonal}	0.3	275	<0.01	0.31	290	<0.01	0.22	172	0.01	-98	30.3	0.27
MRABB _{seasonal}	0.29	2183	<0.01	0.1	550	0.06	0.21	-608	0.01	-315	78.5	0.37
MWELL _{seasonal}	0.44	2026	<0.01	0.2	254	0.04	0.25	285	<0.01	-329	53.4	0.46
MNORT _{seasonal}	0.48	3023	<0.01	0.1	750	0.06	0.21	640	0.01	-729	64.2	0.54
<i>Mesquite</i> _{seasonal}	0.44	796	<0.01	0.01	104	0.20	0.2	-271	0.01	140	36.6	0.29
GIBPE _{seasonal}	0.1	-97	0.09	0.01	-118	0.20	0.14	-395	0.02	634	59.8	0.28
GSUMM _{seasonal}	0.35	1562	<0.01	0.1	1859	0.05	0.14	454	0.02	322	13.9	0.70
GBASN _{seasonal}	0.26	-142	<0.01	0.02	-1106	0.05	0.41	-936	<0.01	875	39.4	0.35
<i>Grass</i> _{seasonal}	0.48	24	<0.01	0.25	-29	<0.01	0.36	-20	<0.01	142	33.6	0.33
CCALI _{seasonal}	0.07	193	0.07	0.33	-209	<0.01	0.21	-139	0.01	170	16.1	0.28
CSAND _{seasonal}	0.24	726	<0.01	0.01	-71	0.60	0.07	-289	0.80	208	35.8	0.38
CGRAV _{seasonal}	0.17	380	0.11	0.05	-260	0.70	0.07	-97	0.70	174	40.8	0.22
<i>Creosote</i> _{seasonal}	0.14	151	0.12	0.01	48	0.70	0.05	-99	0.60	106	41.9	0.23
<i>Landscape</i> _{seasonal}	0.18	107	0.11	0.1	26	0.03	0.1	-131	0.04	96	51.6	0.49
TWEST _{annual}	0.34	1075	<0.01	0.19	676	0.10	0.3	197	<0.01	-274	35.4	0.36
TEAST _{annual}	0.44	1729	<0.01	0.12	892	0.80	0.28	488	<0.01	-512	29.7	0.58
TTAYL _{annual}	0.35	1508	<0.01	0.02	567.6	0.06	0.06	291	0.70	-334	44.8	0.52
<i>Tarbush</i> _{annual}	0.37	1398	<0.01	0.10	642	0.04	0.23	274	<0.01	-329	29.8	0.42
MRABB _{annual}	0.41	2162	<0.01	0.17	1013	0.09	0.25	419	<0.01	-519	74.1	0.45
MWELL _{annual}	0.49	3043	<0.01	0.10	370	0.05	0.37	801	<0.01	-683	55.4	0.51
MNORT _{annual}	0.62	1378	<0.01	0.25	27	<0.01	0.37	-341	<0.01	-683	80.8	0.37
<i>Mesquite</i> _{annual}	0.35	1972	<0.01	0.15	385	0.07	0.27	55	<0.01	-182	44.5	0.37
GIBPE _{annual}	0.21	2.3	0.09	0.05	-845	0.70	0.12	-	0.03	815	57.3	0.53
GSUMM _{annual}	0.73	2512	<0.01	0.08	-15	0.50	0.38	230	<0.01	207	75.3	0.62
GBASN _{annual}	0.41	1219	<0.01	0.03	-31	0.90	0.34	-307	<0.01	178	41.1	0.53
<i>Grass</i> _{annual}	0.31	1675	<0.01	0.13	282	0.70	0.06	1675	0.70	-75	71.5	0.36
CCALI _{annual}	0.39	546	<0.01	0.10	144	0.06	0.18	-37	0.04	-39	12.9	0.47
CSAND _{annual}	0.43	1070	<0.01	0.10	-289	0.07	0.21	-389	0.01	283	33.1	0.53
CGRAV _{annual}	0.26	1118	<0.01	0.12	650	0.70	0.1	-107	0.04	-74.8	31.9	0.24
<i>Creosote</i> _{annual}	0.22	83	0.08	0.10	-128	0.06	0.12	-58	0.03	124	32.6	0.32
<i>Landscape</i> _{annual}	0.18	766	0.09	0.13	111	0.60	0.38	420	<0.01	206	55.1	0.50

The three-variable multiple regressions, utilizing MESMA-derived fractions of GV, NPV, and soil, showed higher overall R^2 when using annual MESMA-derived fractions than when using seasonal MESMA-derived fractions. The tarbush community showed the best overall model ($R^2 = 0.42$, $RMSE = 29.8 \text{ g m}^{-2} \text{ y}^{-1}$, Table 11), with creosote community not yielding a significant model at all. The overall correlations for the grass and mesquite communities were approximately the same. Pooling all communities at the landscape scale, there was almost no difference in the amount of variance explained by the seasonal ($R^2 = 0.49$, $RMSE = 51.6 \text{ g m}^{-2} \text{ y}^{-1}$) and annual ($R^2 = 0.50$, $RMSE = 55.1 \text{ g m}^{-2} \text{ y}^{-1}$) MESMA-derived variable, with both providing significant overall models ($p < 0.01$).

Because NPV did not appear to be significantly correlated with *in situ* NPP (Table 11), we calculated multiple regressions between MESMA-derived fractions of GV and soil (excluding NPV fractions) and *in situ* NPP. The results of these two-variable multiple regressions (Table 12) indicate higher correlations and lower RMSEs for the overall model compared to the three-variable regressions utilizing NPV. We did not calculate Akaike Information Criteria (AIC) values in comparison of two- and three-variable models because prediction improvement associated with removal of a variable clearly indicates that the two-variable models are better (that is, more parsimonious and better predictors). The biggest improvement in this case appears to be for the creosote community, where the overall model R^2 went from 0.23 ($p = 0.73$) to 0.62 ($p < 0.01$) when using seasonal MESMA-derived fractions and from 0.32 ($p = 0.50$) to $R^2 = 0.77$ ($p < 0.01$) when using annual MESMA-derived fractions. These two-variable multiple regression model results explain 62% - 88% of the variance in observed *in situ* NPP. At the landscape scale, modest improvement was seen compared to the three-variable models, with the overall best landscape-

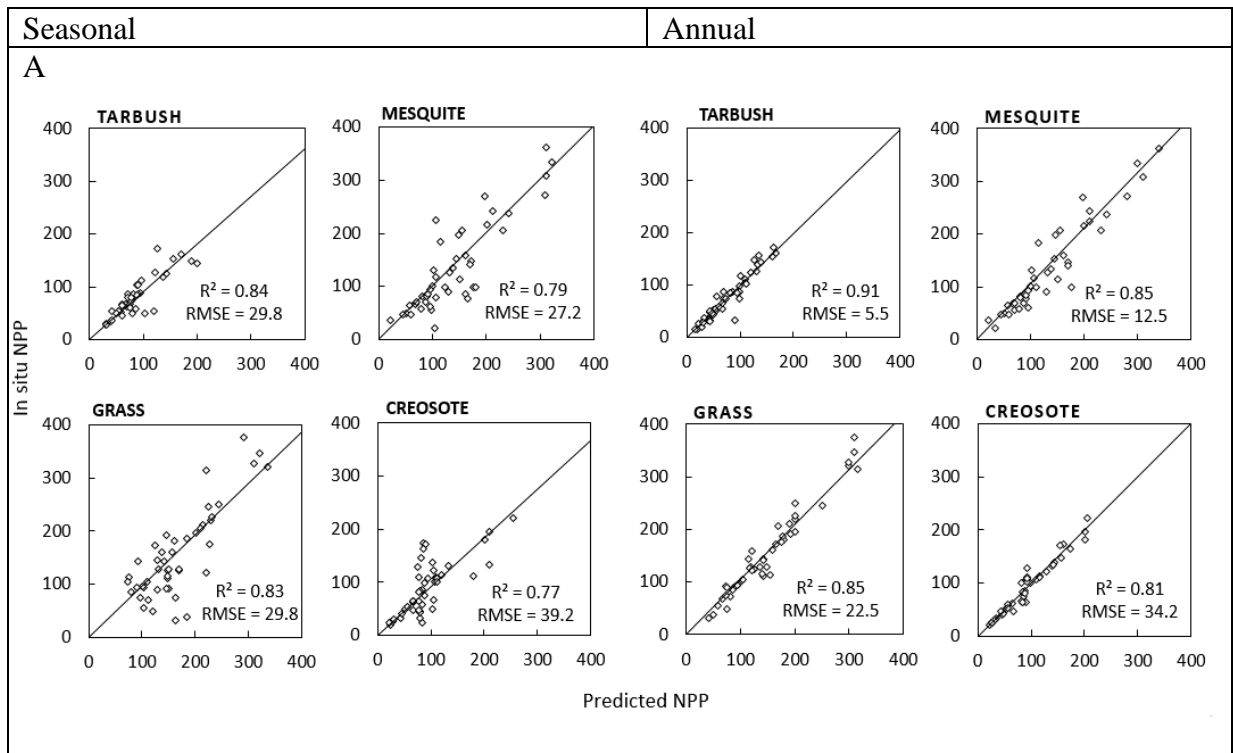
scale model being the two-variable model utilizing annual MESMA-derived fractions of GV and soil ($R^2 = 0.76$, $RMSE = 31.2 \text{ g m}^{-2} \text{ y}^{-1}$).

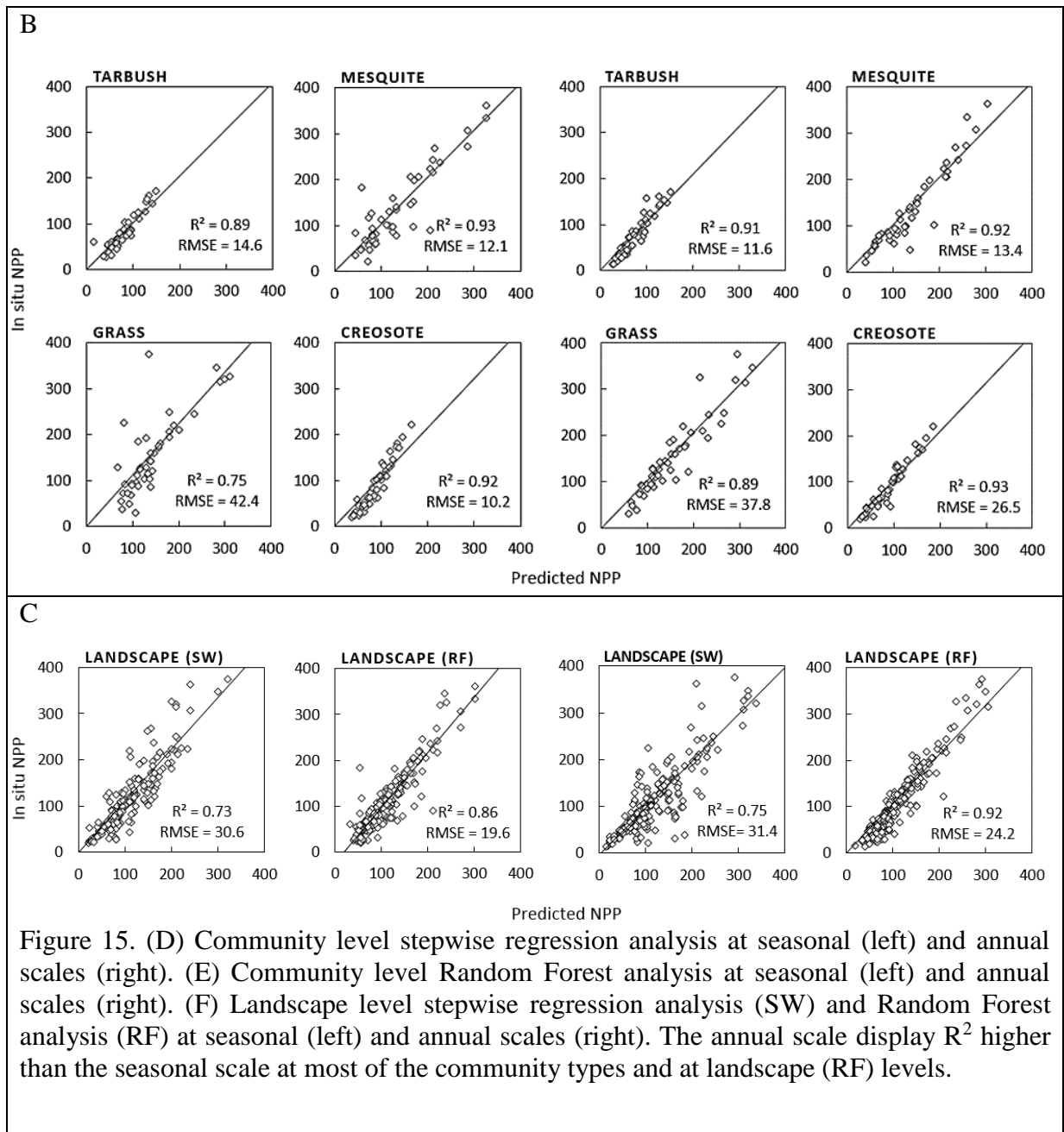
Table 12. Site, variable correlation coefficient (R²), slope (c_{variable}), variable significance (p_{variable}), y-intercept (b), RMSE, R² and the significance of the 2-variable multiple regression model between in situ NPP and GV and soil (seasonal and annual) at plot community type and landscape scales.

Site	GV	c _{GV}	p _{GV}	Soil	c _{soil}	p _{soil}	b	RMSE	R ²	p-value
TWEST _{seasonal}	0.45	605	<0.01	0.30	-142	<0.01	78	30.9	0.62	<0.01
TEAST _{seasonal}	0.51	853	<0.01	0.28	-58	<0.01	20	29.8	0.71	<0.01
TTAYL _{seasonal}	0.03	454	0.12	0.04	-157	0.80	18	40.8	0.44	<0.01
<i>Tarbush</i> _{seasonal}	0.3	271	<0.01	0.22	-53	0.01	51	20.8	0.81	<0.01
MRABB _{seasonal}	0.29	1709	<0.01	0.21	-379	0.01	95	79.6	0.51	<0.01
MWELL _{seasonal}	0.44	1859	<0.01	0.25	141	<0.01	-175	52.5	0.55	<0.01
MNORT _{seasonal}	0.48	2226	<0.01	0.21	091	0.01	-67	67.9	0.48	<0.01
<i>Mesquite</i> _{seasonal}	0.44	144	<0.01	0.2	-72	0.01	58	34.7	0.76	<0.01
GIBPE _{seasonal}	0.1	419	0.09	0.14	-336	0.02	241	53.2	0.28	<0.01
GSUMM _{seasonal}	0.35	1909	<0.01	0.14	129	0.02	-110	13.6	0.73	<0.01
GBASN _{seasonal}	0.26	538	<0.01	0.41	-412	<0.01	288	44.2	0.51	<0.01
<i>Grass</i> _{seasonal}	0.48	38	<0.01	0.36	-49	<0.01	89	35.1	0.83	<0.01
CCALI _{seasonal}	0.07	90	0.07	0.21	-85	0.01	71	14.8	0.42	<0.01
CSAND _{seasonal}	0.24	790	<0.01	0.07	-251	0.80	167	35.9	0.48	<0.01
CGRAV _{seasonal}	0.17	-17	0.11	0.07	647	0.70	67	31.1	0.37	<0.01
<i>Creosote</i> _{seasonal}	0.14	36	0.12	0.05	-81	0.60	166	41.9	0.62	<0.01
<i>Landscape</i> _{seasonal}	0.18	32	0.11	0.1	-44	0.04	81	48.6	0.64	<0.01
TWEST _{annual}	0.34	590	<0.01	0.3	-166	<0.01	95	35.2	0.42	<0.01
TEAST _{annual}	0.44	865	<0.01	0.28	-151	<0.01	83	27.7	0.67	<0.01
TTAYL _{annual}	0.35	1069	<0.01	0.06	-159	0.70	62	44.8	0.66	<0.01
<i>Tarbush</i> _{annual}	0.37	820	<0.01	0.23	-151	<0.01	77	13.6	0.88	<0.01
MRABB _{annual}	0.41	2438	<0.01	0.25	-229	<0.01	19	65.9	0.62	<0.01
MWELL _{annual}	0.49	2696	<0.01	0.37	502	<0.01	-406	22.9	0.58	<0.01
MNORT _{annual}	0.62	1340	<0.01	0.37	-372	<0.01	187	71.3	0.43	<0.01
<i>Mesquite</i> _{annual}	0.35	1699	<0.01	0.27	-261	<0.01	99	22.1	0.87	<0.01
GIBPE _{annual}	0.21	572	0.09	0.12	-401	0.03	247	41.4	0.58	<0.01
GSUMM _{annual}	0.73	3245	<0.01	0.38	411	<0.01	-335	52.7	0.69	<0.01
GBASN _{annual}	0.41	1259	<0.01	0.34	-293	<0.01	159	38.8	0.55	<0.01
<i>Grass</i> _{annual}	0.31	1299	<0.01	0.06	-164	0.70	089	30.2	0.73	<0.01
CCALI _{annual}	0.39	414	<0.01	0.18	-66	0.04	22	12.8	0.58	<0.01
CSAND _{annual}	0.43	1251	<0.01	0.21	-279	0.01	153	22.7	0.50	<0.01
CGRAV _{annual}	0.26	873	<0.01	0.1	-90	0.04	78	28.6	0.43	<0.01
<i>Creosote</i> _{annual}	0.22	80	0.08	0.12	-33	0.03	86	24.3	0.77	<0.01
<i>Landscape</i> _{annual}	0.18	97	0.09	0.38	-313	<0.01	188	31.2	0.76	<0.01

3.4.5 Stepwise Regression

Improved overall model performance is observed for every community (and at the landscape scale) in stepwise regressions (Figure 15:A) compared to multiple regressions, regardless of whether three variables (MESMA-derived fractions of GV, NPV, and soil) or two-variable (MESMA-derived fractions of GV and soil) were used. Using the annual MEMSA derived fractions, grass and mesquite show identical $R^2 = 0.85$ with $RMSE = 22.5 \text{ g m}^{-2} \text{ y}^{-1}$ (grass) and $RMSE = 12.5 \text{ g m}^{-2} \text{ y}^{-1}$ (mesquite). While using the seasonal MEMSA derived fractions, grass coefficient is identical to that found in the two-variable regression ($R^2 = 0.83$), however, shows improvement in RMSE from $35.1 \text{ m}^{-2} \text{ y}^{-1}$ to $29.8 \text{ m}^{-2} \text{ y}^{-1}$. MEMSA-derived annual fractional cover values produced better models in nearly all cases in the community scale (higher R^2 , lower RMSE) than seasonal fractional cover values, but with nearly same landscape coefficient determination ($R^2 = 0.73$ and 0.75).





3.4.6 Random Forest

Table 13. Site, out-of-bag mean error, RMSE, normalized RMSE, relative error and RMS-relative error ($\text{g m}^{-2} \text{y}^{-1}$) at community and landscape scales using seasonal and annual derived-MESMA fractions.

Site	Seasonal					Annual				
	ME	RMSE	Normal RMSE	Rel-error	RMS-Rel error	ME	RMSE	Normal RMSE	Rel-error	RMS-Rel error
<i>Tarbush</i>	0.81	14.6	0.16	0.77	0.16	0.18	11.6	0.19	0.18	0.25
<i>Mesquite</i>	0.21	12.1	0.24	0.33	0.28	0.21	13.4	0.23	0.20	0.21
<i>Grass</i>	0.16	42.4	0.23	0.16	0.19	0.13	37.8	0.17	0.13	0.13
<i>Creosote</i>	0.29	10.2	0.24	0.29	0.28	0.19	26.5	0.2	0.19	0.26
<i>Landscape</i>	0.21	19.6	0.22	0.14	0.23	0.14	24.2	0.23	0.14	0.23

OOB errors for RF were extremely low (Table 13), typically below $1 \text{ g m}^{-2} \text{y}^{-1}$. However, OOB errors often overestimate the quality of RF models (Pal 2005), while predictions based on the final model are a better indicator of the quality of RF model performance. Final RF models indicate that RF model predictions were universally higher for all community types, regardless of whether seasonal or annual MESMA-derived fractions were used (Figure 15). Using the annual MEMSA derived fractions, tarbush, creosote and mesquite show similar R^2 with low RMSE, while grass display lowest R^2 (0.89) and highest RMSE ($37.8 \text{ g m}^{-2} \text{y}^{-1}$). Using the seasonal MESMA-derived fractions mesquite ($R^2 = 0.93$) and creosote ($R^2 = 0.92$) prediction models show high improvement than when using stepwise regression ($R^2 = 0.79$ and $R^2 = 0.77$) with reduced RMSE, where with RF, these models RF explain up to 93% of the variance in the *in situ* NPP. The overall best landscape scale model was the RF prediction using annual MESMA-derived fractions with an overall $R^2 = 0.92$ and $\text{RMSE} = 24.2 \text{ g m}^{-2} \text{y}^{-1}$.

3.5 Discussion

In our study, we compared several statistical methods for estimating NPP using MODIS-derived land cover estimates. Our results indicate that MESMA-derived GV, NPV and soil worked well with stepwise regression and RF in providing the best estimations of NPP.

3.5.1 Standard MODIS NPP and GPP products

There have been several studies that suggest that remote sensing of NPP in drylands may be compromised by contamination of the soil signature (Turner et al. 2006), surface homogeneity (Sims et al. 2007), water content and leaf cycle (Ryu et al. 2011), and high temperature (Running and Zhao 2015). Therefore, MODIS17 products generally, are found to be less reliable in dry regions where the water content of roots and leaves is minimal (Friedl et al. 2000). Indeed, our results indicate that the standard MODIS NPP product had no skill in predicting NPP at the plot, community, or landscape scales. The fact that MODIS GPP estimates were more correlated with the *in situ* estimates of NPP indicates that the problem lies more with the failure of the NPP algorithm to correctly predict respiration losses. In particular, the complexity of the respiration calculations in the standard NPP product appears to be unnecessary, as a deduction of $\sim 100 \text{ g m}^{-2} \text{ y}^{-1}$ from GPP to account for respiration would be sufficient to provide rough estimates of NPP at the landscape scale.

The MODIS estimates of GPP product depends on radiation conversion efficiency, ϵ , which determines the maximum fraction of absorbed photosynthetically active radiation (fPAR) that can be converted to a carbon product (Running et al. 2004). This parameter is primarily dependent on temperature and vapor pressure deficit (VPD), and since the MODIS algorithm uses the temperature of cool regions, it is not surprising to find erroneous estimates for hot and dry regions. In our data, differences in slope at the community scale (Table 10), which vary from 0.36 to ~ 1 , suggest different values of ϵ for different community types. The tarbush community apparently has a value of ϵ close to that used by the GPP algorithm (i.e., with the slope closest to 1), and creosote having a value of ϵ that is the most different from that used by the GPP algorithm. Even then, there are considerable differences within communities among individual plots. Overall,

at the landscape scale (94%), the value of ϵ is approximately close to that assumed by the GPP algorithm (Figure 14, Table 10).

A specific plot by plot comparison between the MODIS NPP and *in situ* NPP show that MODIS NPP overestimates the productivity of vegetation at the basin. We couldn't find a particular pattern of overestimation; however, in years of low productivity, MODIS NPP had overestimated the productivity of vegetation. For example, in 2003, a dry year, MWELL experienced reduced productivity of $46.7 \text{ g m}^{-2} \text{ y}^{-1}$, whereas MODIS NPP estimated high NPP of $195.2 \text{ g m}^{-2} \text{ y}^{-1}$, which is more representative of years of high productivity. Generally, the pattern of overestimation agrees with the conclusions of Turner et al. (2006), who found that MODIS NPP and GPP overestimate productivity at low productivity sites due to elevated values of LUE in the MODIS algorithm.

3.5.4 The utility of MESMA-derived fractions

Conclusions by others that contamination by NPV and soil potentially lead to poor estimates of NPP in dryland regions (e.g., Turner et al. 2006; Sims et al. 2007) suggest that including these terms in estimates of NPP may result in strong and predictive correlations. Our results bear out this conclusion, as even simple regressions including only GV and soil provided RMSEs in the estimation of NPP that were approximately half the corrected NPP estimates derived from MODIS GPP. The utility of GV fractional cover in the prediction of NPP is clear: the fraction of GV represents the portion of the surface that is covered by photosynthetic material, and therefore should be closely correlated with FPAR, a main mechanistic determinant of photosynthesis. The value of soil fractional covers in the prediction of NPP is somewhat less clear. Generally, negative correlations between soil cover and *in situ* NPP require that the complement of soil (i.e. 1-soil cover) must be positively correlated with NPP. The complement of soil cover is equivalent to total

vegetation (GV plus NPV) cover. This suggests that there is an element of cover that is not completely green (as GV is) that also contributes to productivity. This is unclear, but it may be related to functional traits of dryland plants that are useful in preventing overheating and water loss (Okin 2007). Leaves tilted away from the sun in open canopies within which considerable multiple scattering occurs may be part of this relationship. That is, there may be photosynthetic material that is hidden from the nadir view (the satellite's perspective) by non-photosynthetic material. We hypothesize that this photosynthetic material contributes to plant productivity, but is only represented in the nadir view by the total vegetation cover.

The fact that estimates of GV, NPV, and soil fractional cover at annual scales generally predicted NPP better than seasonal fractional cover estimates perhaps reflects the fact that, in these communities, growth can begin in response to moisture from winter storms as soon as temperatures rise, which may be in some years, before April 1st. Additionally, the productivity of grasses and shrubs may continue past October 31st in some years, depending on the amount of moisture in the soil and the fall temperatures (Huenneke et al. 2002). We have provided (Table 7) parameters for the calculation of NPP from GV, NPV, and soil fractional cover so that they may be used by other investigators. Unless individual communities can be delineated in a specific study, we suggest the use of landscape-scale parameters (using annual cover estimates) for NPP estimation in Chihuahuan Desert locations.

More sophisticated regression techniques provide generally better estimates of NPP than simple multiple regression techniques, suggesting the utility of these approaches in the prediction of NPP in drylands. Random Forest, in particular, produced landscape-scale estimates of NPP that had an error of only approximately 5% of the total range of values, compared to the best landscape-scale stepwise regression model, with an error of approximately 8% of the total range. Unlike the

simple multiple regression models which were associated with high prediction errors. We attribute this to the way that these algorithms work, rather than to the fact that seasonal values capture information that annual values do not. Indeed, since seasonal and annual values are calculated as sums, the annual value includes more information than the seasonal value by definition. The improvements in NPP predictions that appear when using simple multiple regression with annual values suggest that this information is not extraneous. Nonetheless, the complex nature of the stepwise and RF approaches, and specifically how they are designed to minimize error, may have resulted in over-optimization on one set of data (seasonal vs. annual), regardless of intrinsic utility or information content.

3.6 Conclusion

Based on a unique set of long-term *in situ* NPP measurements, this study shows that it is possible to develop relationships that allow prediction of NPP in hot deserts from MODIS data. Although these relationships are not mechanistic, i.e., based on the physics of NPP, they succeed where the mechanistic algorithms fail. Indeed, our relationships work better even than the mechanistic MODIS algorithms for GPP, which are mostly dependent upon light absorption by chlorophyll (Zhang et al. 2005), a quantity which is relatively simple estimate from remotely sensed data. This appears to be, in part, because our relationships directly account for factors known to influence the quality of GPP estimates in deserts such as variable soil background and the presence of NPV. Although it is possible that mechanistic algorithms that consider plant architecture, the presence of nonphotosynthetic material, and the effect of the soil background, for the time being, empirical relationships such as the ones produced here must suffice for the production of adequate estimates of NPP in deserts such as the Chihuahuan.

Of course, one of the benefits of mechanistic remote sensing algorithms is that the mechanisms are inferred to be similar in different geographic locations, and therefore there is optimism that mechanistic algorithms can produce robust estimates regardless of location, provided sufficiently complex models and adequate input data. At least in the current version of the MODIS NPP algorithm, this condition has not been met. The advantage of an empirical relationship, in contrast, is that they are easy to produce and provide direct estimates, often associated with estimates of error. The trade-off, however, is there is no guarantee that these relationships will be the same in other geographic locations. In our work, by distilling the surface into component parts (GV, NPV, and soil) that are present everywhere, production of fractional cover estimates that are not susceptible to potentially idiosyncratic factors (e.g., soil color), by including data from years with a range of weather conditions, and by examining communities with often dissimilar composition, we have some optimism that our methods might be, at least, extensible to other portions of the Chihuahuan Desert, if not other hot deserts worldwide. Additional testing using independent data is required to determine whether these empirical relationships are adequate elsewhere.

3.7 Acknowledgments

This research was supported by the NSF-funded Jornada Basin LTER program (DEB-1235828). Special thanks to Kuwait University and Kuwait Embassy for their continuous academic support.

3.8 Bibliography

- Adams, J. B., M. O. Smith, and A. R. Gillespie. 1993. Imaging spectroscopy: interpretation based on spectral mixture analysis. In C. M. Pieters, P. A. J. Englert, Remote Geochemical Analysis: Elemental and mineralogical composition. Press Syndicate of University of Cambridge, Cambridge, England.
- Asner, G. P., and K. B. Heidebrecht. 2002. Spectral unmixing of vegetation, soil and dry carbon cover in arid regions: Comparing multispectral and hyperspectral observations. *International Journal of Remote Sensing* 23: 3939- 3958.
- Auret, L., and C. Aldrich. 2012. Interpretation of nonlinear relationships between process variables by use of random forests. *Minerals Engineering* 35: 27- 42.
- Baldrige, A. M., S. J. Hook, C. I. Grove, G. Rivera. (2009). The ASTER spectral library version 2.0. *Remote Sensing of Environment* 113: 711-715.
- Baudena, M., G. Boni, L. Ferraris, J. von Hardenberg, and A. Provenzale. 2007. Vegetation response to rainfall intermittency in drylands: results from a simple ecohydrological box model. *Advances in Water Resources* 30: 1320- 1328.
- Bell, J. F., W. H. Farrand, J. R. Johanson, and R. V. Morris. 2002. Low abundance material at the MARS Pathfinder landing site: An investigation using spectral mixture analysis and related techniques. *Icarus* 158: 56- 71.
- Breiman, L. 1996. Bagging predictors. *Machine Learning* 24: 123- 140.
- Breiman, L., A. L. Cutler, and M. Wiener. 2006. Breiman and Cutler's Random Forest for classification and regression. [Package version 4.5-16].
- Breiman, L. 1984. *Classification and regression trees*. Routledge, New York, New York, USA.
- Breiman, L. 2001. Random Forests. *Machine Learning* 45: 5- 32.
- Chapin, F. S., E. S. Zavaleta, V. T. Eviner, R. L. Naylor, P. M. Vitousek, H. L. Reynolds, D. U. Hooper, S. Lavorel, O. E. Sala, S. E. Hobbie, M. C. Mack and S. Diaz. 2000. Consequences of changing biodiversity. *Nature* 405: 234- 242.
- Dennison, P. E., and D. A. Roberts. 2003. Endmember selection for multiple endmember spectral mixture analysis using endmember average RMSE. *Remote Sensing of Environment* 87: 123- 135.
- Efroymson, M. A. 1960. "Multiple regression analysis," *Mathematical methods for digital computers*. Edited by A. Ralston and H. S. Wilf. New York: Wiley.

- Escafadel, R., and A. R. Huete. 1991. Improvement in remote sensing of low vegetation cover in arid regions by correcting vegetation indices for soil "noise": C. R. Academie des Sciences Paris 312: 1385- 1391.
- Fredrickson, E. L., R. E. Estell, A. Laliberte, and D. M. Anderson. 2005. Mesquite recruitment in the Chihuahuan Desert: Historic and prehistoric patterns with long-term impacts. *Journal of Arid Environments* 65: 285- 295.
- Friedl, M. A., D. Muchoney, D. McIver, F. Gao, J. C. F. Hodger, and A. H. Strahler. 2000. Characterization of North American land cover from NOAA-AVHRR data using the EOS MODIS land cover classification algorithm. *Geophysics Research* 27: 27- 977.
- Gibbens, R. P., R. P. McNeely, K. M. Hastad, R. F. Beck, and B. Nolen. 2005. Vegetation changes in the Jornada Basin from 1858 to 1998. *Journal of Arid Environments* 61: 651- 668.
- Gitelson, A. A., A. Vina, S. B. Verma, D. C. Rundquist, T. J. Arkebauer, G. Keydan, B. Leavitt, V. Ciganda, G. G. Burba, and A. E. Suyker. 2006. Relationship between gross primary production and chlorophyll content in crops: Implications for the synoptic monitoring of vegetation productivity. *Journal of Geophysical Research* 111: 148- 225.
- Guerschmann, J. P., M. J. Hill, L. J. Renzullo, D. J. Barrett, A. S. Marks, and E. J. Botha. 2009. Estimating fractional cover of photosynthetic vegetation, non-photosynthetic vegetation and bare soil in the Australian tropical savanna region upscaling the EO-1 Hyperion and MODIS sensor. *Remote Sensing of Environment* 113: 928- 945.
- Hartley, A., N. Barger, J. Belnap, and G. S. Okin. 2007. Dryland ecosystems. *Nutrient Cycling in Terrestrial Ecosystems* 10: 271- 308.
- Havstad, K. M., L. F. Huenneke, and W. H. Schlesinger. 2006. Structure and function of a Chihuahuan Desert ecosystem: The Jornada Basin long-term ecological research site. Oxford University Press, New York, USA.
- Helman, D., A. Mussery, I. M. Lensky, and S. Leu. 2014. Detecting Changes in biomass productivity in a different land management regime in drylands using satellite-derived vegetation index. *Soil Use and Management* 30: 32- 39.
- Huenneke, L. F., J. P. Anderson, M. Remmenga, and W. H. Schlesinger. 2002. Desertification alters patterns of aboveground net primary production in Chihuahuan ecosystems. *Global Change Biology* 8: 247- 264.
- Huete, A. R. 1988. A soil-adjusted vegetation index (SAVI). *Remote Sensing of Environment* 25: 295- 309.
- ISRIC. 2010. A Globally Distributed Soil Spectral Library: Visible Near Infrared Diffuse Reflectance Spectra. World Soil Information. http://www.africasoils.net/afsis_files/ICRAF-ISRICSoilVNIRSpectralLibrary.pdf.

- Jobbagy, E. G., O. E. Sala, and J. M. Paruelo. 2002. Patterns and controls of primary production in the Patagonian steppe: A remote sensing approach. *Ecology* 83: 307- 319.
- Meyer, T., G. S. Okin. 2015. Evaluation of spectral unmixing techniques using MODIS in a structurally complex savanna environment for retrieval of green vegetation, nonphotosynthetic vegetation, and soil fractional cover. *Remote Sensing of Environment* 161:122- 130.
- Millennium Ecosystem Assessment. 2005. *Ecosystems and Human Well-Being*. Island Press, Washington, DC, USA.
- Myint, S. W., and G. S. Okin. 2009. Modeling land-cover types using multiple endmember spectral mixture analysis in a desert city. *International Journal of Remote Sensing* 30: 2237-2257.
- Okin, G. S., P. D'Odorico, and S. R. Archer. 2009. Impact of feedbacks on Chihuahuan desert grasslands: Transience and metastability. *Journal of Geophysical Research-Biogeosciences*. [<https://doi.org/10.1029/2008JG000833>].
- Okin, G. S., and J. Gu. 2015. The impact of atmospheric conditions and instrument noise on atmospheric correction and spectral mixture analysis of multispectral imagery. *Remote Sensing of Environment* 164: 130-141.
- Okin, G. S., D. A. Roberts, B. Murray, and W. J. Okin. 2001. Practical limits on hyperspectral vegetation discrimination in arid and semiarid environments. *Remote Sensing of Environments* 77: 212- 225.
- Okin, G. S., K. D. Clarke, and M. M. Lewis. 2012. Comparison of methods for estimation of absolute vegetation and soil fractional cover using. *Remote Sensing of Environment* 130: 266-279.
- Okin, G. S. 2010. The contribution of brown vegetation to vegetation dynamics. *Ecological Society of America* 91: 743-755.
- Okin, W. J., G. S. Okin, D. A. Roberts, and B. Murray. 1999. Multiple endmember spectral mixture analysis: Endmember choice in an arid shrubland. R. O. Green (Ed.). *The 1999 AVIRIS workshop*, Jet Propulsion Laboratory, Pasadena, CA.
- Oliver, J. 2008. *Encyclopedia of World Climatology*. Springer, Dordrecht, The Netherlands.
- Pal, M. 2007. Random forest classifier for remote sensing classification. *International Journal of Remote Sensing* 26: 217-222.
- Peters, A. J, and M. D. Eve. 1995. Satellite monitoring of desert plant community response to moisture availability. *Environmental Monitoring and Assessment* 37: 273-287.

- Peters, D. P.C., I. Mariotto, K. M. Havstad, and L. W. Murry. 2006. Spatial variation in remnant grasses after a grassland-to-shrubland state change: Implications for restoration. *Rangeland Ecology and Management* 59: 343-350.
- Reeves, M. C., M. Zhao, and S. W. Running. 2006. Applying improved estimates of MODIS productivity to characterize grassland vegetation dynamics. *Rangeland Ecology and Management* 59: 1-10.
- Roberts, D. A., M. Gardenr, R. Church, S. Ustin, G. Scheer, and R. O. Green. 1998. Mapping Chaparral in the Santa Monica Mountains using multiple endmember spectral mixture models. *Remote Sensing and Environments* 65: 267–279.
- Roberts, D. A., R. O. Greens, and J. B. Adams. 1997. Temporal and spatial patterns in vegetation and atmospheric properties from AVIRIS. *Remote Sensing of Environment* 62: 223-240.
- Running, S. W., R. R. Nemani, F. A. Heinsch, M. Zhao, M. Reeves, and H. Hashimoto. 2004. A continuous satellite-derived measure of global terrestrial primary production. *Biosciences* 54: 547-560.
- Running, S. W., and M. Zhao. 2015. Daily GPP and Annual NPP Products. NASA Earth Observing System MODIS Land Algorithm. IPDAAC.
- Ryu, Y., D. D. Baldocchi, H. Kobayashi, C. van Ingen, J. Li, A. Black, J. Beringer, E. van Gorsel, A. Knohl, B. E. Law, O. Roupsard. 2011. Integration of MODIS land and atmosphere products with a coupled-process model to estimate gross primary productivity and evapotranspiration from 1km to global scales. *Global Biogeochemical cycle*. [<https://doi.org/10.1029/2011GB004053>].
- Sala, O. E, L. A. Gherardi, L. Reichmann, E. Jobbagy, and D. Peters. 2012. Lags and legacies of precipitation fluctuations on primary production: Theory and data synthesis. *Philosophical Transactions of the Royal Society of London: Biological Sciences* 367: 3135-3144.
- Sala, O. E., W. J. Parton, L. A. Joyce, and W. K. Lauenroth. 1988. Primary production of the central grassland region of the United State. *Ecology* 69: 40-50.
- Shimabukuro, Y. E., and J. A. Smith. 1991. The least-squares mixing models to generate fraction images derived from remote sensing multispectral data. *IEEE Transactions on Geoscience and Remote sensing* 29: 16-20.
- Sims, D. A., A. F. Rahman, V. D. Cordova, B. Z. El-Masari, D. D. Baldocchi, P. V. Bolstad, L. B. Flanagan, A. H. Goldstein, D. Y. Hollinger, L. Misson, R. K. Monson, W. C. Oechel, H. P. Schmid, S. C. Wofsy, L. Xu. 2007. A new model of gross primary productivity for North American ecosystems based solely on the enhanced vegetation index and land surface temperature from MODIS. *Remote Sensing of Environment* 112: 1633-1646.

Smith, M. O., S. L. Ustin, J. B. Adams, and A. R. Gillespie. 1990. Vegetation in deserts: I. A regional measure of abundance from multispectral images. *Remote Sensing of the Environment* 31: 1-26.

Turner, D. P., W. D. Ritts, W. B. Cohen, S. T. Gower, S. W. Running, M. Zhao, M. H. Costa, A. A. Kirschbaum, J. M. Ham, S. R. Saleska, D. E. Ahl. 2006. Evaluation of MODIS NPP and GPP products across multiple biomes. *Remote Sensing of Environment* 102: 282-292.

Wainwright, J., A. J. Parsons, and A. D. Abrahams. 1995. A simulation study of the role of raindrop erosion in the formation of desert pavements. *Earth Surface Processes and Landforms* 20: 277-291.

Yahdjian, L., and O. E. Sala. 2006. Vegetation structure constrains primary production response to water availability in the Patagonian steppe. *Ecology* 87: 952-962.

Zhao, M., F. A. Heinsch, R. M. Nemani, and S. W. Running. 2005. Improvements of the MODIS terrestrial gross and net primary production global data set. *Remote sensing of Environment* 95: 164-176.

Zhao, M., S. W. Running, and R. R. Nemani. 2006. Sensitivity of Moderate Resolution Imaging Spectroradiometer (MODIS) terrestrial primary production to the accuracy of meteorological reanalyses. *Geophysical Research*. [doi:10.1029/2004JG000004.].

Chapter 4. Drone-based monitoring of hillslope-channel coupling by aeolian processes.

4.1 Abstract

There has been an increase in interest in the interaction between aeolian and fluvial processes in drylands over the past several decades and yet, there has been relatively little work investigating how aeolian processes working on hillslopes interact with fluvial features in a form of hillslope-channel coupling. This study used imagery from unmanned aerial vehicles (UAVs) to conduct high-resolution, repeated topographic mapping to study hillslope erosion and sedimentation processes. The purpose of this study was to investigate the contributions of wind and water in soil surface elevation change over the course of 16 months. Detailed analysis indicated that the estimated heights of ground control points (GCPs) were consistent enough to allow calculation of height differences to produce for sediment volume calculations. We compared the elevation values between the total station and the DEMs at ten ground control points (GCP) at three locations for accuracy assessment. We found strong vertical agreement between the UAV and total station for all survey dates over 16 months for three locations (NW, SW, and NE streams). In addition, we classified the morphology of the streams into east and west wall and bed to characterize the effects of wind and water on these sub-morphologies. We found that the majority of the erosion events accrued at the NW and NE stream walls while deposition events at the bed of the NW stream over the course of 16 months.

4.2 Introduction

Drylands are water-limited ecosystems that range from hyperarid to subhumid lands and cover more than 40% of the earth's land and are a home for more than 2 billion people (Reynold et al. 2007). Due to low and discontinuous vegetation cover, drylands are susceptible to both wind and water erosion (Okin et al. 2009). Eighty percent of the world's drylands may be affected by

moderate to severe soil degradation (Lal et al. 2003; Pimentel 1993), much of which has a component of wind and water erosion (Belnap et al. 2011; Field et al. 2009). Both types of erosion have contributed to one billion ton of soil loss per year in the United States (NRCS 2000A; NRCS 2000B). The combined effects of wind and water erosion in the U.S. are estimated to cost about 9.6 and 7.4 billion dollars per year due to on-site and off-site agricultural impacts (Pimentel et al. 1995). The coupled effect of wind and water has major long-term impacts on dryland degradation that could lead to various environmental, ecological, and economic consequences.

From a scientific perspective, there has been an increase in interest in the interaction between aeolian and fluvial processes in drylands over the past several decades (Bullard and McTainsh 2003; Maroulis et al. 2007; Okin et al. 2009; Field et al. 2009; Belnap et al. 2011; Sankey & Draut 2014; Okin et al. 2018). Much of the work that has been done has concerned the interaction of dunes and river systems in both modern and ancient systems (Bullard & McTainsh 2003; Maroulis et al. 2007; Sankey & Draut 2014) or the influence of fluvial sediment delivery to dry lakes on dust emission (Reheis 1997; Reheis 2006; Okin & Reheis 2001; Bullard & McTainsh 2003; Schepanski et al. 2012). Other work has focused on processes, either aeolian or fluvial, at work on hillslopes and potential feedbacks with vegetation (Field et al. 2009; Stewart et al. 2014; Okin et al. 2009; Okin et al. 2018).

There has been relatively little work at the intersection of all these areas: how aeolian processes working on hillslopes interact with fluvial processes occurring in channels inset in those hillslopes (Belnap et al. 2011; Sankey & Draut 2014). This is a potentially revealing area of research which may indicate more extensive and more consequential interactions between fluvial and aeolian processes than generally acknowledged due to the ubiquity of inset channels on hillslopes and generally higher rates of aeolian transport than expected in the few locations where

it has been measured together with hillslope water transport. (Breshears et al. 2003a; Breshears et al. 2003b; Field et al. 2011; Whicker et al. 2002). For instance, sediment blown by wind into ephemeral, inset channels and then subsequently cleared during flooding events, represents a coupling that is rarely considered (but see Belnap et al. 2011), but that represents a potentially important mechanism of hillslope-channel coupling through aeolian mechanisms.

The purpose of this study is to investigate the coupling of hillslopes and channels through aeolian transport. Due to the episodic nature of both wind and water transport, a strategy of infrequent surveys of coupled channel systems was devised, using novel drone-based methods for accurate estimation of changes in surface height that are due to transport events. In particular, we investigate the effects of wind and water transport in erosion/deposition in ephemeral streams in Moab, UT. Our investigation of the cumulative effect of sediment flow occurred during dry and wet periods, which helps guide interpretation of changes in microtopography in terms of the dominant process (aeolian or fluvial) responsible for changes to surface elevation and sediment storage.

4.2.1 Background

The relationship between aeolian and fluvial processes has been observed at various spatial and temporal scales (Bullard & McTanish 2003; Field 2009). The interactions between wind and water transport are deeply linked and controlled by landscape and land formations (Belnap 1995). Soil particles under the effect of one type of erosion, either wind or water, can become available for another type of erosion over time, which may intensify the amount of soil loss, redistribution, and contributing to long-term pedogenesis, including the development of desert pavements (McFadden & Well 1987; Wells et al. 1995). For example, sand dunes can encroach drainages during dry periods and deposit sediments directly into channels (Field 2009). The aeolian

sediments can be stored until the next rainfall events, where rain transport sediments downstream by surface runoff (Belnap et al. 2011). Aeolian transport of fluvial deposits in drylands can occur in a variety of settings, including re-working of material deposited in dry lakes (Reheis 1997; Reheis 2006), aeolian transport of bar sediments (Sankey & Draut 2014), and aeolian transport of delta sediments (Belnap et al. 2011; Okin et al. 2001).

In general, the magnitude of the combined effect of soil erosion is dependent on the speed of wind and of the amount and intensity of rainfall, as well as physical characteristics of soil, such as texture, hydrophobicity, crusting, and wetness (Ravi et al. 2010). Due to the temporal separation and spatial scale differences, wind and water have been often studied in separation (Breshears et al. 2003; Toy et al. 2002; Visser et al. 2004). The magnitude of transport is different between aeolian and fluvial processes (Whicker et al. 2002) and is dependent on the magnitude and frequency characteristics of transport events. In particular, aeolian transport events may be more frequent than fluvial transport events, however, the amount of material transported in a single, infrequent fluvial transport event can be much greater than the amount of material transported in strong aeolian events (Okin et al. 2018).

Another important difference between wind and water transport processes is the directionality of transport. Aeolian transport, observed throughout the year, is omni-directional, controlled by wind speed and direction which, in many locations, can be any direction. Wind speed and direction are typically not strongly affected by hillslope characteristics. Water transport, on the other hand, is strongly directional since water flows downslope carving its way into channels within watershed boundaries (Ravi et al. 2010). In practice, these differences mean that while water can only move sediment within a channel or down a hillslope, wind can move sediment orthogonal or even opposite to the direction of water flow.

Despite the relative isolation in the combined study of the two transport mechanisms in research, numerous attempts have been made to re-evaluate this separation (Breshears et al. 2003; Bullard and Mctanish 2003; Visser et al. 2004). Various techniques have been developed to estimate soil erosion and deposition by detecting changes in soil surface elevation due to multiple processes (Capolupo et al. 2015; Gillan et al. 2017). Although there are other methods used for quantifying sediment transport, such as sediment traps, there is no standard method for simultaneously measuring both wind and water transport from trapped sediment. Indeed, attempts to measure both wind and water transport simultaneously (Breshears et al. 2002; Whicker et al. 2003) have been criticized due to the differences in measurement techniques and different temporal characteristics of transport.

Detecting soil surface elevation change does not quantify soil mass transport, but can provide valuable information about spatial distribution of sediments following erosion events, which can be used to infer transport using a mass-balance approach. Due to their high accuracy, terrestrial laser scanners are commonly used to detect soil loss and microtopographic change on various scales (Elner et al. 2014). However, the high cost of hardware acquisition limits their user base (Niethammer et al. 2012). Methods using topographical data derived from unmanned aerial vehicles (UAVs, also called drones) are potentially an efficient alternative for monitoring microtopography and soil loss at various scales (Elner et al. 2014). Recent advances in computer vision and digital 3D surface reconstruction have resulted in developments in structure-from-motion (SfM) techniques that employ drone-based photography (Elner et al. 2014). SFM technologies are dependent on camera positions and matching points of multiple images, using real world and translated coordinates and UAVs are efficient tools that can be used for producing such imagery in order to derive repeatable soil surface elevation estimates (Gillan et al. 2016; Gillan et al. 2017).

The low cost of UAV acquisition and maintenance and the availability of SfM software have expanded the usage and applications of SfM (Westoby et al. 2012). Digital surface models from drone imagery potentially provide a reliable alternative for estimating the changes in surface height and can be used in detecting temporal changes in microtopography (Gillan et al. 2016).

4.3 Methods

4.3.1 Study area

Three streams located in the outskirts of Moab, UT ($38^{\circ} 33' 26.34''$ N, $109^{\circ} 30' 28.8''$ W) were selected as study plots for our UAV surveys (Figure 16). The area has a mean elevation of ~1,370 meters, a mean annual rainfall of ~235 millimeters, and mean annual wind speed of ~3.5 meters per second (USGS Moab, UT). The windy season starts in late February and ends in early July, while the monsoon season starts in early July and ends in late September. Each of the three streams are given a label in reference to their direction (Table 14; Figure 16). The largest (widest) stream is the NW and smallest is the NE (Table 14). The width is the mean of three transect measurements.

Table 14. Stream location reference direction, field transect measurements of length of survey (m) and mean width (m).

Stream	Length (m)	Width (m)
NW	151	4.3
SW	98	2.5
NE	96	2.9

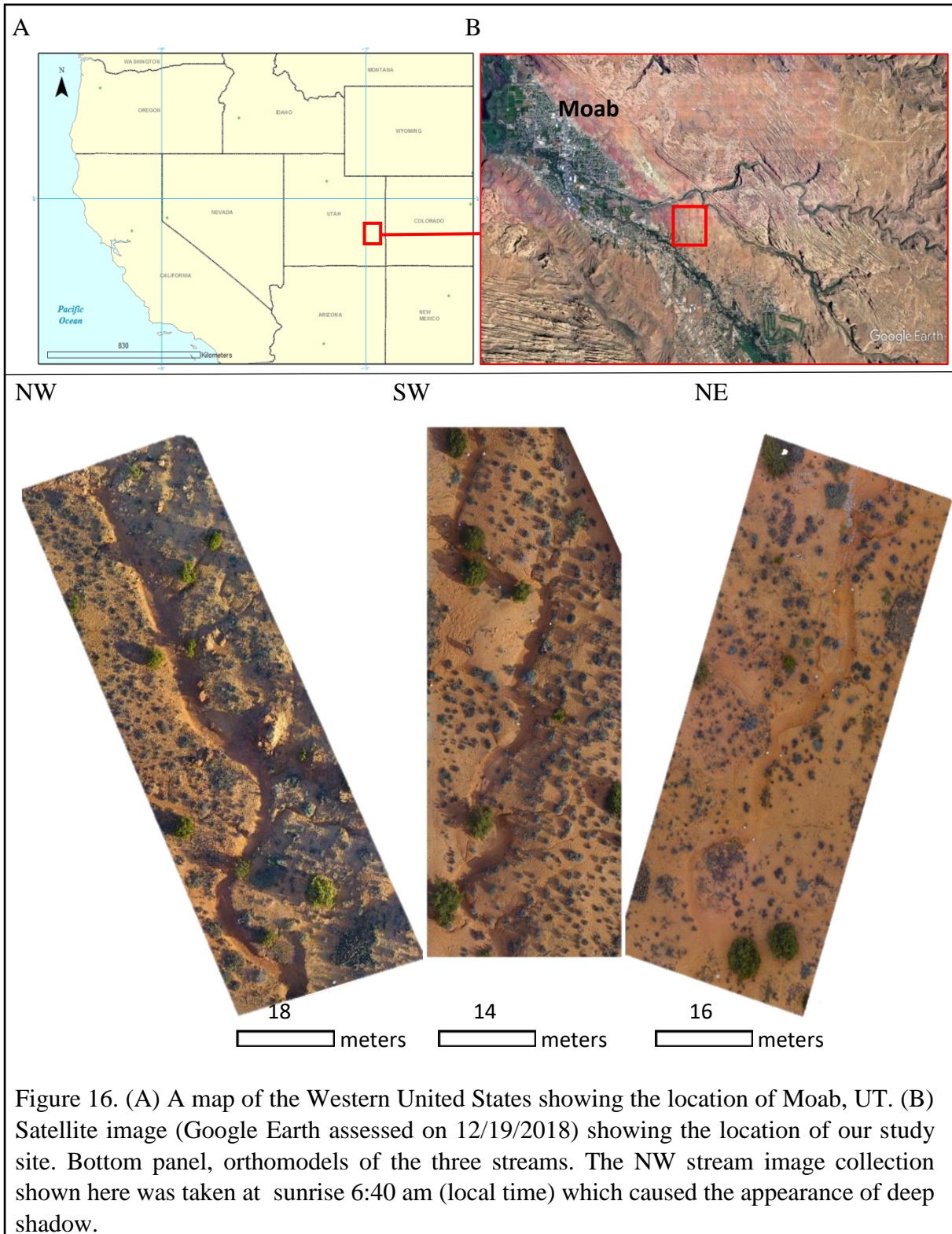


Figure 16. (A) A map of the Western United States showing the location of Moab, UT. (B) Satellite image (Google Earth assessed on 12/19/2018) showing the location of our study site. Bottom panel, orthomodels of the three streams. The NW stream image collection shown here was taken at sunrise 6:40 am (local time) which caused the appearance of deep shadow.

Five surveys spanning a period of 16 months from July 2017 to November 2018 were made: (1) July 1, 2017, (2) September 24, 2017; (3) March 10, 2018; (4) May 10, 2018 and (5) November 20, 2018, each survey date is given a number to represent the order of the survey, these orders are used to clarify soil Δh calculation. The area experienced an intense storm cycle from September 9th, 2017 to September 15th, 2017 (i.e., between acquisition 1 and 2) and recorded a total of ~ 67.5 mm of rain (Utah Water Science Center 2017), causing visible flow in these streams (J. Belnap, *personal communication*). Maximum wind gusts of 29.3 m s⁻¹ were recorded for the same period of time (Table 15), with south being the predominant wind direction (ASOS Network 2017).

Table 15. Survey dates, max wind speed (m s⁻¹), 95th percentile wind speed (m s⁻¹), total rainfall (mm), number of days with maximum windspeed > 7 m/s (WS>7), and number of days with more than 10 mm rainfall (R>10) during the survey periods from Canyonland Weather Station near Moab, UT (ASOS Network 2017). Numbers in parentheses represent the percent of days during a time period with WS>7 and R>10.

Survey period	Max wind speed	95 th percentile wind speed	Total rainfall	WS> 7	R>10
July 1, 2017 - September 24, 2017	29.3	6.7	108	59 (69%)	11 (13%)
September 24, 2017 - March 10, 2018	21.9	6.2	119	56 (34%)	5 (3%)
March 10, 2018 - May 10, 2018	18.6	7.2	48.8	44 (72%)	2 (3%)
May 10, 2018 - November 20, 2018	19.4	8.2	71.3	66 (34%)	4 (2%)

4.3.2. Ground control point (GCP)

Ten unique GCPs were established for each plot using bars of rebar driven at least 80 cm into the ground with 30 cm above the surface to orient the drone flights and register the 3D models: five on each side of the streams. During the surveys, 58 cm diameter prints of coded targets (Agisoft LLC St. Petersburg, Russia), mounted on wooden plates, were placed on each of the poles. Care was taken to ensure that the same target was placed on the same pole for every flight at each plot. The coded targets can be automatically identified by PhotoScan Pro software to aid automated matching of photographs. We used Trimble Net R9 with 2-cm accuracy (Trimble Sunnyvale, CA)

to collect high-accuracy GPS locations for each of the GCPs. The GPS coordinates were used to georegister the models. The GPS points were all in the WGS 84 geographic coordinate system.

4.3.2. Image acquisition

A DJI Phantom 4 equipped with a 4K camera was used for image acquisition (Dà-Jiāng Innovations Science and Technology Co. Shenzhen, China). The camera is mounted on an adjustable gimbal that allows control of its viewing direction while also reducing vibration. Stabilizing the camera position and viewing direction is important to eliminate vibrations and motion blur caused by wind and flight speed. For this work, the camera position was always set to 90 degrees (nadir) during flights. Drone flights were designed (flight height and speed) and controlled using Map Pilot V2.6.4 (Drones Made Easy San Diego, CA). A double grid (two directions: east-west and north-south) flight design was initially used for our surveys. The double grid flight eliminates blind spots and gaps in the models, which in turn increases the accuracy of matching viewpoints. Images were taken at ~16 m above the ground with a 75% forward and 75% sidelap (Table 16); these overlap parameters are sufficient for most digital elevation model (DEM)-based surface feature detection, i.e., soil and vegetation models (Daftry et al. 2015; Cunliffe et al. 2016).

Table 16. Acquisition and processing parameters used for designing drone flights and generating 3D models.

aircraft	DJI Phantom 4
Camera model	FC330 (3.61mm)
Camera type	Frame
FOV (degree)	94
Image size	4000 x 3000
Flying height above the ground (m)	16
Forward overlap (%)	75
Side overlap (%)	75
Image count	80 - 120
Average point density (points/ m ²)	60
DEM cell size (cm)	2 - 3
Orthomosaic resolution (mm)	5.8 - 6.2

4.3.3. Image processing

The collected imagery was processed in Agisoft PhotoScan 1.4.4 (Agisoft LLC, St. Petersburg, Russia) SFM software to generate DEMs and orthomosaics. We followed the four major SFM steps to process images and generate DEMs: 1) photo alignment and sparse cloud building, 2) GCP identification and sparse point cloud optimization, 3) dense point cloud building, and 4) building orthomosaics and DEMs.

We first aligned the photos using “high” accuracy and created sparse point clouds for each plot separately. The alignment algorithm is designed to search for identifiable features in the images and determines the location of the cameras to calculate the 3D coordinates of the surface features (Lowe 2004). This step results in a sparse cloud that includes features that are matched with their calculated x, y, and z geographic coordinates (WGS 84) according to the DJI Phantom 4 built-in GPS.

Next, we manually navigated and identified GCPs in the images for each plot. In Photoscan, identification of GCP “Add marker tool” enables the software to automatically estimate locations of GCPs in all of the uploaded images. The estimated GCPs were checked and adjusted to the center pixel of each GCP. Each GCP was assigned the appropriate GPS-derived geographical coordinate.

With these parameters, the final ground resolution of the orthophotos was as small as 5.8 mm per pixel, with 0.5 cm geometric accuracy. Geometric errors were quantified by comparing the ground GPS coordinates of the GCPs to their georeferenced image coordinates at each plot (Table 17).

About 100 images were used to construct a 3D mosaic for each plot with 120,000-125,000 tie points, and an average point density of 46–60 points/m². Orthomosaics and DEMs were constructed using a “high accuracy” dense point cloud. The coverage area of our models was 5,670

m², 4,270 m² 4,740 m² with average DEM resolution of 2.6 cm, 2 cm, 2.4 cm for NW, NE and SW, respectively.

4.3.4 Height accuracy/consistency assessment

Two types of height accuracy assessment were conducted. In the first, relative heights of GCPs derived from UAV imagery were compared against an independent set of relative height measurements using a total station. In the second, UAV-derived relative heights were compared with one another and were tracked through time. For both analyses, the height of the pixel closest to the center of each GCP in each UAV imagery was used.

For the first analysis we collected heights using a Trimble Total Station (Trimble Sunnyvale, CA) in each plot on July 1, 2017. The total station measurements were taken at the center of each GCP by placing the prism pole on the center of each GCP plate. Using the logic that the absolute heights of the Total Station and UAV-derived GCPs would not agree, but the relative differences between them should agree, one GCP was chosen as the standard (GCP1 for all plots) and in both datasets (Total Station and UAV-derived), this height was subtracted from the others. For the first analysis, these relative heights could be compared directly with each other using two metrics, the mean absolute difference (MAD), given as:

$$MAD = \frac{|\Delta h_1 - \Delta h_2|}{N} \quad (8)$$

where Δh is a measure of height, 1 and 2 refer to the two measures under consideration, and N is the number of points used, and the mean difference (MD), given as:

$$MD = \frac{\Delta h_1 - \Delta h_2}{N} \quad (9)$$

For the comparison between Total Station and UAV heights, Δh refers to the height difference between a GCP and the height of the standard GCP, the index '1' was used for the UAV-derived height measures and '2' was used for the Total Station height measures, meaning

that a positive MD indicated that the UAV height differences were greater, on average, than the Total Station height differences. N , in this case was the number of GCPs (10) minus one because one of the GCPs is used as the standard.

For the second analysis, in which we compared UAV heights for consistency through time, two approaches were used. First, we checked to see that relative heights of individual GCPs changed through time; this was quantified by calculating the standard deviation of the UAV-derived (absolute) height measures for the 5 times the imagery was acquired. Comparison of relative heights through time required a slightly different approach from the Total Station-UAV comparison. In particular, use of a single GCP as the ‘standard’ could potentially inflate the estimate of MAD if the ‘standard’ GCP height measurement was in error. Therefore, the differences in height between all possible combinations of GCPs (excluding the height difference between a GCP and itself) at each stream was used to calculate MD and MAD, with N in these cases equal to 45, the number of possible combinations. In practice, Δh for MAD and MD calculations were calculated as the difference between a GCP’s height on one survey date (index 2) minus the height of that GCP on the first survey data (index 1). A positive MD indicates that the estimated height at the later date was greater than the estimated height on the original date.

4.3.5 Object classification and differencing analysis

In the PhotoScan Pro software, we used “Classify Point Cloud” to eliminate vegetation and other objects that were not soil; see Cunliff et al. (2016) and Gillan et al. (2017). Next, the DEM models were imported into ArcMap 10.5 (ESRI Redlands, CA, USA) and were reprojected to UTM.

The ArcMap “Minus” tool was used to perform a mathematical procedure to identify soil surface elevation change (Δh) on a per-pixel basis according to:

$$\Delta h_{total} = DEM_{(1)} - DEM_{(5)} \quad (10)$$

$$\Delta h_1 = DEM_{(1)} - DEM_{(2)} \quad (11)$$

$$\Delta h_2 = DEM_{(2)} - DEM_{(3)} \quad (12)$$

$$\Delta h_3 = DEM_{(3)} - DEM_{(4)} \quad (13)$$

$$\Delta h_4 = DEM_{(4)} - DEM_{(5)} \quad (14)$$

Where $DEM_{(x)}$ is the DEM derived from (x) survey date (see survey date orders). To analyze patterns of soil erosion and deposition in relation to stream morphology, we partitioned the soil elevation differenced maps using three morphological classes: 1) stream bed, 2) stream east wall and 3) stream west wall. Due to the fine scale of the surface models, ArcMap could not recognize the stream morphologies with watershed tools, therefore masks were created manually by tracing the areas of interest. We created masks (Figure 17) for each class to cover the desired area at each site, then summed the values of soil Δh (cm) for erosion and deposition and multiplied them by the pixel size (cm^2) of each DEM for each class.

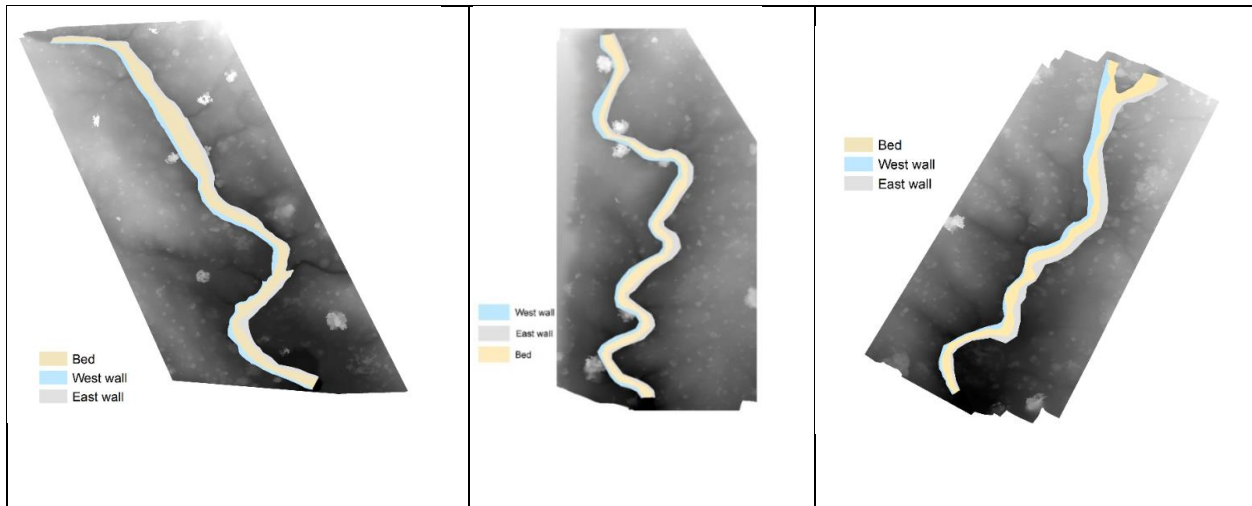


Figure 17. Masks were created for NW, SW, and NE streams indicating stream morphologies (bed, east wall, and west wall).

4.4 Results

Georeferencing error during SfM construction in the X- and Y- directions was under 0.5 cm for all streams for all surveys (Table 17). Z-direction errors were less than 0.8 cm for all surveys. Overall locational error was less than 0.7 cm for all surveys, with overall locational error never greater than 0.08 pixel widths.

Table 17. X, y and z errors (cm), overall error (cm), and reprojection pixel error of the estimated GCP marker positions.

Stream	Survey	X error	Y error	Z error	Overall Error	Error (pixel)
NW	July 2017	0.1	0.3	0.5	0.4	0.08
	September 2017	0.4	0.2	0.6	0.5	0.06
	March 2018	0.2	0.5	0.8	0.7	0.08
	May 2018	0.3	0.2	0.7	0.4	0.05
	November 2018	0.4	0.3	0.6	0.3	0.07
NE	July 2017	0.1	0.3	0.5	0.4	0.08
	September 2017	0.4	0.2	0.6	0.5	0.06
	March 2018	0.2	0.5	0.8	0.7	0.08
	May 2018	0.3	0.2	0.7	0.4	0.05
	November 2018	0.4	0.3	0.6	0.3	0.07
SW	July 2017	0.2	0.3	0.5	0.4	0.04
	September 2017	0.1	0.3	0.6	0.3	0.03
	March 2018	0.3	0.4	0.7	0.4	0.03
	May 2018	0.2	0.1	0.5	0.3	0.02
	November 2018	0.3	0.4	0.5	0.2	0.06

Comparisons between Total Station heights and UAV-derived heights indicated that there was always more variability in the Total Station heights than UAV heights from the same date (Table 18), with MAD ranging from 5.1 – 13.1 cm and |MD| ranging from 1.5 – 12.1 cm. Agreement between UAV-derived heights through time indicated considerably less variability, with MAD ranging from 1.4 – 2.9 cm and |MD| ranging from 0.2 – 1.6 cm. Overall MAD for the three streams was 2.0 – 2.3 mm and overall |MD| for the three streams was 0.2 – 0.5. Average standard for (absolute) UAV-derived heights was 1.2 – 1.4 cm (Table 18). To estimate uncertainty in UAV-derived heights, we used the overall MAD because, to be conservative, this was greater

than the standard deviation (Table 20). Volume uncertainties for each stream were estimates as the overall UAV-derived MAD multiplied by the pixel area (Table 19).

Table 18. Comparison between heights (cm) measured with Trimble Total Station (TS) and heights retrieved from UAV (cm) for July 2017, and between heights of GCP retrieved from UAV (cm) for each survey date and overall for each site, mean difference (MD) cm, mean difference (MD) cm, mean absolute difference (MAD) cm.

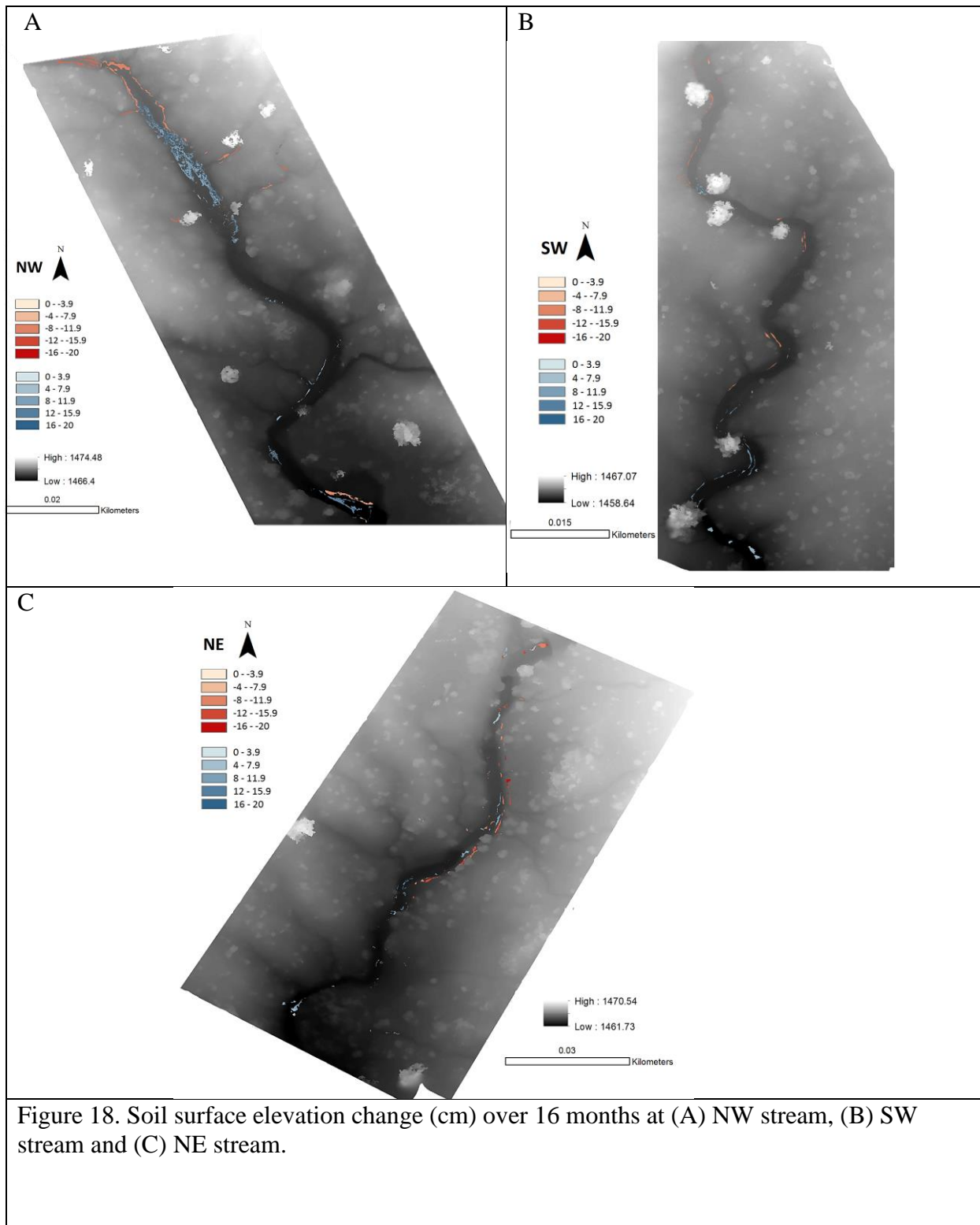
Site	Comparison	Survey	MD	MAD
NW	TS vs. UAV	July 2017	-3.0	10.0
	UAV	July 2017	-0.4	1.8
	UAV	September 2017	0.2	1.8
	UAV	March 2018	0.7	2.7
	UAV	May 2018	1.3	2.8
	UAV	November 2018	1.3	2.8
	UAV	overall	0.5	2.3
SW	TS vs. UAV	July 2017	-1.5	5.1
	UAV	July 2017	-1.2	1.5
	UAV	September 2017	-0.2	1.8
	UAV	March 2018	-0.2	2.9
	UAV	May 2018	-0.7	2.9
	UAV	November 2018	-0.7	2.0
	UAV	Overall	2.0	-0.5
NE	TS vs. UAV	July 2017	-12.2	13.1
	UAV	July 2017	0.4	1.4
	UAV	September 2017	-0.4	2.0
	UAV	March 2018	-0.6	2.4
	UAV	May 2018	1.6	2.5
	UAV	November 2018	1.6	2.5
	UAV	Overall	0.2	2.1

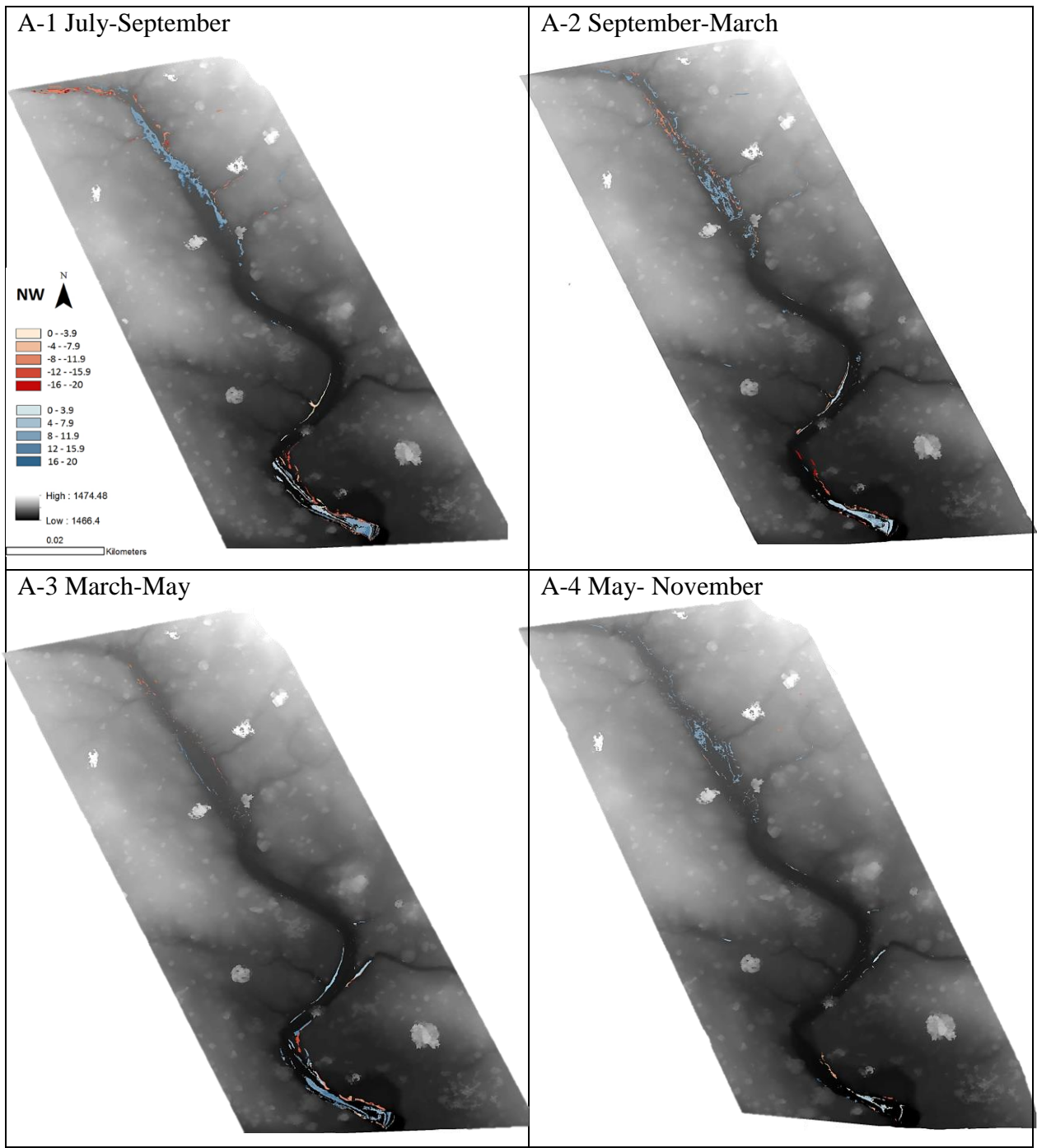
Table 19. Height uncertainty (MAD), pixel size, and volume uncertainty for each stream in the study.

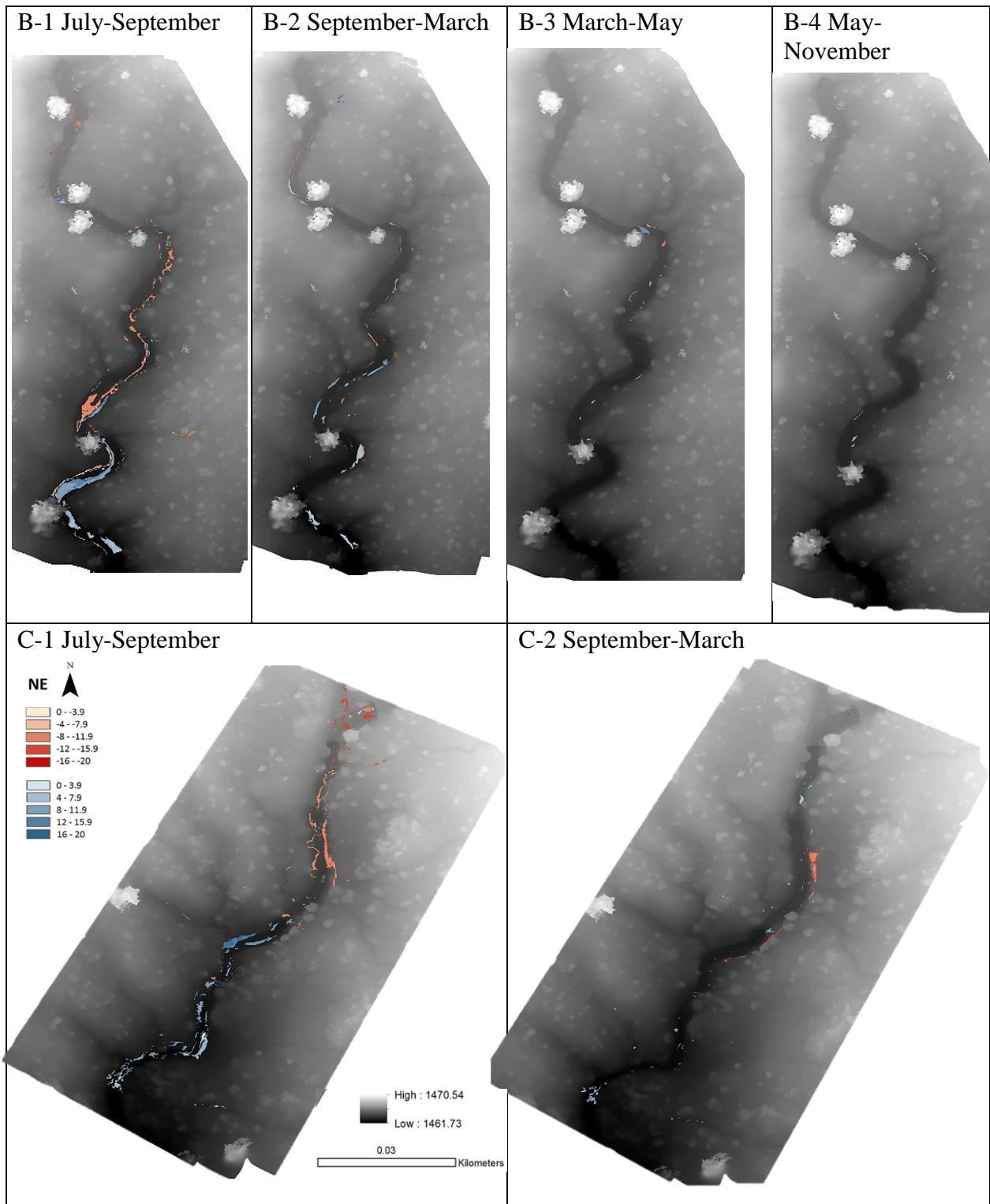
Site	Overall MAD (cm)	Pixel Size (cm ²)	Volume uncertainty (cm ³)
NW	2.1	4.0	8.2
SW	2.0	5.8	11.6
NE	2.1	6.8	14.3

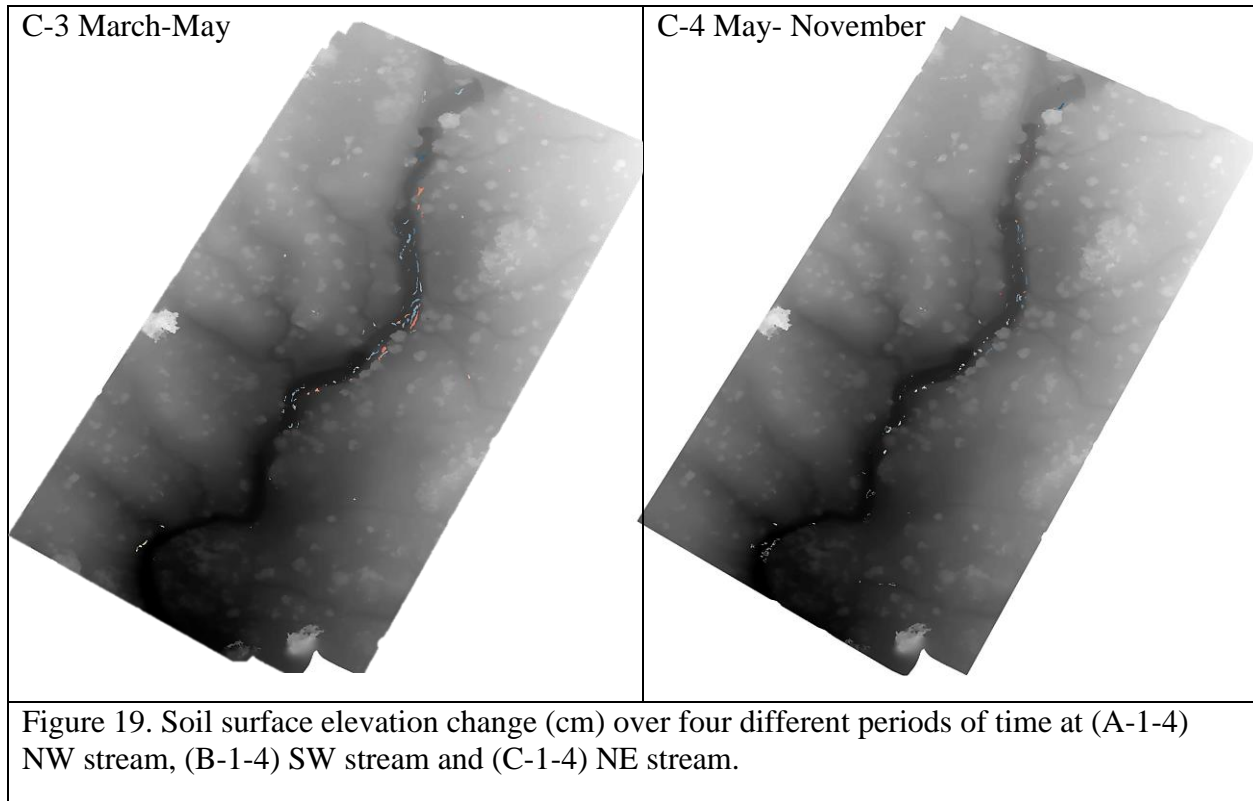
Table 20. Site, GCP order, GCP heights for each survey date (cm), and standard deviation cm (STDEV) for each GCP at all survey dates and average STDEV cm for each site.

Site	GCP	Jul-17	Sep-17	Mar-18	May-18	Nov-18	STDEV
NW	GCP1	51.1	52.1	51.2	52.1	53.6	1.0
	GCP2	58.6	58.4	58.4	56.7	56.6	1.0
	GCP3	56.2	55.7	55.9	56.1	56.1	0.2
	GCP4	44.4	45.6	45.8	47.3	46.5	1.1
	GCP5	52.1	50.4	49.4	49.3	50.7	1.1
	GCP6	59.5	59.4	58.3	58.1	59.8	0.8
	GCP7	51.3	53.5	54.1	54.1	45.7	3.6
	GCP8	57.6	54.1	55.4	54.8	55.3	1.3
	GCP9	55.4	55.3	54.7	52.1	52.7	1.5
	GCP10	55.6	55.8	55.4	55.6	55.5	0.1
Average = 1.2							
SW	GCP1	40.1	38.7	39.1	38.7	38.1	0.7
	GCP2	36.5	38.5	36.1	38.6	37.3	1.1
	GCP3	36.8	38.8	37.6	39.1	37.5	1.0
	GCP4	34.4	33.3	34.5	38.6	38.5	2.5
	GCP5	41.1	39.1	40.1	41.9	40.1	1.1
	GCP6	40.2	41.3	42.1	43.2	38.7	1.7
	GCP7	42.7	44.3	43.3	43.5	39.5	1.9
	GCP8	44.2	45.4	46.4	44.7	46.1	0.9
	GCP9	47.3	45.3	48.4	48.1	47.1	1.2
	GCP10	44.6	45.2	47.1	47.1	48.6	1.6
Average = 1.4							
NE	GCP1	44.1	44.2	45.1	43.2	50.1	2.7
	GCP2	50.1	49.3	50.7	50.4	51.3	0.7
	GCP3	56.4	56.1	55.7	54.5	55.4	0.7
	GCP4	50.9	49.7	50.8	49.2	49.3	0.8
	GCP5	49.4	49.1	48.7	47.1	47.4	1.0
	GCP6	43.2	44.5	48.1	48.1	45.2	2.2
	GCP7	45.3	43.2	44.9	45.3	44.2	0.9
	GCP8	47.2	47.0	48.2	46.3	45.6	1.0
	GCP9	56.9	59.1	60.1	59.1	55.9	1.7
	GCP10	58.8	58.7	58.6	57.7	58.2	0.5
Average = 1.2							









Areas outside of the channels exhibited no discernible change in height (Figure 18 and 19). Within the channels, the streams exhibited spatially coherent patterns of erosion and deposition over the entire 16 months of the study (Figure 18) and between individual surveys (Figure 19), with changes in height up to 20 cm in some locations. The areas of the greatest volume change in each stream was typically isolated to a few locations, which remained relatively consistent between time periods during which there was significant volume change.

The NW stream, which has both the longest reach in this study and is the widest stream, exhibited the greatest changes in sediment volume in its channel from the beginning to the end of the study period, as well as between individual surveys (Table 19). Although the SW and NE streams have about the same reach in the study (98 and 96 m, respectively), and are about the same width (2.5 and 2.9 m, respectively), the NE stream exhibited considerably less overall volume change (-1.2 cm^3) than the SW stream (9.2 cm^3).

For all streams, soil volume changes (erosion and deposition) were greatest between July 1, 2017 and September 24, 2017 (Table 19). During this period, which also has the greatest number of days with > 10 mm rainfall, the highest total rainfall and the highest maximum windspeed, all three streams exhibited net erosion. The period from September 24, 2017 and March 10, 2018 exhibited the next-highest change in channel sediment volume. During this period, the NE stream exhibited net erosion, but the other two streams exhibited net deposition. During all other time periods, all streams exhibited net deposition.

Except for SW stream during the period between July 1, 2017 and September 24, 2017, the stream beds exhibited net soil volume deposition. The channel walls all exhibited net erosion during this period as well. Net erosion was also exhibited on the channel walls of the NW and NE streams during the September 24, 2017 and March 10, 2018 period. Net wall erosion for the entire 16 months of the study period was only experienced by NE stream.

There were no clear patterns in erosion, deposition, or net sediment storage between the east and west channel walls for any of the streams.

Table 21. Total erosion and deposition (cm³) at different portions of each stream.

Stream	Survey	Event	Bed	East Wall	West Wall	Total
NW	July-September	Deposition	147.3	25.4	37.2	209.9
		Erosion	115.9	72.6	44.2	232.7
		Deposition-Erosion	31.4	-47.2	-7.0	-22.8
	September-March	Deposition	145.5	21.8	26.2	193.5
		Erosion	118.6	32.4	27.6	178.6
		Deposition-Erosion	26.9	-10.6	-1.4	14.9
	March-May	Deposition	100.1	43	23	166.1
		Erosion	81.9	25.8	19.6	127.3
		Deposition-Erosion	18.2	17.2	3.4	38.8
	May-November	Deposition	87.4	31.4	20.8	139.6
		Erosion	60.6	25.2	18.8	104.6
		Deposition-Erosion	26.8	6.2	2.0	35.0
July-November	Deposition	125.4	21.6	20.8	167.8	
	Erosion	48.3	16.4	15.4	80.1	
	Deposition-Erosion	77.1	5.2	5.4	87.7	

NE	July-September	Deposition	124.3	19.2	15.8	159.3
		Erosion	88.1	66.2	59.6	213.9
		Deposition-Erosion	36.2	-47.0	-43.8	-54.6
	September-March	Deposition	72.7	19.4	24.4	116.5
		Erosion	72.6	50.4	18.8	141.8
		Deposition-Erosion	0.1	-31.0	5.6	-25.3
	March-May	Deposition	102.6	19.6	23	145.2
		Erosion	49.6	25.8	13.4	88.8
		Deposition-Erosion	53.0	-6.2	9.6	56.4
	May-November	Deposition	69.5	20.2	13.2	102.9
		Erosion	27.7	14.8	10.4	52.9
		Deposition-Erosion	41.8	5.4	2.8	50.0
	July-November	Deposition	87.4	29.8	14.4	131.6
		Erosion	54.8	67.2	10.8	132.8
		Deposition-Erosion	32.6	-37.4	3.6	-1.2
SW	July-September	Deposition	72	25.6	7.2	104.8
		Erosion	81.8	34.8	23	139.6
		Deposition-Erosion	-9.8	-9.2	-15.8	-34.8
	September-March	Deposition	55.2	25.4	20.4	101.0
		Erosion	27.1	19.6	17.2	63.9
		Deposition-Erosion	28.1	5.8	3.2	37.1
	March-May	Deposition	28.4	15.2	5.6	49.2
		Erosion	22.6	9.8	0	32.4
		Deposition-Erosion	5.8	5.4	5.6	16.8
	May-November	Deposition	22.9	5.4	5	33.3
		Erosion	0	0	0	0
		Deposition-Erosion	22.9	5.4	5.0	33.3
	July-November	Deposition	58.5	19.6	15.6	93.7
		Erosion	51.3	11	22.2	84.5
		Deposition-Erosion	7.2	8.6	-6.6	9.2

4.5 Discussion

The UAV approach used here appears generally capable of making reliable, repeated measures of soil surface height at the scale of ~ 100 m. Changes in UAV-derived heights, whether measured as standard deviations of absolute heights during different surveys (Table 19), or as overall MAD and MD (Table 18) were considerably smaller than measures of height between the Total Station and UAV. Given the complexity of accurately using a Total Station and the difficulty

of obtaining high-accuracy angle measurements, we interpret this to mean that the Total Station accuracy was actually less than that of the UAV. The repeatability of the UAV-derived height estimates is thus between 1 - 2 cm from our measurements, and considerably smaller than many of the height differences measured in the streams (Figures 18 and 19).

Although camera and flight parameters such as overlap and cell size have a major effect on accuracy of UAV-derived heights, our results are generally in agreement, if smaller than, other estimates of UAV-derived heights. For instance, Glendell et al. (2017) compared vertically differenced DEMs using a terrestrial laser scanner against UAV surface models and found a vertical difference of 5 to 6 cm. Goncalves and Henriques (2015) reported a vertical difference error of 4 cm. Fonstad et al. (2013) reported 18 cm accuracy, whereas Gillan et al. (2017) reported difference errors between 2.2 to 4.4 cm.

The fact no change was observed in areas that were not expected to see significant erosion or deposition, such as the hillslopes away from the channels, provides added confirmation that the height differences measured within the channel were real. This is further supported by the spatially coherent and consistent patterns of erosion and deposition within the streams, which would not be expected if there was significant uncertainty or variability in height measurements. In all but a few cases deposition or erosional volume differences were greater than the volume change uncertainty (Table 19).

Thus, with few exceptions, we have confidence that the estimated volume changes are representative of reality. Taking them at face value, then, indicates that highly variable sediment storage in the observed streams. Our differencing analysis, alone, does not make it possible to distinguish the dominant mode of transport (aeolian or fluvial) that led to changes in sediment storage. However, local observations indicate that flow within channels only occurred during

September, 2017. And, indeed, we observed evidence of rill erosion in the NE stream during the second survey in September 2017, indicating recent flow, consistent with the storm cycle in the areas from September 9th, 2017 to September 15th, 2017. The fact that all streams experienced net erosion during this period indicates the efficacy of these storms in flushing sediment out of the channel reaches that we studied. Although no direct observations of stream flow were made from September 24, 2017 to March 10, 2018, there is evidence of net erosion in the NE stream suggesting that, perhaps some flow may have occurred during this period.

The March to May, and May to November periods only experienced 2 and 4 days with > 10 mm rain, respectively. But, they experienced the strongest 95th percentile wind speeds and erosive wind (>7 m/s) were experienced at the Moab ASOS station in nearly three-quarters of the days between the March and May surveys and nearly one-third of the days between the May and November surveys with significant rain only 3% and 2% of the days, respectively. Thus, we interpret the majority of transport that occurred during these two periods as being aeolian.

The changes in sediment volume in the streams we studied during these aeolian-dominant periods could either be due to reworking of sediment within the channel or transfer of sediment into/out of the channel from/to the adjacent hillslope. Given the considerable quantities of net deposition observed during the March to November time periods in all three streams, and the fact that much of that deposition is on the margins of the streams where sand ramps form, we interpret these changes in sediment storage to net transfer of sediment into the channel from the hillslope through aeolian transport.

4.6 Conclusion

The study of three ephemeral streams in Utah using UAV-derived heights indicates highly complex changes in sediment storage reflecting a combination of fluvial and aeolian processes.

Fluvial processes appear to have flushed considerable amount of sediments from the stream in Fall, 2017. However, much of this was replenished in the following months through deposition by wind into the channel. One of the streams, in fact, experienced a dramatic net increase in sediment storage during the 16-month duration of this study.

It is impossible to know the exact source of the wind-erodible hillslope sediment that was deposited in the channels. The fact that deposition occurred all along the stream reaches studied suggests, however, that it may have a diffuse source, rather than coming from a few large sources. Regardless, our data suggest an important coupling between the hillslope and its inset channels that has received little attention in the geomorphic literature. Although this study spanned only 16 months, the net sediment balance within the reach of these streams suggests that much of the sediment that is flushed out of streams like these may have entered not through overland flow but, rather, through aeolian transport. Thus, although aeolian transport, and saltation especially, is often seen as a mechanism for small-scale reworking of available sediments, in the context of hillslope-channel coupling, it could be an important mechanism of overall hillslope erosion.

4.7 Acknowledgment

I would like to thank Dr. Jayne Belnap for hosting the research in Moab UT and for support and guidance. Special thanks to Kuwait University for their academic support.

4.8 Bibliography

ASOS Network. 2017. Iowa State University: Department of Agriculture. Iowa, United States. URL: <https://mesonet.agron.iastate.edu>.

Belnap, Jayne. 1995. "Surface disturbances: Their Role in accelerating desertification." *Environmental Monitoring and Assessment* 37 (1-3): 39-57.

Belnap, Jayne, Seth M Munson, and Jason P Field. 2011. "Aeolian and fluvial processes in drylands regions: the need for integrated studies." *Ecohydrology* 4: 615-622.

Breshears, D D, J J Whicker, M P Johansen, and J E Pinder. 2003a. "Wind and water erosion and transport in semi-arid shrubland, grassland and forest ecosystems: Quantifying dominance of horizontal wind-drive transport." *Earth Surface Processes and Landforms* 28: 1189-1209.

Breshears, David D, Jeffrey J Whicker, Mathew P Johansen, and John E Pinder. 2003b. "Wind and water erosion and transport in semi-arid shrubland, grassland, and forest ecosystems: Quantifying dominance of horizontal wind-driven transport." *Earth Surface Processes and Landforms* 28: 1189-1209.

Bull, L J, and M J Kirkby. 2002. "Dryland rivers: Hydrology and geomorphology of semi-arid channels". Chichester, England: John Wiley & Sons.

Bullard, Joanna E, and Grant H McTanish. 2003. "Aeolian-fluvial interactions in dryland environments: Example, concepts and Australia case Study." *Progress in Physical Geography* 27 (4): 471-501.

Capolupo, Alessandra, Stefania Pindozi, Collins Okello, Nunzio Fiorentino, and Lorenzo Boccia. 2015. "Photogrammetry for environmental monitoring: The use of drones and hydrological models for detection of soil contaminated by copper." *Science Of The Total Environment* 514: 298-306.

Castillo, C, R Perez, M R James, J N Quinton, E V Taguas, and J A Gomez. 2012. "Comparing the accuracy of several field methods for measuring Gully Erosion." *Science Society of America Journal* 76 (4): 1319-1332.

Cunliff, A M, R E Brazier, and K Anderson. 2016. "Ultra-fine grain landscape-scale quantification of dryland vegetation structure with drone-acquired structure-from-motion photogrammetry." *Remote Sensing of Environment* 183: 129-143.

Daftry, S, C Hoppe, H Bischof. 2015. "Building with drones: Accurate 3D facade reconstruction using MAVs". *IEEE International Conference on Robotics and Automation (ICRA)*. Seattle, WA, USA.

DJI. 2019. Los Angeles, CA, United States. URL: <https://www.dji.com>.

d'Oleire-Oltmanns, Sebastian, Irene Marzloff, Klaus Daniel Peter, and Johannes Ries. 2012. "Unmanned aerial vehicle (UAV) for monitoring soil erosion in Morocco." *Remote Sensing* 4 (11): 3390-3416.

Drones Made Easy. 2018. San Diego, CA, United States. URL: <https://www.dronesmadeeasy.com/>.

Elner, A, P Baumgart, H G Maas, and D Faust. 2014. "Multi-temporal UAV data for automatic measurements of rill and interill erosion on loess soil." *Earth Surface Processes and Landform* 40 (6): 741-755.

Field, Jason P, David D Breshears, and Jeffrey J Whicker. 2009. "Toward a more holistic perspective of soil erosion: Why aeolian research needs to explicitly consider fluvial processes and interactions." *Aeolian Research* 1 (1-2): 9-17.

Field, J D, D D Breshears, J J Whicker, and C B Zou. 2011. "On the ratio of wind- to water-driven sediment transport: Conserving soil under global-change-type extreme events". *Journal of Soil and Water Conservation* 66:51A-56A.

Fonstad, Mark A, James T Dietrich, Brittany C Courville, L Jennifer Jensen, and Patrice E Carbonneau. 2013. "Topographic structure from motion: A new development in photogrammetric measurement." *Earth Surface Processes and Landforms* 38 (4): 421-430.

Gillan, J K, J W Karl, A Elaksher, and M Duniway. 2017. "Fine-resolution repeat topographic surveying of dryland landscapes using UAS-based structure-from-motion photogrammetry: Assessing accuracy and precision against traditional ground-based erosion measurements." *Remote Sensing* 69: 95-107.

Gillan, J K, J W Karl, Nichole N Barger, Ahmed Elaksher, and Michael C Duniway. 2016. "Spatially explicit rangeland erosion monitoring using high-resolution digital aerial imagery." *Rangeland Ecology and Management* 69 (2): 95-107.

Glendell, M, G McShane, L Farrow, M R James, J Quinton, K Anderson, M Evans, et al. 2017. "Testing the utility of structure from motion photogrammetry reconstructions using small unmanned aerial vehicles and ground photography to estimate the extent of upland soil erosion." *Earth Surface Processes and Landforms* 42 (12): 1860-1871.

Goncalves, J A, and R Henriques. 2015. "UAV photogrammetry for topographic monitoring of coastal areas." *ISPRS J. Photogrammetry and Remote Sensing* 104: 101-111.

Goudie, A S, and N J Middleton. 2006. *Desert dust in the global system*. Heidelberg: Springer.

James, M R, and S Robson. 2012. "Straightforward reconstruction of 3D surfaces and topography with a camera: Accuracy and geoscience application." *Journal of Geophysical Research* 117 (F3).

James, Mike R, and Stuart Robson. 2014. "Mitigating systematic error in topographic models derived from UAV and ground-based image network." *Earth Surface Processes and Landforms* 39 (10): 1413-1420.

Lal, Rattan, Terry M Sobecki, John M Kimble, and Thomas Livari. 2003. *Soil degradation in the United States: Extent, Severity, and Trends*. Boca Raton: Lewis Publishers.

Lowe, D G. "Distinctive Image Features from Scale-Invariant Keypoints". 2004. *International Journal of Computer Vision* 60: 91-110.

Maroulis, J C, G C Nanson, D M Price, T Pietsch. 2007. "Aeolian-fluvial interaction and climate change: source-bordering dune development over the past ~100 ka on Cooper Creek, central Australia". *Quaternary Science Reviews* 26: 386-404.

McFadden L D, S G Wells, and M J Jercinovich. 1987. "Influence of eolian and pedogenic processes on the origin and evolution of desert pavements". *Geology* 15:504-508.

Niethammer, U, M R James, S Rothmund, J Travelletti, and M Joswing. 2012. "UAV-based remote sensing of the Super-Sauze landslide: Evaluation and results." *Engineering Geology* 129: 2-11.

Okin, G S, M C Rehies. 2001. "An ENSO predictor of dust emission in the southwestern United States". *Geophysical Research Letters* 29: 461-463.

Okin, G S, A J Parsons, J Wainwright, J E Herrick, B T Bestelmeyer, D P.C Peters, and E L Fredrickson. 2009. "Do changes in connectivity explain desertification." *Biosciences* 59: 237-244.

Okin, G S, D A Gillette, and J E Herrick. 2006. "Multi-scale controls on and consequences of aeolian processes in landscape change in arid and semi-arid environment." *Journal of Arid Environments* 65 (2): 253-275.

Okin G S, O E Sala, E N Vivoni, J Zhang, A Bhattachan. "The interactive role of wind and water in functioning of drylands: What does the future hold?". 2018. *Bioscience* 68: 670-677.

Osman, Khan Towhid. 2014. *Soil degradation, Conservation and Remediation*. Dordrecht, Netherlands: Springer.

Pimentel, D, C Harvey, P Resosudarmo, K Sinclair, D Kurz, M McNair, S Crist, et al. 1995. "Environmental and Economic cost of soil erosion and conservation benefits." *Science* 267: 1117-1123.

Pimentel, D. 1993. World Soil Erosion and conservation. Cambridge, UK: Cambridge University Press.

Ravi, Sujith, David Breshears, Travis E Huxman, and D'Odorico Paolo. 2010. "Land Degradation in drylands: Interactions among hydrologic-aeolian erosion and vegetation dynamics." *Geomorphology* 116 (3-4): 236-245.

Reheis, M C. 1997. "Dust deposition downwind of Owens (dry) Lake, 1991–1994: Preliminary findings". *JGR Atmospheres* 102:D22.

Reheis, M C. 2007. "A 16-year record of eolian dust in Southern Nevada and California, USA: Controls on dust generation and accumulation." *Journal of Arid Environment* 67: 487-520.

Reynold, F James, D Mark Stafford Smith, Eric F Lambin, B L Turner II, Michael Mortimore, Simon P J Butterbury, Thomas E Dowing, et al. 2007. "Global desertification: Building a Science for Dryland Development." *Science* 316 (5826): 847-851.

Sankey, J A, E Draut. 2014. "Gully annealing by aeolian sediment: field and remote-sensing investigation of aeolian–hillslope–fluvial interactions, Colorado River corridor, Arizona, USA". *Geomorphology* 220: 68-80.

Schepanski K, I Tegen, A Macke. 2012. "Comparison of satellite based observations of Saharan dust source areas" *Remote Sensing of Environment* 123: 90-97.

Toy, T J, G R Foster, and K G Renard. 2002. *Soil Erosion: Processes, prediction, measurement and control*. New York: John Wiley & Sons.

Trimble Inc. 2018. Sunnyvale, CA, United States. <https://www.trimble.com>.

Utah Water Science Center. 2017. U.S Geological Survey, UT, United States. URL: <http://ut.water.usgs.gov/index.html>.

Visser, S M, G Sterk, and O Ribolzi. 2004. "Techniques for simultaneous quantification of wind and water erosion in semi-arid regions." *Journal of Arid Environment* 59: 699-717.

Wells S G, L D McFadden, J Poths, and C T Olinger. 1995. "Cosmogenic ³He surface-exposure dating of stone pavements: implications for landscape evolution in deserts". *Geology* 23:613-616.

Westoby, M J, J Brasington, N F Glasser, M J Hambrey, and J M Reynolds. 2012. "'Structure-from-motion' photogrammetry: A low-cost effective tool for geoscience application." *Geomorphology* 179: 300-314.

Whicker, Ward, and Vincent Schutlz. 1982. Radioecology:Nuclear energy an the environment. Boca Ralton, Florida: CRC Press.

Whicker, J J, D D Breshears, P T Wasiolek, T B Kirchner, R A Tavani, D A Schoep, J C Rodgers. 2002. "Temporal and spatial variation of episodic wind erosion in unburned and burned semiarid shrubland". Journal of Environmental Quality 31: 599-612.

Chapter 5: Discussion and Conclusion

Drylands account for 41% of the earth's land surface and 23% of the land surface of the United States (Le Houérou 1996). Dryland ecosystems are directly affected by changes in climate and land use (Nicholson 2001; Nicholson and Kim 1997). The global climate change and the rapid expansion of the human population and their activities cause drylands to experience accelerated rates of soil loss via erosion, reduction in productivity of biomass, reduction in resource quality, and a decline in potential support for economic activities. Climate models have suggested that climate change may reduce soil moisture due to increasing temperature and evaporation (Sheffield and Wood 2007). Drier soil might not be sufficient for biogeochemical processes that support microbial activities and plant production. It is expected that the supply of wind-borne soil particle will increase due to the decrease in vegetation cover and the expansion of bare soil surface. In this case, soil movement and dust emission would be more likely to increase, as well.

Over the past 150 years, most drylands have experienced drastic changes in the vegetation cover represented in the form of shrub encroachment into grasslands. Research has been widely conducted on grazing, droughts, fires, temperature fluctuations, and precipitation inputs. Many LTER studies have highlighted the processes that control patterns of productivity and the establishment of grasses versus shrubs (Peters et al. 2006). Least studied has been aeolian erosion, due to the complexity of the dynamics and the mechanisms involved with it. The lack of understanding of the implications associated with soil movement makes it difficult to assess potential consequences of climate change.

In our sandblasting-vegetation impacts study, we showed, for the very first time, that soil movement might have played a major role in shrub encroachment in the United States. Our experiment at the Jornada Experimental Range allowed us to cross the traditional boundaries of

shrub encroachment studies and explore the role of aeolian processes on biomass health and mortality in drylands. Our results have positively supported our hypothesis that aeolian processes are responsible for above-ground biomass reduction to varying degrees. In addition, our results confirmed that grasses are more vulnerable to damage from sandblasting, due to their sensitive leaf and stolon structure and their growing point, while shrubs are more resilient to damage from sandblasting and chances of their recovery are higher. *Lerrea Tridentata* and *Artiplex* showed high resilience to disturbances, which explains their expansion and high rates of establishing in regions that were formally occupied by grasses. The damaging effects of aeolian processes found in our study can extend the field of shrub encroachment into a comprehensive ecological framework. Understanding the dynamics of the controls that dominate shrub encroachment in drylands is of great importance, as it helps to understand past climates and thereby predict future ones.

Changes in vegetation cover have the potential to alter net primary productivity of plants and the contribution of drylands' NPP to global NPP rates. Net primary productivity is a critical measure of the ecosystem's functionality. Drylands are regions of extreme drought that are suffering from ongoing degradation; yet they produce about 30% of the global net primary production (Parton et al. 1995). The Jornada Basin has a well-documented history of vegetation cover changes and shrub encroachment, including plant activities and productivity fluctuations. It has been documented that some plant species experience severe stress, which has led to their withdrawal. Methods of field-based NPP measurements vary, while remote sensing of NPP is still limited due to the nature of dryland surfaces and vegetation characteristics. Our remote sensing study of NPP displays a high probability of predicting NPP using advanced remote sensing techniques, such as spectral unmixing and non-linear statistical approaches, i.e., a Random Forest.

Remote sensing of drylands is rather complicated and is usually associated with an overestimation of vegetation productivity. Spectral unmixing approaches facilitate studying ground components by spectrally separating them. With this approach, we were able to characterize the photosynthetic vegetation cover and the non-photosynthetic vegetation cover, in addition to soil. The critical aspect of our study is the characterization of NPV, which remains a challenge in most studies. Our findings indicate that long-term NPP prediction could accurately represent vegetation activities using sophisticated methods, where basic retrieval of NPP fractions using MODIS NPP have yielded erroneous estimations.

Wind and water activities can accelerate the degradation of drylands. This can lead to major environmental consequences worldwide (Bridges and Oldeman 2010; Lal 2001). Changes in climate, land use, and land cover are likely to increase the intensity of soil erosion. Climate is predicted to be warmer and drier in many dry regions, which will increase environmental stress (IPCC 2013). The vegetation cover and distribution is expected to decline as a result of climate change (Bridges and Oldeman 2010), which in turn will increase soil surface exposure and soil movement. Increased rates of wind and water erosion are found in regions of the world where there is expansion of urban areas, cultivation, suburbanization, and increasing populations. Wind and water interactions in drylands are more complex than previously anticipated because of rapid changes in the climatic variables and dryness conditions. The patterns and intensity of soil movement are unpredictable. Our findings indicate that the episodic fluvial events not only intensify soil movement by water, but also intensify aeolian activities' post fluvial events, where during flash floods, much of the vegetation that holds the soil in place is stripped, exposing the soil to the next wind event. Our study shows that morphological features such as channels could

eventually change in shape and size due to the excessive removal of surface material. When wind and water encounter loose soil particles without obstacles, the removal of soil increases.

Methods of studying fluvial and aeolian interactions are limited, and few guidelines and frameworks have been introduced in the literature, which makes it difficult to study interactions between wind and water and relate them to land use and climate alterations.

The interactions and feedbacks between dryland ecosystem drivers and environmental changes and their impact on the ecosystems have been recognized by academics and policy makers. However, the high spatial and temporal heterogeneity of dryland surfaces require deeper investigation to understand the dynamics that control drylands.

5.1 Bibliography

Bridges, E M, and L R Oldeman. 2010. "Global Assessment of Human-induced Soil Degradation (GLASOD)." *Arid Soil Research and Rehabilitation* 13 (4): 319-325.

IPCC. 2013. *Climate Change. The physical science basis. Contribution of working group I to the fifth assessment report of the intergovernmental panel on climate change.* Cambridge, United Kingdom: Cambridge University Press.

Lal, R. 2001. "Potential of desertification control to sequester carbon and mitigate the greenhouse effect." *Climate Change* 51: 35-72.

Le Houérou, H N. 1996. "Climate change, drought and desertification." *Journal of Arid Environments* 34 (2): 133-185.

Nicholson, S E. 2001. "Climatic and environmental change in Africa during the last two centuries." *Climate Research* 17: 123-144.

Nicholson, S E, and J Kim. 1997. "The relationship of the El Nino-Southern Oscillation to African Rainfall." *International Journal of Climatology* 17: 123-135.

Parton, W J, J M Scurlock, D S Ojima, D S Schimel, D O Hall, and M Scopegram Group. 1995. "Impact of climate change on grassland production and soil carbon worldwide." *Global Change Biology* 1: 13-22.

Peters, D PC, and R Gibbons. 2006. "Plant communities in the Jornada Basin: the dynamic landscape." In *Structure and function of a Chihuahuan Desert ecosystem: the Jornada Basin long-term ecological research site*, by W H Havstad, 211-231. Oxford, UK: Oxford University Press.